

Author Manuscript

This is the author manuscript accepted for publication and has undergone full peer review but has not been through the copyediting, typesetting, pagination and proofreading process, which may lead to differences between this version and the [Version of Record](#). Please cite this article as [doi: 10.1002/mp.13264](https://doi.org/10.1002/mp.13264)

This article is protected by copyright. All rights reserved

Received Date:

Revised Date:

Accepted Date:

Article Type: Review Article

Deep learning in medical imaging and radiation therapy

Berkman Sahiner, Aria Pezeshk, Lubomir M. Hadjiiski, Xiaosong Wang, Karen Drukker, Kenny H. Cha, Ronald M. Summers, Maryellen L. Giger

Berkman Sahiner: DIDSR/OSEL/CDRH, U.S. Food and Drug Administration, Silver Spring, MD 20993 USA

Aria Pezeshk: DIDSR/OSEL/CDRH, U.S. Food and Drug Administration, Silver Spring, MD 20993 USA

Lubomir M. Hadjiiski: Department of Radiology, University of Michigan, Ann Arbor, MI 48109

Xiaosong Wang: Imaging Biomarkers and Computer-aided Diagnosis Lab, Radiology and Imaging Sciences, NIH Clinical Center, Bethesda, MD 20892-1182

Karen Drukker: Department of Radiology, University of Chicago, Chicago, IL 60637

Kenny H. Cha: DIDSR/OSEL/CDRH, U.S. Food and Drug Administration, Silver Spring, MD 20993 USA

Ronald M. Summers: Imaging Biomarkers and Computer-aided Diagnosis Lab, Radiology and Imaging Sciences, NIH Clinical Center, Bethesda, MD 20892-1182

23 Maryellen L. Giger: Department of Radiology, University of Chicago, Chicago, IL 60637

24 **Corresponding Author:** Berkman Sahiner, berkman.sahiner @fda.hhs.gov,

25 DIDS/OSEL/CDRH, U.S. Food and Drug Administration, Silver Spring, MD 20993 USA

26 **Deep learning in medical imaging and radiation therapy**

27 Berkman Sahiner¹, Aria Pezeshk¹, Lubomir M. Hadjiiski², Xiaosong Wang³, Karen Drukker⁴,

28 Kenny H. Cha¹, Ronald M. Summers³, Maryellen L. Giger⁴

29 **Abstract**

30 The goals of this review paper on deep learning (DL) in medical imaging and radiation therapy
31 are to: 1) summarize what has been achieved to date; 2) identify common and unique challenges,
32 and strategies that researchers have taken to address these challenges; and 3) identify some of the
33 promising avenues for the future both in terms of applications as well as technical innovations.
34 We introduce the general principles of DL and convolutional neural networks, survey five major
35 areas of application of DL in medical imaging and radiation therapy, identify common themes,
36 discuss methods for data set expansion, and conclude by summarizing lessons learned, remaining
37 challenges, and future directions.

38 **1. INTRODUCTION**

39 In the last few years, artificial intelligence (AI) has been rapidly expanding and permeating both
40 industry and academia. Many applications such as object classification, natural language

¹ DIDS/OSEL/CDRH, U.S. Food and Drug Administration, Silver Spring, MD 20993 USA

² Department of Radiology, University of Michigan, Ann Arbor, MI 48109

³ Imaging Biomarkers and Computer-aided Diagnosis Lab, Radiology and Imaging Sciences, NIH Clinical Center, Bethesda, MD 20892-1182

⁴ Department of Radiology, University of Chicago, Chicago, IL 60637

41 processing and speech recognition, which until recently seemed to be many years away from
42 being able to achieve human levels of performance, have suddenly become viable.¹⁻³ Every
43 week, there is a news story about an AI system that has surpassed humans at various tasks
44 ranging from playing board games⁴ to flying autonomous drones.⁵ One report shows that
45 revenues from AI will increase by around 55% annually in the 2016-2020 time period from
46 roughly \$8 billion to \$47 billion.⁶ Together with breakthroughs in other areas such as
47 biotechnology and nanotechnology, the advances in AI are leading to what the World Economic
48 Forum refers to as the fourth industrial revolution.⁷ The disruptive changes associated with AI
49 and automation are already being seriously discussed among economists and other experts as
50 both having the potential to positively improve our everyday lives, e.g., by reducing healthcare
51 costs, as well as to negatively affect society, e.g., by causing large scale unemployment and
52 rising income inequality^{8,9} (according to one estimate, half of all working activities can be
53 automated by existing technologies¹⁰). The advances in AI discussed above have been almost
54 entirely based on the groundbreaking performance of systems that are based on deep learning
55 (DL). We now use DL-based systems on a daily basis when we use search engines to find images
56 on the web or talk to digital assistants on smart phones and home entertainment systems. Given
57 its widespread success in various computer vision applications (among other areas), DL is now
58 poised to dominate medical image analysis and has already transformed the field in terms of
59 performance levels that have been achieved across various tasks as well as its application areas.

60 **1.A. Deep learning, history, and techniques**

61 DL is a subfield of machine learning, which in turn is a field within AI. In general, DL consists
62 of massive multi-layer networks of artificial neurons that can automatically discover useful

63 features, i.e. representations of input data (in our case images) needed for tasks such as detection
64 and classification, given large amounts of unlabeled or labeled data.^{11, 12}

65 Traditional applications of machine learning using techniques such as support vector machines
66 (SVM) or random forests (RF) took as input hand-crafted features, which are often developed
67 with a reliance on domain expertise, for each separate application such as object classification or
68 speech recognition. In imaging, hand-crafted features are extracted from the image input data
69 and reduce the dimensionality by summarizing the input into what is deemed to be the most
70 relevant information that helps with distinguishing one class of input data from another. On the
71 other hand, using the image pixels as the input, the image data can be flattened into a high-
72 dimensional vector; for example, in mammographic mass classification, a 500x500 pixel region
73 of interest will result in a vector with 250,000 elements. Given all the possible variations of a
74 mass's appearance due to differences in breast type, dose, type and size of a mass, etc., finding
75 the hyperplane that separates the high dimensional vectors of malignant and benign masses
76 would require a very large number of examples if the original pixel values are used. However,
77 each image can be summarized into a vector consisting of a few dozen or a few hundred
78 elements (as opposed to over a million elements in the original format) by extracting specialized
79 features that for instance describe the shape of the mass. This lower dimensional representation
80 is more easily separable using fewer examples if the features are relevant. A key problem with
81 this general approach is that useful features are difficult to design, often taking the collective
82 efforts of many researchers over years or even decades to optimize. The other issue is that the
83 features are domain or problem specific. One would not generally expect that features developed
84 for image recognition should be relevant for speech recognition, but even within image
85 recognition different types of problems such as lesion classification and texture identification

86 require separate sets of features. The impact of these limitations has been well demonstrated in
87 experiments that show performance of top machine learning algorithms to be very similar when
88 they are used to perform the same task using the same set of input features.¹³ In other words,
89 traditional machine learning algorithms were heavily dependent on having access to good feature
90 representations, otherwise it was very difficult to improve the state-of-the-art results on a given
91 data set.

92 The key difference between DL and traditional machine learning techniques is that the former
93 can automatically learn useful representations of the data, thereby eliminating the need for hand-
94 crafted features. What is more interesting is that the representations learned from one data set can
95 be useful even when they are applied to a different set of data. This property, referred to as
96 transfer learning^{14, 15}, is not unique to DL but the large training data requirements of DL make it
97 particularly useful in cases where relevant data for a particular task is scarce. For instance, in
98 medical imaging, a DL system can be trained on a large number of natural images or those in a
99 different modality to learn proper feature representations that allow it to “see”. The pre-trained
100 system can subsequently use these representations to produce an encoding of a medical image
101 that is used for classification.¹⁶⁻¹⁸ Systems using transfer learning often outperform the state-of-
102 the-art methods based on traditional hand-crafted features that were developed over many years
103 with a great deal of expertise.

104 The success of DL compared to traditional machine learning methods is primarily based on two
105 inter-related factors: depth and compositionality.^{11, 12, 19} A function is said to have a compact
106 expression if it has few computational elements used to represent it (“few” here is a relative term
107 that depends on the complexity of the function). An architecture with sufficient depth can
108 produce a compact representation, whereas an insufficiently deep one may require an

109 exponentially larger architecture (in terms of the number of computational elements that need to
110 be learned) to represent the same function. A compact representation requires fewer training
111 examples to tune the parameters and produces better generalization to unseen examples. This is
112 critically important in complex tasks such as computer vision where each object class can exhibit
113 many variations in appearance which would potentially require several examples per type of
114 variation in the training set if a compact representation is not used. The second advantage of
115 deep architectures has to do with how successive layers of the network can utilize the
116 representations from previous layers to compose more complex representations that better
117 capture critical characteristics of the input data and suppress the irrelevant variations (for
118 instance, simple translations of an object in the image should result in the same classification). In
119 image recognition, deep networks have been shown to capture simple information such as
120 presence or absence of edges at different locations and orientations in the first layer. Successive
121 layers of the network assemble the edges into compound edges and corners of shapes, and then
122 into more and more complex shapes that resemble object parts. Hierarchical representation
123 learning is very useful in complicated tasks such as computer vision where adjacent pixels and
124 object parts are correlated with each other and their relative locations provide clues about each
125 class of object, or speech recognition and natural language processing where the sequence of
126 words follow contextual and grammatical rules that can be learned from the data. This
127 distributed hierarchical representation has similarities with the function of the visual and auditory
128 cortexes in the human brain where basic features are integrated into more complex
129 representations that are used for perception.^{20, 21}

130 As discussed earlier, DL is not a completely new concept, but rather mostly an extension of
131 previously existing forms of artificial neural networks (ANNs) to larger number of hidden layers

132 and nodes in each layer. In the late 1990s until early 2000s, ANNs started to lose popularity in
133 favor of SVMs and decision-tree-based methods such as random forests and gradient boosting
134 trees that seemed to be more consistently outperforming other learning methods.²² The reason for
135 this was that ANNs were found to be both slow and difficult to train aside from shallow
136 networks with one to two hidden layers, as well as prone to getting stuck in local minima.
137 However, starting around 2006 a combination of several factors led to faster and more reliable
138 training of deep networks. One of the first influential papers was a method for efficient
139 unsupervised (i.e. using unlabeled data, as opposed to supervised training that uses data labeled
140 based on the ground truth) layer by layer training of deep restricted Boltzmann machines.²³ As
141 larger data sets became more commonplace, and with availability of commercial gaming
142 graphical processing units (GPUs) it became possible to explore training of larger deeper
143 architectures faster. At the same time, several innovations and best practices in network
144 architecture and training led to faster training of deep networks with excellent generalization
145 performance using stochastic gradient descent. Some examples include improved methods for
146 network initialization and weight updates,²⁴ new neuron activation functions,²⁵ randomly cutting
147 connections or zeroing of weights during training,^{26,27} and data augmentation strategies that
148 render the network invariant to simple transformations of the input data. Attention to these
149 improvements was still mostly concentrated within the machine learning community and not
150 being seriously considered in other fields such as computer vision. This changed in 2012 in the
151 ImageNet²⁸ competition in which more than a million training images with 1000 different object
152 classes were made available to the challenge participants. A DL architecture that has since been
153 dubbed AlexNet outperformed the state-of-the-art results from the computer vision community

154 by a large margin and convinced the general community that traditional methods were on their
155 way out.²⁹

156 The most successful and popular DL architecture in imaging is the convolutional neural network
157 (CNN).³⁰ Nearby pixels in an image are correlated with one another both in areas that exhibit
158 local smoothness and areas consisting of structures (e.g. edges of objects or textured regions).
159 These correlations typically manifest themselves in different parts of the same image.
160 Accordingly, instead of having a fully connected network where every pixel is processed by a
161 different weight, every location can be processed using the same set of weights to extract various
162 repeating patterns across the entire image. These sets of trainable weights, referred to as kernels
163 or filters, are applied to the image using a dot product or convolution and then processed by a
164 non-linearity (e.g. a sigmoid or tanh function). Each of these convolution layers can consist of
165 many such filters resulting in the extraction of multiple sets of patterns at each layer. A pooling
166 layer (e.g. max-pooling where the output is the maximum value within a window) often follows
167 each convolution layer to both reduce the dimensionality as well as impose translation invariance
168 so that the network becomes immune to small shifts in location of patterns in the input image.
169 These convolution and pooling layers can be stacked to form a multi-layer network often ending
170 in one or more fully connected layers as shown in Fig **Error! Reference source not found.**
171 followed by a softmax layer. The same concepts can be applied in 1D and 3D to accommodate
172 time-series and volumetric data, respectively. Compared to a fully connected network, CNNs
173 contain far fewer trainable parameters and therefore require less training time and fewer training
174 examples. Moreover, since their architecture is specifically designed to take advantage of
175 presence of local structures in images they are a natural choice for imaging applications and a
176 regular winner of various imaging challenges.

177 Another very interesting type of network is the recurrent neural network (RNN) which is ideal
178 for analyzing sequential data (e.g. text or speech) due to having an internal memory state that can
179 store information about previous data points. A variant of RNNs, referred to as long short term
180 memory (LSTM),³¹ has improved memory retention compared to a regular RNN and has
181 demonstrated great success across a range of tasks from image captioning^{32, 33} to speech
182 recognition^{1, 34} and machine translation.³⁵

183
184 Generative adversarial networks (GANs) and its different variants (e.g. WGAN³⁶, CycleGAN³⁷,
185 etc.) are another promising class of DL architectures that consist of two networks: a generator
186 and a discriminator.³⁸ The generator network produces new data instances that try to mimic the
187 data used in training, while the discriminator network tries to determine the probability of
188 whether the generated candidates belong to the training samples or not. The two networks are
189 trained jointly with backpropagation, with the generative network becoming better at generating
190 more realistic samples and the discriminator becoming better at detecting artificially generated
191 samples. GANs have recently demonstrated great potential in medical imaging applications such
192 as image reconstruction for compressed sensing in magnetic resonance imaging (MRI).³⁹

193 **1.B. Deep learning in medical imaging**

194 In medical imaging, machine learning algorithms have been used for decades, starting with
195 algorithms to analyze or help interpret radiographic images in the mid-1960's.⁴⁰⁻⁴² Computer-
196 aided detection/diagnosis (CAD) algorithms started to make advances in the mid 1980's, first
197 with algorithms dedicated to cancer detection and diagnosis on chest radiographs and
198 mammograms,^{43, 44} and then widening in scope to other modalities such as computed

199 tomography (CT) and ultrasound.^{45,46} CAD algorithms in the early days predominantly used a
200 data-driven approach as most DL algorithms do today. However, unlike most DL algorithms,
201 most of these early CAD methods heavily depended on feature engineering. A typical workflow
202 for developing an algorithm for a new task consisted of understanding what types of imaging and
203 clinical evidence clinicians use for the interpretation task, translating that knowledge into
204 computer code to automatically extract relevant features, and then using machine learning
205 algorithms to combine the features into a computer score. There were, however, some notable
206 exceptions. Inspired by the neocognitron architecture,⁴⁷ a number of researchers investigated the
207 use of CNNs⁴⁸⁻⁵¹ or shift-invariant ANNs^{52,53} in the early and mid-1990's, and massively-trained
208 artificial neural networks (MTANNs)^{54,55} in the 2000's for detection and characterization tasks
209 in medical imaging. These methods all shared common properties with current deep CNNs
210 (DCNNs): Data propagated through the networks via convolutions, the networks learned filter
211 kernels, and the methods did not require feature engineering, i.e., the inputs into the networks
212 were image pixel values. However, severely restricted by computational requirements of the
213 time, most of these networks were not deep, i.e., they mostly consisted of only one or two hidden
214 layers. In addition, they were trained using much smaller data sets compared to a number of
215 high-profile DCNNs that were trained using millions of natural images. Concepts such as
216 transfer learning,¹⁴ residual learning,⁵⁶ and fully convolutional networks with skip connections⁵⁷
217 were generally not well-developed. Thus, these earlier CNNs in medical imaging, as competitive
218 as they were compared to other methods, did not result in a massive transformation in machine
219 learning for medical imaging.

220 With the advent of DL, applications of machine learning in medical imaging have dramatically
221 increased, paralleling other scientific domains such as natural image and speech processing.

222 Investigations accelerated not only in traditional machine learning topics such as segmentation,
223 lesion detection and classification,⁵⁸ but also in other areas such as image reconstruction and
224 artifact reduction that were previously not considered as data driven topics of investigation. Fig.
225 2 22 shows the number of peer-reviewed publications in the last six years in the areas of focus
226 for this paper, DL for radiological images, and shows a very strong trend: For example, in the
227 first three months of 2018, more papers were published on this topic than the whole year of
228 2016.

229
230 Using DL involves making a very large number of design decisions such as number of layers,
231 number of nodes in each layer (or number and size of kernels in the case of CNNs), type of
232 activation function, type and level of regularization, type of network initialization, whether to
233 include pooling layers and if so what type of pooling, type of loss function, and so on. One way
234 to avoid using trial and error for devising the best architecture is to follow the same exact
235 architectures that have shown to be successful in natural image analysis such as AlexNet,²⁹
236 VGGNet,⁵⁹ ResNet,⁵⁶ DenseNet,⁶⁰ Xception,⁶¹ or Inception V3.⁶² These networks can be trained
237 from scratch for the new task.⁶³⁻⁶⁷ Alternatively, they can be pre-trained on natural images that
238 are more plentiful compared to medical images so that the weights in the feature extraction
239 layers are properly set during training (see Sec 3.B for more details). The weights only in the last
240 fully-connected layer or last few layers (including some of the convolutional layers) can then be
241 retrained using medical images to learn the class associations for the desired task.

242 1.C. Existing platforms and resources

243 A large number of training examples are required to estimate the large number of parameters of a
244 DL system. One needs to perform backpropagation throughout many iterations using stochastic
245 gradient descent over mini-batches consisting of a small subset of samples at any given time to
246 train hundreds of thousands to hundreds of millions or even billions of parameters. A single or
247 multi-core central processing unit (CPU) or a cluster of CPU nodes in a high-performance
248 computing (HPC) environment could be used for training, but the former approach would take an
249 extremely long amount of time while the latter requires access to costly infrastructure.

250 Fortunately, in the last ten years gaming GPUs have become cheaper, increasingly powerful, and
251 easier to program. This has resulted in simultaneously far cheaper hardware requirements for
252 running DL (compared to HPC solutions) and training times that are several orders of magnitude
253 shorter compared to a solution run on a CPU.^{27, 68} The most common setup for training DL
254 models is therefore to train networks on a desktop workstation containing one or more powerful
255 gaming GPUs that can be easily configured for a reasonable price. There are also several cloud-
256 based solutions including Amazon Web Services (AWS)⁶⁹ and Nvidia GPU cloud⁷⁰ that allow
257 users to train or deploy their models remotely. Recently, Google has developed Application-
258 Specific Integrated Circuit (ASIC) for neural networks to run its wide variety of applications that
259 utilize DL. These accelerators, referred to as Tensor Processing Units (TPUs), are several times
260 faster than CPU or GPU solutions and have recently been made available to general users via
261 Google Cloud.⁷¹

262 In line with the rapid improvements in performance of GPUs, several open-source DL libraries
263 have been developed and made public that free the user from directly programming GPUs. These
264 frameworks allow the users to focus on how to set up a particular network and explore different

265 training strategies. The most popular DL libraries are TensorFlow,⁷² Caffe,⁷³ Torch,⁷⁴ and
266 Theano.⁷⁵ They all have Application Programming Interfaces (APIs) in different programming
267 languages, with the most popular language being Python.

268 **1.D. Organization of the paper**

269 Throughout the paper, we strived to refer to published journal articles as much as we could.
270 However, DL is a very fast-changing field, and reports of many excellent and new studies either
271 appear as a conference proceeding paper only, or as a pre-print in online resources such as arxiv.
272 We did not refrain from citing articles from these resources whenever necessary. In sections
273 other than Section 2, to better summarize the state-of-the-art, we have included publications from
274 many different medical imaging, and natural imaging. However, to keep the length of the paper
275 reasonable, in Section 2, we focused only on applications in radiological imaging and radiation
276 therapy, although there are other areas in medical imaging that have seen influx of DL
277 applications, such as digital pathology and optical imaging. This paper is organized as follows:
278 In Section 2, we summarize applications of DL to radiological imaging and radiation therapy. In
279 Section 3, we describe some of the common themes among DL applications, which include
280 training and testing with small data set sizes, pretraining and fine tuning, combining DL with
281 radiomics applications, and different types of training, such as supervised, unsupervised and
282 weakly supervised. Since data set size is a major bottleneck for DL applications in medical
283 imaging, we have devoted Section 4 to special methods for data set expansion. In Section 5, we
284 summarize some of the perceived challenges, lessons learned, and possible trends for the future
285 of DL in medical imaging and radiation therapy.

286 2. APPLICATION AREAS IN RADIOLOGICAL IMAGING AND RADIATION

287 THERAPY

288 2.A. Image Segmentation

289 DL has been used to segment many different organs in different imaging modalities, including
290 single-view radiographic images, CT, MR, and ultrasound images.

291 Image segmentation in medical imaging based on DL generally uses two different input
292 methods: 1) patches of an input image, and 2) the entire image. Both methods generate an output
293 map that provides the likelihood that a given region is part of the object being segmented. While
294 patch-based segmentation methods were initially used, most recent studies use the entire input
295 image to give contextual information and reduce redundant calculations. Multiple works
296 subsequently refine these likelihood maps using classic segmentation methods, such as level
297 sets,⁷⁶⁻⁷⁹ graph cuts,⁸⁰ and model-based methods,^{81, 82} to achieve a more accurate segmentation
298 than using the likelihood maps alone. Popular deep-learning frameworks used for segmentation
299 tasks include Caffe, Matlab™ and cuda-convnet.

300 2.A.1. Organ and substructure segmentation

301 Segmentation of organs and their substructures may be used to calculate clinical parameters such
302 as volume, as well as to define the search region for computer-aided detection tasks to improve
303 their performance. Patch-based segmentation methods, with refinements using traditional
304 segmentation methods, have been shown to perform well for different segmentation tasks.^{76, 83}

305 Table **Error! Reference source not found.** briefly summarizes published performance of DL
306 methods in organ and substructure segmentation tasks using either Dice coefficient or Jaccard
307 index, if given, as the performance metric.

308 A popular network architecture for segmentation is the U-net.⁸⁴ It was originally developed for
309 segmentation of neuronal structures in electron microscope stacks. U-nets consist of several
310 convolution layers, followed by deconvolution layers, with connections between the opposing
311 convolution and deconvolution layers (skip connections), which allow for the network to analyze
312 the entire image during training, and allow for obtaining segmentation likelihood maps directly,
313 unlike the patch-based methods. Derivatives of U-net have been used for multiple tasks,
314 including segmenting breast and fibroglandular tissue⁸⁵ and craniomaxillofacial bony
315 structures.⁸⁶

316 Another DL structure that is being used for segmentation of organs is holistically nested
317 networks (HNN). HNN uses side-outputs of the convolutional layers, which are multi-scale and
318 multi-level, and produce a corresponding edge map at different scale levels. A weighted average
319 of the side-outputs is used to generate the final output, and the weights for the average are
320 learned during the training of the network. HNN has been successfully implemented in
321 segmentation of the prostate⁸⁷ and brain tumors.⁸⁸

322 2.A.2. Lesion segmentation

323 Lesion segmentation is a similar task to organ segmentation; however, lesion segmentation is
324 generally more difficult than organ segmentation, as the object being segmented can have
325 varying shapes and sizes. Multiple papers covering many different lesion types have been
326 published for DL lesion segmentation (Table **Error! Reference source not found.**). A common
327 task is the segmentation of brain tumors, which could be attributed to the availability of a public
328 database with dedicated training and test sets for use with the brain tumor segmentation
329 challenge held by the Medical Image Computing and Computer Assisted Intervention (MICCAI)

330 conference from 2014 to 2016, and continuing in 2017 and 2018. Methods evaluated on this data
331 set include patch-based auto-encoders,^{115, 116} U-net-based structures,¹¹⁷ as well as HNN.⁸⁸

332

333 **2.B. Detection**

334 2.B.1. **Organ detection**

335 Anatomical structure detection is a fundamental task in medical image analysis, which involves
336 computing the location information of organs and landmarks in 2D/3D image data. Localized
337 anatomical information can guide more advanced analysis of specific body parts or pathologies
338 present in the images, e.g. organ segmentation, lesion detection, and radio-therapy planning. In a
339 similar fashion to counterparts using traditional machine learning techniques, DL based organ /
340 landmark detection approaches can be mainly divided into two groups, i.e. classification based
341 methods and regression based ones. While classification based methods focus on discriminating
342 body parts / organs on the image or patch level, regression based methods target at recovering
343 more detailed location information, e.g., coordinates of landmarks. Table **Error! Reference**
344 **source not found.** illustrates a list of the DL based anatomical structure detection methods
345 together with their performance on different evaluation settings.

346 Early classification based approaches often utilized off-the-shelf CNN features to classify image
347 or image patches that contain anatomical structures. Yang et al.¹³⁵ adopted a CNN classifier to
348 locate 2D image patches (extracted from 3D MR volumes) that contain possible landmarks as an
349 initialization of the follow-up segmentation process for the femur bone. Chen et al.¹³⁶ adopted an
350 ImageNet pre-trained model and fine-tuned the model using fetal ultrasound frames from
351 recorded scan videos to classify the fetal abdominal standard plane images.

352 A variety of information in addition to original images could also be included to help the
353 detection task. For the same standard plane detection task in fetal ultrasound, Baumgartner et
354 al.¹³⁷ proposed a joint CNN framework to classify 12 standard scan planes and also localize the
355 fetal anatomy using a series of ultrasound fetal mid-pregnancy scans. The final bounding boxes
356 were generated based on the saliency maps computed as the visualization of network activation
357 for each plane class.

358 Improvements were also achieved by adapting the CNN network with more advanced
359 architecture and components. Kumar et al.¹³⁸ composed a two-path CNN network with features
360 computed from both original images and pre-generated saliency maps in each path. The final
361 standard plane classification was performed using SVM on a set of selected features.

362 Another category of methods tackle the anatomy detection problems with regression analysis
363 techniques. Ghesu et al.¹³⁹ formulated the 3D heart detection task as a regression problem,
364 targeting at the 3D bounding box coordinates and affine transform parameters in transesophageal
365 echocardiogram images. This approach integrated marginal space learning into the DL
366 framework and learned sparse sampling to reduce computational cost in the volumetric data
367 setting.¹⁴⁰

368 Yan et al.^{141, 142} formulated body part localization using DL. The system was developed using an
369 unsupervised learning method with two inter-sample CNN loss functions. The unsupervised
370 body part regression built a coordinate system for the body and output a continuous score for
371 each axial slice, representing the normalized position of the body part in the slice.

372 Besides the two common categories of methods discussed above, modern techniques (e.g.,
373 reinforcement learning) are also adopted to tackle the problem from a different direction. Ghesu

374 et al.¹⁴³ present a good example of combining reinforcement learning and DL in anatomical
375 detection task. With the application in multiple image data sets across a number of different
376 modalities, the method could search the optimal paths from a random starting point to the
377 predefined anatomical landmark via reinforcement learning with the help of effective
378 hierarchical features extracted via DCNN models. Furthermore, the system was further extended
379 to search 3D landmark positions with 3D volumetric CNN features.^{144, 145} Later on, Xu et al.¹⁴⁶
380 further extended this approach by turning the optimal action path searching problem into an
381 image partitioning problem, in which a global action map across the whole image was
382 constructed and learned by a DCNN network to guide the searching action.

383

384 2.B.2. **Lesion detection**

385 Detection of abnormalities (including tumors and other suspicious growths) in medical images is
386 a common but costly and time-consuming part of the daily routine of physicians, especially
387 radiologists and pathologists. Given that the location is often not known a priori, the physician
388 should search across the 2D image or 3D volume to find deviations compared to surrounding
389 tissue and then to determine whether that deviation constitutes an abnormality that requires
390 follow-up procedures or something that can be dismissed from further investigation. This is often
391 a difficult task that can lead to errors in many situations either due to the vast amount of data that
392 needs to be searched to find the abnormality (e.g. in the case of volumetric data or whole-slide
393 images) or because of the visual similarity of the abnormal tissue with normal tissue (e.g. in the
394 case of low-contrast lesions in mammography). Automated computer detection algorithms have
395 therefore been of great interest in the research community for many years due to their potential
396 for reducing reading costs, shortening reading times and thereby streamlining the clinical

397 workflow, and providing quality care for those living in remote areas who have limited access to
398 specialists.

399 Traditional lesion detection systems often consist of long processing pipelines with many
400 different steps.^{158, 159} Some of the typical steps include pre-processing the input data e.g. by
401 rescaling the pixel values or removing irrelevant parts of the image, identification of locations in
402 the image that are similar to the object of interest according to rule-based methods, extraction of
403 hand-crafted features, and classification of the candidate locations using a classifier such as SVM
404 or RF. In comparison, DL approaches for lesion detection are able to avoid the time-consuming
405 pipeline design approach. Table 4 presents a list of studies that used DL for lesion detection,
406 along with some details about the DL architecture.

407 Many of the papers focused on detection tasks use transfer learning with architectures from
408 computer vision.¹⁶⁰ Examples of this approach can be found in many publications, including
409 those for lesion detection in breast ultrasound,¹⁶¹ for detection of bowel obstructions in
410 radiography,¹⁶² and for detection of the third lumbar vertebra slice in a CT scan.¹⁶³ Usage of
411 CNNs in lesion detection is not limited to architectures taken directly from computer vision, but
412 also includes some applications where custom architectures are used.¹⁶⁴⁻¹⁶⁷

413 Most of the early applications used 2D CNNs, even if the data was 3D. Due to prior experience
414 with 2D architectures, limitations in the amount of available memory of GPUs, and higher
415 number of samples needed for training the larger number of parameters in a 3D architecture,
416 many DL systems used multi-view 2D CNNs for analysis of CT and MRI data sets in what is
417 referred to as 2.5D analysis. In these methods, orthogonal views of a lesion or multiple views at
418 different angles through the lesion were used to train an ensemble of 2D CNNs whose scores

419 would be merged together to obtain the final classification score.^{166, 168} More recently, 3D CNNs
420 that use three-dimensional convolution kernels are successfully replacing 2D CNNs for
421 volumetric data. A common approach to deal with the small number of available cases is to train
422 the 3D CNNs on 3D patches extracted from each case. This way, each case can be used to extract
423 hundreds or thousands of 3D patches. Combined with various data augmentation methods, it is
424 possible to generate sufficient number of samples to train 3D CNNs. Examples of using 3D
425 patches can be found for detection of pulmonary nodules in chest CT,¹⁶⁹ and for detection of
426 lacunar strokes in brain MRI.¹⁷⁰ Due to the large size of volumetric data, it would be very
427 inefficient to apply the CNN in a sliding window fashion across the entire volume. Instead, once
428 the model is trained on patches the entire network can be converted into a fully convolutional
429 network¹⁷¹ so that the whole network acts as a convolution kernel that can be efficiently applied
430 to an input of arbitrary size. Since convolution operations are highly optimized, this results in
431 fast processing of the entire volume when using a 3D CNN on volumetric data.¹⁷²

432

433 **2.C. Characterization**

434 Over the past decades, characterization of diseases has been attempted with machine learning
435 leading to computer-aided diagnosis (CADx) systems. Radiomics, the –omics of images, is an
436 expansion of CADx to other tasks such as prognosis and cancer sub-typing. Radiomic features
437 can be described as (a) “hand-crafted”/“engineered”/“intuitive” features or (b) deep-learned
438 features. Characterization of disease types will depend on the specific disease types and the
439 clinical question. With hand-crafted radiomic features, the features are devised based on imaging
440 characteristics typically used by radiologists in their interpretation of a medical image. Such
441 features might include tumor size, shape, texture, and/or kinetics (for dynamic contrast-enhanced

442 imaging). Various review papers have already been written about these hand-crafted radiomic
443 features that are merged with classifiers to output estimates of, for example, the likelihood of
444 malignancy, tumor aggressiveness, or risk of developing cancer in the future.^{158, 159}

445 DL characterization methods, on the other hand, may take as input a region of the image around
446 the potential disease site, such as a region of interest (ROI) around a suspect lesion. How that
447 ROI is determined will likely affect the training and performance of the DL. Thinking of how a
448 radiologist is trained during residency will lend understanding of how a DL system needs to be
449 trained. For example, an ROI that is cropped tightly around a tumor will provide different
450 information to a DL system than an ROI that is much larger than the encompassing tumor since
451 with the latter more anatomical background is also included in the ROI.

452 More and more DL imaging papers are published each year but there are still only a few methods
453 that are able to characterized among the vast range of radiological presentations across subtle
454 disease states. Table 5 presents a list of published DL characterization studies in radiological
455 imaging.

456

457 2.C.1. **Lesion characterization**

458 When it comes to computer algorithms and specific radiological interpretation tasks, there is no
459 one-size-fits-all for either conventional radiomic machine learning methods or DL approaches.
460 Each computerized image analysis method requires customizations specific to the task as well as
461 the imaging modality.

462 Lesion characterization is mainly being conducted using conventional CAD/radiomics computer
463 algorithms, especially when the need is to characterize (i.e., describe) a lesion rather than

464 conduct further machine learning for disease assessment. For example, characterization of lung
465 nodules as well as characterization of the change in lung nodules over time, are used to track the
466 growth of lung nodules in order to eliminate false positive diagnoses of lung cancer.

467 Other examples involving computer characterization of tumors occurs in research in imaging-
468 genomics. Here, radiomic features of tumors are used as image-based phenotypes for correlative
469 and association analysis with genomics as well as histopathology. A well-documented, multi-
470 institutional collaboration on such was conducted through the TCGA/TCIA Breast Phenotype
471 Group.²²⁰⁻²²⁴

472 Use of DL methods as feature extractors can lend itself to tumor characterization; however, the
473 extracted descriptors (e.g., CNN-based features) are not intuitive. Similar to ‘conventional’
474 methods that use hand-crafted features, DL-extracted features could characterize a tumor relative
475 to some known trait – such as receptor status – during supervised training, and that subsequent
476 output could be used in imaging-genomics discovery studies.

477 Additional preprocessing and data use methods can further improve characterization such as in
478 the past use of unlabeled data with conventional features to enhance the machine learning
479 training.^{225, 226} Here, the overall system can learn aspects of the data structure without knowledge
480 of the disease state, leaving the labeled information for the final classification step.

481 2.C.2. **Tissue characterization**

482 Tissue characterization is sought when specific tumor regions are not relevant. Here we focus on
483 analysis of non-diseased tissue to predict a future disease state (such as texture analysis on
484 mammograms in order to assess the parenchyma with the goal to predict breast cancer risk¹⁵⁹)

485 and characterization of tissue that includes diffuse disease, such as in various types of interstitial
486 lung disease and liver disease.^{227, 228}

487 In breast cancer risk assessment, computer-extracted characteristics of breast density and/or
488 breast parenchymal patterns are computed and related to breast cancer risk factors. Using
489 radiomic texture analysis, Li et al. have found that women at high risk for breast cancer have
490 dense breasts with parenchymal patterns that are coarse and low in contrast.²²⁹ DL is now being
491 used to assess breast density.^{194, 195} In addition, parenchymal characterization is being conducted
492 using DL, in which the parenchymal patterns are related through the CNN architecture to groups
493 of women using surrogate markers of risk. One example is shown by Li et al. assessing the
494 performance of DL in the distinction between women at normal risk of breast cancer and those at
495 high risk based on their BRCA1/2 status.¹⁹²

496 Lung tissue has been analyzed with conventional texture analysis and DL for a variety of
497 diseases. Here, characterization of the lung pattern lends itself to DL as patches of the lung may
498 be informative of the underlying disease, commonly interpreted by the radiologist's eye-brain
499 system. Various investigators have developed CNNs, including those to classify interstitial lung
500 diseases characterized by inflammation of the lung tissue.²⁰⁷⁻²⁰⁹ These disease characterizations
501 can include healthy tissue, ground glass opacity, micronodules, consolidation, reticulation, and
502 honeycombing patterns.¹⁷⁹

503 Assessing liver tissue lends itself to DCNNs in the task of staging liver fibrosis on MRI by
504 Yasaka et al.²¹⁶ and ultrasonic fatty liver disease characterization by Bharath et al.²¹⁷

505 2.C.3. **Diagnosis**

506 Computer-Aided Diagnosis (CADx) involves the characterization of a region or tumor, initially
507 indicated by either a radiologist or a computer, after which the computer characterizes the
508 suspicious region or lesion and/or estimates the likelihood of being diseased (e.g., cancerous) or
509 non-diseased (e.g., non-cancerous), leaving the patient management to the physician.^{158, 159} Note
510 that CADx is not a localization task but rather a characterization/classification task. The subtle
511 difference between this section and the preceding two sections, is that here the output of the
512 machine learning system is related to the likelihood of disease and not just a characteristic
513 feature of the disease presentation.

514 Many review papers have been written over the past two decades on CADx, radiomic features,
515 and machine learning,^{158, 159} and thus details will not be presented in this paper.

516 An active area of DL is CADx of breast cancer. Training CNNs “from scratch” is often not
517 possible for CAD and other medical image interpretation tasks, and thus methods to use CNNs
518 trained on other data (transfer learning) are considered. Given the initial limited data sets and
519 variations in tumor presentations, investigators explored the use of transfer learning to extract
520 tumor characteristics using CNNs trained on nonmedical tasks. The outputs from layers can be
521 considered as characteristic features of the lesion and serve as input to classifiers, such as linear
522 discriminant analysis and support vector machines. Fig. 3a shows an example in which AlexNet
523 is used as a feature extractor for an SVM, and Fig. 3b shows the performance of the SVM based
524 on features from each layer of AlexNet.

525 Researchers have found that performance of the conventional radiomics CADx and that of the
526 CNN-based CADx yielded similar levels of diagnostic performance in the task of distinguishing
527 between malignant and benign breast lesions, and thus when combined, via a deep feature fusion

528 methodology, gave a statistically significant level of performance.^{196, 197} Fig. 4 shows one
529 possible method for combining CNN-extracted and conventional radiomics features.

530
531 In an effort to augment, under limited data set constraints, CNN performance with dynamic
532 contrast-enhanced MRI, investigators have looked to vary the image types input to the CNN. For
533 example, instead of replicating a single image region to the three RGB channels of VGG19Net,
534 investigators have used the temporal images obtained from DCE-MRI, inputting the pre-contrast,
535 the first post-contrast, and the second post-contrast MR images to the RGB channels,
536 respectively. In addition, to exploit the 4D nature of DCE-MRI (3D and temporal), Antropova et
537 al. have input MIP (maximum intensity projections) images to the CNN.²⁰⁰ Incorporation of
538 temporal information into the DL efforts has resulted in the use of recurrent neural network, such
539 as a long short-term memory (LSTM) recurrent networks.^{201, 230}

540 Instead of using transfer learning for feature extraction, investigators have used transfer learning
541 for fine tuning by either (i) freezing the earlier layers of a pre-trained CNN and training the later
542 layers, i.e., fine tuning or (ii) training on one modality, such as digitized screen/film
543 mammography (dSFM), for use on a related modality, such as full-field digital mammography
544 (FFDM). The latter has been shown by Samala et al.¹⁹⁹ to be useful in the training of CNN-based
545 CADx for lesion diagnosis on FFDMs.

546 Investigations on DL for CADx are continuing across other cancers, e.g., lung cancer, and other
547 disease types, and similar methods can be used.²⁰⁴⁻²¹⁹ The comparison to more conventional
548 radiomics-based CADx is also demonstrated further, which is potentially useful for both
549 understanding the CNN outputs as well as for providing additional decision support.

550 2.C.4. Prognosis and staging

551 Once a cancer is identified, further workup through biopsies gives information on stage,
552 molecular subtype, and/or genomics to yield information on prognosis and potential treatment
553 options. Cancers are spatially heterogeneous, and therefore, investigators are interested whether
554 imaging can provide information on that spatial variation. Currently, many imaging biomarkers
555 of cancerous tumors include only size and simple enhancement measures (if dynamic imaging is
556 employed) and, thus, there is interest in expanding, through radiomic features, the knowledge
557 that can be obtained from images. Various investigators have used radiomics and machine
558 learning in assessing the stage and prognosis of cancerous tumors.^{220, 231} Now, those analyses are
559 being investigated further with DL. It is important to note that when using DL to assess
560 prognosis, one can analyze the tumor from medical imaging, such as MRI or ultrasound, or from
561 pathological images. Also, in the evaluation, one needs to determine the appropriate comparison
562 – a radiologist, a pathologist, or some other histopathological/genomics test.

563 The goal is to better understand the imaging presentation of cancer, i.e., to obtain prognostic
564 biomarkers from image-based phenotypes, including size, shape, margin morphology,
565 enhancement texture, kinetics, and variance kinetic phenotypes. For example, enhancement
566 texture phenotypes can characterize the tumor texture pattern of contrast-enhanced tumors on
567 DCE-MRI through analysis the first post-contrast images, and thus quantitatively characterize the
568 heterogeneous nature of contrast uptake within the breast tumor.²²⁰ Here, the larger the
569 enhancement texture entropy, the more heterogeneous is the vascular uptake pattern within the
570 tumor, which potentially reflects the heterogeneous nature of angiogenesis and treatment
571 susceptibility, and serves as a location-specific “virtual digital biopsy”. Understanding the
572 relationships between image-based phenotypes and the corresponding biopsy information could

573 potentially lead to discoveries useful for assessing images obtained during screening as well as
574 during treatment follow-up, i.e., when an actual biopsy is not practical.

575 Shi et al.²⁰³ demonstrated the prediction of prognostic markers using DL on mammography in
576 distinguishing between DCIS with occult invasion from pure DCIS. Staging on thoracic CTs is
577 being investigated by Masood et al. through DL by relating CNN output to metastasis
578 information for pulmonary nodules.²¹⁰ In addition, Gonzalez et al. evaluated DL on thoracic CTs
579 in the detection and staging of chronic obstructive pulmonary disease (COPD) and acute
580 respiratory disease (ARD).²¹¹ While use of DL in the evaluation of thoracic CTs is promising,
581 more development is needed to reach clinical applicability.

582 2.C.5. Quantification

583 Use of DL in quantification requires a CNN output that correlates significantly with a known
584 quantitative medical measurement. For example, DL has been used in automatic calcium scoring
585 in low-dose CTs by Lessmann et al.²¹² and in cardiac left ventricle quantification by Xue et al.²¹³
586 Similar to cancer workup, in cardiovascular imaging, use of DL is expected to augment clinical
587 assessment of cardiac defect/function or uncover new clinical insights.²³² Larson et al. turned to
588 DL to assess skeletal maturity on pediatric hand radiographs with performance levels rivaling
589 that of an expert radiologist.²¹⁹ DL has been used to predict growth rates for pancreatic
590 neuroendocrine tumors²³³ on PET-CT scans.

591 2.D. Processing and reconstruction

592 In the previous parts of this section, we focused on applications in which image pixels or ROIs
593 are classified into multiple classes (e.g., segmentation, lesion detection and characterization), the
594 subject is classified into multiple classes (e.g., prognosis, staging), or a feature in the image (or

595 the ROI) is quantified. In this part, we focus on applications in which the output of the machine
596 learning algorithm is also an image (or a transformation) that potentially has a quantifiable
597 advantage over no processing or traditional processing methods.

598

599 2.D.1. **Filtering, noise/artifact reduction, and reconstruction**

600 Filtering: Going back to the early days of application of CNNs to medical images, one can find
601 examples of CNNs that produced output images for further processing. Zhang et al.⁵² trained a
602 shift-invariant ANN that aimed at having a high or low pixel value in an output image depending
603 on whether the pixel was determined to be the center of a microcalcification by an expert
604 mammographer. Suzuki et al.²³⁴ trained an MTANN as a supervised filter for the enhancement
605 lung nodules on thoracic CT scans. More recently, Yang et al.²³⁵ used a cascade of CNNs for
606 bone suppression in chest radiography. Using ground-truth images extracted from dual-energy
607 subtraction chest X-rays, the authors trained a set of multi-scale networks to predict bone
608 gradients at different scales and fuse these results to obtain a bone image from a standard chest
609 x-ray. Another advantage of CNNs for image filtering is speed: Mori²³⁶ investigated several
610 types of residual convolutional autoencoders and residual CNNs for contrast-limited adaptive
611 histogram equalization filtering and denoising of X-ray fluoroscopic imaging during treatment,
612 without specialized hardware.

613 Noise reduction: The past couple of years have seen a proliferation of applications of DL to
614 improve the noise quality of reconstruction medical images. One application area is low-dose
615 image reconstruction. This is important in modalities with ionizing radiation such as CT or PET
616 for limiting patient dose,^{237-239, 241} or for limiting damage to samples in synchrotron-based X-ray

617 CT.²⁴⁰ Chen et al.²³⁷ designed a DL algorithm for noise reduction in reconstructed CT images.
618 They used the mean-squared pixelwise error between the ideal image and the denoised image as
619 the loss function, and synthesized noisy projections based on patient images to generate training
620 data.²³⁸ They later combined a residual autoencoder with a CNN in an architecture called the
621 RED-CNN²³⁸, which has a stack of encoders and a symmetrical stack of decoders that are
622 connected with shortcuts for the matching layers. Kang et al.²³⁹ applied a DCNN to the wavelet
623 transform coefficients of low-dose CT images, and similar to the work of Chen et al.²³⁸, used a
624 residual learning architecture for faster network training and better performance. Their method
625 won the second-best place at the 2016 “Low-Dose CT Grand Challenge.”²⁶⁶ Xiang et al used low-
626 dose PET images combined with T1-weighted images acquired on a PET/MRI scanner to obtain
627 standard acquisition quality PET images. In comparison to the papers above that started
628 denoising with reconstructed images, Yang et al. aimed at improving the quality of recorded
629 projections. They used a CNN-based approach for learning the mapping between a number of
630 pairs of low- and high-dose projections. After training with a limited number of high-dose
631 training examples, they used the trained network to predict high-dose projections from low-dose
632 projections, and then used the predicted projections for reconstruction.

633 Artifact reduction: Techniques similar to those described for denoising have been applied to
634 artifact reduction. Jin et al.²⁴² described a general framework for the utilization of CNNs for
635 inverse problems, applied the framework to reduce streaking artifacts in sparse-view
636 reconstruction on parallel beam CT, and compared their approach to filtered-backprojection
637 (FBP) and total variation (TV) techniques. Han et al.²⁴⁴ used DL to reduce streak artifacts
638 resulting from limited number of radial lines in radial k-space sampling in MRI. Zhang et al.²⁴³
639 used a CNN-based approach to reduce metal artifacts on CT images. They combined the original

640 uncorrected image with images corrected with the linear interpolation and beam hardening
641 correction methods to obtain a three-channel input. This input was fed into a CNN, whose output
642 was further processed to obtain “replacement” projections for the metal-affected projections.

643 Reconstruction: Several studies indicated that DL may be useful in directly attacking the image
644 reconstruction problem. In one of the early publications in this area, Golkov et al.²⁴⁵ applied a
645 deep-learning approach to diffusion-weighted MR images (DWI) to derive rotationally invariant
646 scalar measures for each pixel. Hammernik et al.²⁴⁶ designed a variational network to learn a
647 complete reconstruction procedure for multi-channel MR data, including all free parameters
648 which would otherwise have to be set empirically. To obtain a reconstruction, the undersampled
649 k-space data, coil sensitivity maps and the zero-filling solution are fed into the network.

650 Schlemper et al.²⁴⁷ evaluated the applicability of CNNs for reconstructing undersampled
651 dynamic cardiac MR data.. Zhu et al.²⁴⁸ introduced an automated transform by manifold
652 approximation approach to replace the conventional image reconstruction with a unified image
653 reconstruction framework that learns the reconstruction relationship between sensor and image
654 domain without expert knowledge. They showed examples in which their approach resulted in
655 superior immunity to noise and a reduction in reconstruction artifacts compared with
656 conventional reconstruction methods.

657 2.D.2. **Image registration**

658 To establish accurate anatomical correspondences between two medical images, both hand-
659 crafted features and features selected based on a supervised method are frequently employed in
660 deformable image registration. However, both types of features have drawbacks.²⁴⁹ Wu et al.²⁴⁹
661 designed an unsupervised DL approach to directly learn the basis filters that can effectively
662 represent all observed image patches, and used the coefficients by these filters for

663 correspondence detection during image registration. They subsequently further refined the
664 registration performance by using a more advanced convolutional stacked autoencoder, and
665 comprehensively evaluated the registration results with respect to current state-of-the-art
666 deformable registration methods.²⁵⁰ A deep encoder-decoder network was used for predictions
667 for the large deformation diffeomorphic metric mapping model by Yang et al.²⁵¹ for fast
668 deformable image registration. In a feasibility study, Lv et al.²⁵² trained a CNN for respiratory
669 motion correction for free-breathing 3D abdominal MRI. For the problem of 2D/3D registration,
670 Miao et al.²⁵³ used a supervised CNN regression approach to find a rigid transformation from the
671 object coordinate system to the x-ray imaging coordinate system. The CNNs were trained using
672 synthetic data only. The authors compared their method with for intensity-based 2-D/3-D
673 registration methods and a linear regression- based method, and showed that their approach
674 achieved higher robustness and larger capture range, as well as higher computational efficiency.
675 A later study by the same research group identified a performance gap when the model trained
676 with synthetic data is tested on clinical data.²⁵⁴ To narrow the gap, the authors proposed a
677 domain adaptation method by learning domain invariant features with only a few paired real and
678 synthetic data.

679 2.D.3. **Synthesis of one modality from another**

680 A number of studies have recently investigated using DL to generate synthetic CT (sCT) images
681 from MRI. This is important for at least two applications: First, for accurate PET image
682 reconstruction and uptake quantification, tissue attenuation coefficients can be readily estimated
683 from CT images. Thus, estimation of sCT from MRI in PET/MRI imaging is desirable. Second,
684 there is an interest in replacing CT with MRI in the treatment planning process mainly because
685 MRI is free of ionizing radiation. Nie et al.²⁵⁵ used a 3D CNN to learn an end-to-end nonlinear

686 mapping from an MR image to a CT image. The same research group in their later research
687 added a context-aware GAN for improved results.²⁵⁹ Han et al.²⁵⁶ adopted and modified the U-
688 net architecture for sCT generation from MRI. Current commercially available MR attenuation
689 correction (MRAC) methods for body PET imaging use a fat/water map derived from a two-echo
690 Dixon MRI sequence. Leynes et al.²⁵⁷ used multi-parametric MRI consisting of Dixon MRI and
691 proton-density-weighted zero (ZTE) echo-time MRI to generate sCT images with the use of a
692 DL model that also adopted the U-net architecture.²⁶⁷ Liu et al.²⁵⁸ trained a deep network (deep
693 MRAC) to generate sCT from T1-weighted MRI, and compared deep MRAC with Dixon
694 MRAC. Their results showed that significantly lower PET reconstruction errors were realized
695 with deep MRAC. Choi et al.²⁶⁰ investigated a different type of synthetic image generation. They
696 noted that although PET combined with MRI is useful for precise quantitative analysis, not all
697 subjects have both PET and MR images in the clinical setting, and used a GAN-based method to
698 generate realistic structural MR images from amyloid PET images. Ben-Cohen et al.²⁶¹ aimed at
699 developing a system that can generate PET images from CT, to be used in applications such as
700 evaluation of drug therapies and detection of malignant tumors that require PET imaging, and
701 found that a conditional GAN is able to create realistic looking PET images from CT.

702 2.D.4. **Quality assessment**

703 In addition to traditional characterization tasks in medical imaging, such as classification of ROIs
704 as normal or abnormal, DL has been applied to image quality assessment. Wu et al.²⁶² proposed a
705 DCNN for computerized fetal US image quality assessment to assist the implementation of US
706 image quality control in the clinical obstetric examination. The proposed system has two
707 components: The L-CNN that locates the ROI of the fetal abdominal region in the US image, and
708 the C-CNN evaluates the image quality by assessing the goodness of depiction for the key

709 structures of stomach bubble and umbilical vein. Neylon et al.²⁶³ used a deep neural network as
710 an alternative to image similarity metrics to quantify deformable image registration performance.

711 Since the image quality strongly depends on both the characteristics of the patient as well as the
712 imager, both of which are highly variable, using simplistic parameters like noise to determine the
713 quality threshold is challenging. Lee et al.²⁶⁴ showed that DL using fine-tuning of a pre-trained
714 VGG19 CNN was able to predict whether CT scans meet the minimal image quality threshold
715 for diagnosis, as deemed by a chest radiologist.

716 Esses et al.²⁶⁵ used a DCNN for automated task-based image quality evaluation of T2-weighted
717 liver MRI acquisition, and compared this automated approach to image quality evaluation by two
718 radiologists. Both the CNN and the readers classified a set of test images as diagnostic or non-
719 diagnostic. The concordance between the CNN and reader 1 was 0.79, that between the CNN and
720 reader 2 was 0.73, and that between the two readers was 0.88. The relatively lower concordance
721 of the CNN with the readers was mostly due to cases that the readers agreed to be diagnostic, but
722 the CNN did not agree with readers. The authors concluded that although the accuracy of the
723 algorithm needs to be improved, the algorithm could be utilized to flag cases as low-quality
724 images for technologist review.

725 **2.E. Tasks involving imaging and treatment**

726 Radiotherapy and assessment of response to treatment are not areas that are traditionally
727 addressed using neural networks or data-driven approaches. However, these areas have recently
728 seen a strong increase in the application of deep learning techniques. Table 7 summarizes
729 studies in this fast-developing DL application area.

730

731 2.E.1. **Discovery: Imaging-genomics (Radiogenomics)**

732 A major need in breast cancer research is the elucidation of the relationship between the
733 macroscopic image-based presentation of the tumor and its environment and cancer biology
734 indicators of risk, diagnosis, prognosis, or treatment response. Imaging-genomics, i.e.,
735 “radiogenomics”, aims to find these relationships between imaging data and clinical data,
736 molecular data, genomic data, and outcome data.^{222, 224} Of interest is whether DL can provide
737 sufficient detailed information to relate to genetic data as have hand-crafted radiomic
738 phenotypes.²⁸⁵

739 2.E.2. **Radiotherapy**

740 The goals of DL in radiation oncology are to assist in treatment planning, assess response to
741 therapy, and provide automated adaptation in treatments over time. Deep reinforcement learning
742 using both prior treatment plans and methods for assessing tumor local control were used to
743 automatically estimate dose protocols.²⁷⁸ Such adaptive radiotherapy methods may provide
744 clinical decision support for dose adaptation.

745 Much of the needs in treatment planning relate to the segmentation of organs (discussed earlier)
746 and in the prediction of dose distributions from contours. Nguyen et al.²⁸⁰ used a U-net to predict
747 dose from patient image contours on prostate intensity-modulated radiation therapy (IMRT)
748 patients, and demonstrated desired radiation dose distributions. Foote et al.²⁷⁹ combined a DCNN
749 with motion tracking to recover anatomical positions from a single projection radiographic image
750 in real time in order to achieve dynamic tracking of a lung tumor volume.

751 As discussed earlier, DL can be used to convert between modalities (Section 2.D.3), which can
752 benefit both diagnosis and therapy. Maspero et al.²⁸² have developed a DL method for creating

753 synthetic CTs from MR-only radiotherapy, leading to online adaptive replanning. Such methods,
754 in order to allow for real time changes, need to rapidly generate synthetic CTs, thus modeling the
755 radiation attenuation and dose calculations.

756 While DL methods are being developed to plan and predict radiation therapy to specific tumor
757 sites, they are also being investigated to assess toxicity to normal organs and tissue. Zhen et al.²⁸³
758 used a transfer learning strategy to predict rectum dose toxicity for cervical cancer radiotherapy.

759 Segmentation methods to aid in the assessment of treatment plans have been developed as well;
760 Tong et al. developed a CNN-based method for multi-organ segmentation for use in head and
761 neck cancer radiotherapy²⁷⁴, Men et al developed a target tumor volume segmentation for rectal
762 cancer²⁷² and breast cancer,²⁸⁶ while Jackson et al. focused on renal segmentation for automated
763 radiation dose estimation.²⁷⁵ Dose estimation was also the aim of Kajikawa et al. who
764 investigated the feasibility of DL in the automated determination of dosimetric eligibility of
765 prostate cancer patients undergoing intensity modulated radiation therapy.²⁸¹

766 Just as with imaging-genomics, as discussed earlier, incorporation of both image-based
767 phenotypes and genomics in treatment planning and response assessment may yield new
768 relationships and improved therapeutics.²⁷³

769 Overall, however, use of DL in radiation planning is still at a very early stage in development.

770 2.E.3. **Response to treatment**

771 Just as DL is used to extract tumor characteristics for diagnosis and prognosis, it can also be used
772 in decision making for assessing response to therapy. In machine learning, various classifiers can
773 be used to merge the tumor image-based phenotypes into a response prediction. Thus, DL can
774 also be used to analyze medical image(s) over time to predict response. For example, CNNs were

775 used with breast DCE-MRI to assess response to neoadjuvant chemotherapy, where the inputs
776 varied over contrast time points as well as treatment exam times.²⁷⁰

777 Cha et al.²⁶⁸ have explored the feasibility of DL through CNNs on pre- and post-treatment CT of
778 bladder cancer patients to assist in assessment of treatment response. In addition, assessing
779 prognosis of a tumor contributes to decision making on treatment options and predicting
780 survival. Lao et al.²¹⁸ investigated MRI radiomic features and DL as a means to predict survival
781 in glioblastoma multiforme. Bibault et al. used DL to predict pathologic complete response after
782 chemoradiation in locally advanced rectal cancer,²⁸⁴ while Ibramov et al. predicted hepatobiliary
783 toxicity after liver stereotactic body radiotherapy.²⁷⁷ In research unrelated to oncology the
784 interest in using DL to assess response to treatment has increased as well. Shehata et al.²⁷⁶ used
785 autoencoders for early detection/prediction of acute renal rejection after kidney transplant.
786 Nielsen et al. used DL to predict outcome and to assess the effect of treatment with recombinant
787 tissue-type plasminogen activator in ischemic stroke patients.²⁶⁹

788 3. COMMON THEMES

789 3.A. Training and testing with size-limited data sets

790 The rapid and immense success of DCNNs in many challenging computer vision problems is
791 achieved through accessibility to large-scale well-annotated data sets, e.g., PASCAL VOC,²⁸⁷
792 ImageNet²⁸ and MS COCO.²⁸⁸ ImageNet pre-trained DCNN models^{29, 73} serve as the foundation
793 in many higher level tasks, e.g. image captioning,²⁸⁹ visual question answering,²⁹⁰ and instance
794 relationship extraction.²⁹¹ Compared to natural image data sets, existing medical image data sets
795 are typically smaller in size. This is because the collection of medical image data sets is often a
796 challenging, time consuming process, which involves multiple steps, such as searching in large

797 hospital PACS systems with moderately structured clinical information, selection of a relatively
798 small number of useful clinical cases, and further data annotation by expert physicians. In this
799 sub-section, we explore some of the challenges for applying DL on relatively small data sets.
800 The concepts and principles discussed below, such as overfitting, the need for independent
801 training and test data sets, and dependence of performance on training data set size, apply to
802 most machine learning algorithms, including traditional (shallow) neural networks. However,
803 some aspects may be exacerbated due to the large number of tunable parameters in DL networks.

804 **Overfitting:** It has long been recognized that training a complex classifier with a small data set
805 invites the risk of overfitting (also termed overtraining). According to the Oxford English
806 dictionary overfitting is “the production of an analysis that corresponds too closely or exactly to
807 a particular set of data, and may therefore fail to fit additional data or predict future observations
808 reliably”. In other words, overfitting occurs when a classifier models the training data too well,
809 resulting in it failing to generalize and performing poorly on new unseen data. John von
810 Neumann famously said ‘With four parameters I can fit an elephant, and with five I can make
811 him wiggle his trunk’.²⁹² Both shallow neural networks and DL exhibit overtraining.

812 Surprisingly, compared to the huge number of tunable parameters in DL networks, they may
813 exhibit a more limited amount of overfitting compared to a shallow network designed to achieve
814 the same functionality. One possible explanation for this, as discussed in the introduction, is that
815 DL learns a hierarchical representation that matches the composition of the individual
816 components that the data consists of.²⁹³ Another possible explanation, using concepts from
817 information theory, contends that a deep networks helps better compress the irrelevant
818 information in the input data and thus can achieve better generalization.²⁹⁴

819 A number of ways have been suggested in the literature to reduce overfitting, including
820 regularization,²⁹⁵ early stopping,²⁹⁶ and drop-out.^{11, 26} Regularization involves the addition of an
821 extra term to the loss function during training akin to the use of a Lagrange multiplier to satisfy
822 certain boundary conditions. The regularization term is typically chosen to penalize overly
823 complex solutions and for example imposes rules for the smoothness of the solution. Early
824 stopping can be seen as regularization in time. The longer a network is trained, the more complex
825 its solutions become, so by regularizing on time (through early stopping) the complexity will be
826 reduced and generalizability improved. When to stop training is usually determined by
827 monitoring the loss on a validation set (see next paragraph). Dropout is another very efficient
828 way to prevent overfitting and the term "dropout" refers to dropping out units in a neural
829 network.

830 Training, validation and testing: Ideally, one has access to three large independent data sets to
831 serve as training, validation, and test set for the training and evaluation of any machine learning
832 approach. Although the terms 'validation set' and 'test set' may not be defined consistently
833 among all communities, here we use the term 'validation set' for the set used for fine-tuning as
834 part of training and 'test set' for the set used for final performance evaluation. Fig. 5 shows how
835 the training, validation, and test sets can be used in a supervised machine learning system in an
836 ideal scenario with a large number of available cases. However, when the total number of
837 available cases is small, such a scenario may be inadequate to make full use of the limited-size
838 data set. For example, if a total of a hundred cases is available, then it may not be reasonable to
839 randomly assign 20% as a test set and divide the remaining 80 cases into training and validation.
840 The statistical variability of the classification performance for 20 cases will typically be large,
841 limiting the usefulness of the reported performance. Instead, it may be clinically more useful to

842 use a cross-validation approach (with multiple training/validation and testing data splits) for
843 obtaining a more realistic performance estimate. Using a cross-validation training/validation and
844 testing approach is a way to obtain a realistic performance estimate for the entire data set when
845 done correctly but does not result in a single model. Care must be taken to perform all training
846 and validation steps only within the training fold of the cross-validation, so that there is no
847 leakage of information from the different folds into each other that might bias the cross-
848 validation performance estimate. In Section 4, methods to help overcome problems related to
849 training DL on a small data set are discussed, but one should keep in mind that these methods do
850 not overcome the most important limitation of having a small data set, i.e., that the small sample
851 may not accurately represent the population of interest.

852 Dependence of test performance on training set size: A number of studies in the literature have
853 investigated the effect of training size on the performance of the machine learning system.²⁹⁷⁻³⁰¹
854 The general trend is that as the number of training cases increases, overtraining decreases and the
855 performance on the targeted population improves. There is also a number beyond which
856 increasing the training set size only marginally improves the test performance. However, this
857 number is believed to be a function of the machine learning system architecture, the task, and the
858 system inputs. A few papers studied the effect of varying the training set size on the performance
859 of their DL network.^{16, 63, 193, 302, 303} Mohamed et al.¹⁹³ found that for breast density classification,
860 there is a small increase in test performance (the area under the receiver operating characteristic
861 curve increases from 0.95 to 0.99, $p < 0.001$) when their training set size increased from 2000
862 images to 6000 images. Azizi et al.¹⁶ also found that increasing the training data set increased the
863 performance of a DL model used for prostate cancer detection in ultrasound Gulshan et al.⁶³
864 showed that for their detection algorithm of diabetic retinopathy in retinal fundus photographs,

865 the relative specificity at a given sensitivity on their validation set consistently increased as the
866 number of training samples increased from around 200 samples to around 60,000 samples, at
867 which point the performance plateaued. Using natural images data sets, where the available
868 labeled data are much more abundant compared to medical images, Sun et al.³⁰³ demonstrated
869 that the test performance of the DL network continued to increase when going from 10 million
870 training samples up to 300 million training samples for both object detection and semantic
871 segmentation tasks. While it is difficult to obtain data sets of annotated medical images similar in
872 size to data sets for natural images, the trend that increasing the training data set size increases
873 the performance of the DL network on a target population still applies.

874

875 **3.B. Transfer learning and fine tuning**

876 Transfer learning is a technique in which a DL network trained on a large data set from one
877 domain is used to retrain or fine-tune the DL network with a smaller data set associated with
878 another domain.¹⁶⁰ The limited size of the annotated medical image data sets, and the current
879 trend of using deeper and larger structures increase the risk of overtraining and makes transfer
880 learning more appealing in medical imaging.

881 Transfer learning in medical imaging commonly starts with a CNN that was already trained on
882 natural images, i.e., a pre-trained model. The limited medical image data set is then used to fine-
883 tune the pre-trained model or, in some applications, no fine-tuning is performed at all. During
884 fine-tuning, the DL architecture typically remains fixed, and only a subset of the weights may be
885 re-trained.

886 A commonly used data set for pre-training of DL structures is ImageNet²⁸ composed of natural
887 scene images. It has been used in more than 75% of the reported transfer learning studies.
888 Different data sets also used for pre-training include CIFAR-10,²⁰⁴ Places205,³⁰⁴ and texture data
889 sets, such as ALOT, DTD, FMD, and KTH-TIPS-2b, as discussed in the literature.²⁰⁹

890 Transfer learning within the same domain of the target task has also been performed. Kooi et
891 al.²⁰² pre-trained DCNN on a large mammogram data set and then re-trained the DCNN on a
892 different smaller mammogram data set for the task of discriminating benign solitary cysts from
893 malignant masses in digital mammography. Samala et al. first pre-trained a DCNN on
894 ImageNet¹⁹⁸ or a larger mammogram data set¹⁷ and then fine-tuned on a digital breast
895 tomosynthesis (DBT) data set for classification and detection of masses on DBT. Zheng et al.²⁵⁴
896 pre-trained on synthetic data and retrained on clinical data for two-dimensional to three-
897 dimensional (2D/3D) registration of preoperative 3D image data. Azizi et al.¹⁶ used
898 radiofrequency (RF) ultrasound images as a source domain to pre-train the DCNN and fine-tuned
899 it on B-mode images as a target domain for prostate cancer detection.

900 A number of studies used pre-trained CNNs for extracting features, which are sometimes
901 referred to as the off-the-shelf CNN features.³⁰⁵ A relatively small labeled data set can then be
902 used to train a classifier such as an SVM for the problem at hand. A number of studies^{173, 181, 192,}
903 ^{196, 306-308} extracted the outputs of the fully-connected layers of a DL network that has been pre-
904 trained ImageNet, and used those features as input to SVMs to build classification models, which
905 suggests that a network pre-trained on natural images is useful for extracting features for medical
906 image analysis purposes.

907 Many of the studies that use transfer learning fine-tune their models by performing additional
908 training on all the network layers, thus using transfer learning like a weight-initialization step.
909 With the assumption that the earlier layers perform more common filtering tasks and later layers
910 (usually fully connected layers) focus more on semantic and high-level features for specific
911 purposes, others have fine-tuned only a few of the last layers within the network.¹¹⁰ Samala et
912 al.¹⁹⁹ studied the effects of fine-tuning different layers of the AlexNet architecture, and found
913 that fine-tuning different layer combinations resulted in different performance. For their task,
914 they found that freezing the weights of just the first convolution layer achieved higher
915 performance compared to freezing additional layers, or fine-tuning all the convolution layers.
916 Similar trends were observed by Lee et al.³⁰⁹. However, the data set size for the fine-tuning may
917 also need to be taken into consideration when using transfer learning, as Samala et al.³¹⁰ saw a
918 trend where the performance of the fine-tuned network increased with increasing data set size of
919 the target task domain used for fine-tuning.

920 **3.C. Combining deep learning with radiomics approaches**

921 Before DL was applied to medical imaging, hand-crafted-features-based approaches were
922 generally used to analyze the images. By using DL, it is expected that given enough data, the
923 network will learn image descriptors useful for analysis. However, it is possible to combine the
924 outputs of DL methods with the knowledge the field of medical imaging analysis has
925 accumulated with computer-extracted, hand-crafted features.¹⁶⁶ Several works, including
926 Antropova et al.,¹⁹⁷ Li et al.,¹⁹² Huynh et al.,¹⁹⁶ and Ben-Cohen et al.,³⁰⁷ combined features
927 extracted from the fully-connected layers of a DL architecture, with traditional hand-crafted
928 features (morphology, intensity, texture). Feature selection was performed to reduce the number
929 of features, then a machine learning classifier, such as SVM or RF, were used to generate a

930 model using the extracted features. These studies suggest that supplementing DL with
931 information already known to be useful, may improve the performance of these DL models.

932 **3.D. Supervised / Weakly supervised / Unsupervised learning**

933 The majority of the DL applications utilize supervised learning: there is ground truth or labels
934 that the system is trying to match. However, there are also unsupervised methods that attempt to
935 draw inferences from unlabeled data, i.e., without the help of a supervisor (or label) that provides
936 a degree of error for each observation, and weakly-supervised methods, that use noisy labels, or
937 images labeled as positive or negative, without localization information, to train for a specific
938 task.

939 Unsupervised learning in DL is generally performed by auto-encoders or independent subspace
940 analysis (ISA).^{249, 250, 311} The outputs of these networks may be further processed in a supervised
941 manner, by extracting the features from the network and applying a machine learning classifier.
942 In weakly-supervised learning, the reference standard used to train does not contain the full
943 information.^{311, 312} For example, Feng et al.³¹³ trained a system for lung nodule segmentation
944 with a binary label if a nodule was present for a given image slice. Yang et al.¹⁶⁷ used a weakly-
945 supervised network in a system that aimed to generate a cancer response map with each pixel
946 indicating the likelihood to be cancerous. Both methods refined the initial results with additional
947 deep learning networks. There are also methods that use a combination of weakly supervised and
948 supervised methods.^{180, 314} Wang et al.¹⁸⁰ and Rajpurkar et al.³¹⁴ used supervised learning to label
949 chest x-rays with one or multiple specific lung diseases, and used weakly-supervised learning to
950 localize the region with the disease.

951 **4. EXPANDING DATA SETS FOR DEEP LEARNING**

952 As discussed above, DL performs significantly better than previous shallow learning methods
953 and hand-crafted image features. However, this comes at the cost of requiring greater amounts of
954 training data compared to previous methods. In the medical domain, publicly-available large-
955 scale image data sets that contain images from tens of thousands of patients are not available
956 (except the recently released ChestX-ray14 data set.¹⁸⁰) Although vast amounts of clinical
957 images/annotations/reports are stored in many hospitals' digital warehouse, e.g., picture
958 archiving and communication systems (PACS) and oncology information system (OIS),
959 obtaining semantic labels on a large scale medical image database is another bottleneck to train
960 highly effective DL models for image analysis.

961 It is difficult to directly borrow conventional means of collecting image annotations that are used
962 for annotating natural scene images (e.g., Google image search uses terms from NEIL
963 knowledge³¹⁵ base followed by crowd-sourcing²⁸) and apply them in medical images. Medical
964 annotations are difficult to obtain from clinically untrained annotators. On the other hand, using
965 well-trained radiologists is expensive. Moreover, the task of “assigning labels to images” is not
966 aligned with their regular clinical routine, which can cause drastic inter-observer variations or
967 inconsistency. There is a lot of definition ambiguity to assign image labels based on visible
968 anatomic structures, pathological findings or using both cues. In addition, a high quality or large
969 capacity medical image search engine is a prerequisite to locate relevant image studies. For
970 example, the radiological data stored in the PACS server are only indexed with dates, patient
971 names, and scan protocols, and it often takes extra effort to find all the cases with a disease
972 pattern of interest. Natural language processing based systems that text mine radiology reports
973 are just beginning to become available.³¹⁶

974 A wide variety of techniques have been developed for tackling the data shortage problem for
975 both the general computer vision and medical image analysis domain. Data augmentation is the
976 most straightforward way to increase the size of a data set for training purposes. It has been
977 proved to be extremely effective for currently existing data sets,¹⁶⁰ which often contain a small
978 number (hundreds of cases) of hand-labeled data. Others believe that DL and humans-in-the-loop
979 inspection may have to be interleaved and integrated to construct labels for a large-scale image
980 database, rather than being employed as two independent labeling processes. It can involve
981 selectively labeling critical samples via active learning. A few recent works focus on transferring
982 the tremendous number of imaging studies accompanied by radiological reports (i.e., loosely
983 labeled samples) into machine trainable data format. Both image and textual features could be
984 utilized for this retrospective and cost-effective process. In addition to using hand-labeled
985 ground-truth, others^{317, 318} utilize the algorithm-generated ground-truth of existing image data for
986 training the CNN models. They assume the model can learn from these less accurate examples
987 and produce refined results in an iterative training process. Furthermore, approaches based on
988 generative adversarial networks³⁸ (GAN) can create image samples for training, either from
989 random initialization or from more advanced clues for image generation. Recent results have
990 shown examples of its promising and useful outcomes. In the following sections, we will
991 summarize these techniques individually.

992 **4.A. Data augmentation**

993 Data augmentation creates new samples based on existing samples in a data set or according to a
994 generative model. These new samples can then be combined with the original samples to
995 increase the variability of data points in a data set. This class of techniques has become a
996 common practice in DL based applications since it has been shown to be extremely effective for

997 increasing the size of training sets, reducing the chance of overfitting and eliminating the
998 unbalance issue in multi-class data sets, which is critical for achieving generalizable models and
999 testing results.

1000 Common data augmentation techniques adopted in medical image analysis applications^{84, 107, 319}
1001 include **cropping**, translation, rotation, flipping, and scaling of images. Instead of augmenting
1002 whole images, Gao et al.²⁰⁶ randomly jittered and cropped sub-images as patches from each
1003 original CT slice to generate more samples for classifying interstitial lung diseases. Pezeshk et
1004 al.³²⁰ introduced an image blending tool that can seamlessly embed a lesion patch into a CT scan
1005 or mammography. Furthermore, the lesion patches could be inserted with various types of
1006 transformations to the lesion shape and characteristics. Improved classification performances
1007 were presented even for small training data sets. Zhang et al.³²¹ intended to tackle the unbalanced
1008 data issue for common medical image classification tasks. They proposed a new data
1009 augmentation method called unified learning of feature representation and similarity matrix. A
1010 single DCNN was trained on the seed labeled data set to obtain image feature representations and
1011 a similarity matrix simultaneously, which could be used for searching more similar images to
1012 each class of colonoscopy and upper endoscopy images.

1013 Another type of data augmentation involves synthesizing images or data using an object model
1014 and physics principles of image formation. Depending on the ultimate purpose of the DL
1015 algorithm, the degree of sophistication for the models and image formation approximations can
1016 vary.³²² Yang et al.²⁴⁰ created a synthetic CT data set through the use of the Radon transform for
1017 a known object and modeled different exposure conditions through adding noise to the data, for
1018 the purpose of training a CNN to estimate high-dose projections from low-dose ones. Cui et al.³²³
1019 simulated dynamic PET emission data in order to train a stacked sparse autoencoder based

1020 reconstruction framework for dynamic PET imaging. Chen et al.²³⁷ synthesized noisy projections
1021 based on patient images to generate training data for developing a DL algorithm for noise
1022 reduction in reconstructed CT images. Miao et al.²⁵³ used synthetic data only to train a CNN for
1023 2D/3D image registration.

1024 **4.B. Data annotation via mining text reports**

1025 Over the decades, large amounts of radiological data (e.g., images, clinical annotations, and
1026 radiological reports) have accumulated in many hospitals' PACS. How to transform those
1027 retrospective radiological data into a machine-learnable format has become a big challenge in the
1028 DL era. A radiological report could contain many types of information. Generally speaking, it is
1029 a free-text summary of all the clinical findings and impressions determined during examination
1030 of a radiological image study. It can contain richer information than just the description of
1031 disease findings, but also may consist of negation and uncertainty statements. In the 'findings'
1032 section, a list of normal and abnormal observations is listed for each part of the body examined
1033 in the image. Attributes of the disease patterns, e.g., specific location and severity, are also noted.
1034 Furthermore, critical diagnosis information is often presented in the 'impression' section by
1035 considering all findings, patient history, and previous studies. Additional or follow-up imaging
1036 studies are recommended if suspicious findings are located. As such, reports consist of a
1037 challenging mixture of information. A key for machine learning is extracting the relevant parts
1038 for particular applications.³²⁴

1039 Schlegl et al.³²⁵ relied on existing optical coherence tomography (OCT) volume data and
1040 corresponding diagnostic reports to correlate image content and geometry with semantic
1041 concepts described in the reports. Increasing classification accuracy for intraretinal cystoid fluid,

1042 subretinal fluid and normal retinal tissue was demonstrated while mining the voxel-level
1043 annotation of class labels.

1044 Following an initial work using MeSH (medical subject headings) manual annotations on chest
1045 radiographs,³²⁶ Shin et al.³³ extracted sentences from the original radiology reports describing
1046 key images (images identified during clinical image interpretation as having important findings).
1047 The authors used natural language processing (NLP) to analyze about 780,000 patients'
1048 radiology reports and found 215,786 key images mentioned in the reports from scans of 61,845
1049 unique patients. The key images were then extracted from their institution's PACS.

1050 Corresponding image labels were then mined via unsupervised hierarchical Bayesian document
1051 clustering, i.e. generative latent Dirichlet allocation topic modeling, to form 80 classes at the first
1052 level of hierarchy. Zech et al.³¹⁶ applied a similar methodology to a set of 96,303 head computed
1053 tomography reports. While mining topic labels in a fully unsupervised manner,³³ they adopted
1054 latent Dirichlet allocation together with bag of words to compute the feature representation of
1055 corpuses. Then, a regression model was trained using a small subset (1,004) of annotated reports
1056 to initialize the clustering of those unlabeled text reports.

1057 The purely text-computed information offers some coarse level of radiology semantics but is
1058 often limited and disconnected from the associated image. First, the classes could be highly
1059 unbalanced, which means that one dominating category may contain many more images while
1060 other classes may contain few. Furthermore, the images in a class assigned purely by text
1061 analysis may not be visually coherent since the image appearance is not considered in the
1062 clustering process. Wang et al.³²⁷ exploited a combination of image features and textual
1063 information extracted from reports to label groups of images to alleviate these limitations. Fig. 6
1064 shows the flowchart of the framework. A CNN based joint mining framework was developed to

1065 iteratively improve the extracted CNN image features and clustering labels. Consequently, NLP-
1066 mined disease keywords were assigned to each image cluster.

1067

1068 More advanced NLP techniques have demonstrated better performances in extracted disease
1069 keywords for image labeling task in recent studies. Wang et al.¹⁸⁰ introduced a two-stage
1070 pathology extraction approach by first detecting all disease keywords mentioned in the report
1071 using ontology-based tools and then building negation and uncertainty elimination rules on the
1072 dependency graph of sentences. Fig. 7 shows sample disease categories mined from the
1073 retrospective data. The authors publicly released their data set of 112,120 frontal-view chest x-
1074 ray images of 30,805 unique patients along with image annotations of 14 disease categories.
1075 Subsequent research led to a 6% average improvement in the area under the receiver operating
1076 characteristic curve through the use of a multi-level attention model in a DL pipeline that
1077 included both CNNs and recurrent neural networks.³²⁸

1078 Chen et al.³²⁹ applied a CNN based textual classification framework to find the presence,
1079 chronicity, and location of pulmonary embolism in CT examination reports. A human-in-the-
1080 loop NLP annotation strategy was adopted to reduce the labeling cost for CNN training. The
1081 final CNN model was trained using a total of 2,512 radiologist-annotated CT reports.

1082

1083 Yan et al.^{330, 331} mined radiology reports and images to extract lesion measurements. The lesion
1084 measurements were made in the course of routine clinical interpretation of CT scans. They were
1085 bidimensional measurements performed for RECIST (Response Evaluation Criteria in Solid
1086 Tumors) assessment, many as part of oncology clinical trials. Their data set, named

1087 “DeepLesion”, consisted of 32,120 axial CT slices, each containing a measured lesion, from
1088 10,594 CT imaging studies of 4,459 unique patients. The data set consists of a large variety of
1089 lesion types, including those involving lung, liver, kidney, pancreas and lymph nodes. The
1090 authors’ deep learning algorithm, which used a triple network and ImageNet pretrained weights,
1091 was able to retrieve images of specified type, location and size with an average accuracy of
1092 90.5%.

1093 Possibilities for text mining do not need to be limited to radiology reports but extend to other
1094 clinical reports. The presence of electronic health records (EHR) yields the potential to collect
1095 both imaging and clinical/pathology data in order to input to DL to predict diagnosis, outcome,
1096 and guide treatments within a clinical workflow.³³² Dai et al.³³³ proposed a clinical report guided
1097 CNN which leverages a small amount of supervised information in clinical reports to identify the
1098 potential microaneurysms in fundus images. During training, both fundus images and clinical
1099 reports are presented to the network. In the testing stage, the input is a fundus image only, and
1100 the output is a probabilistic map of the lesion types in the image. Zhang et al.³³⁴ proposed a
1101 multimodal network that jointly learns from medical images and their diagnostic reports, in
1102 which semantic information interacts with visual information to improve the image
1103 understanding ability by teaching the network to distill informative features. Applied to bladder
1104 cancer images and the corresponding diagnostic reports, the network demonstrated improved
1105 performance compared to baseline CNN that only use image information for training.

1106 **4.C. Data annotation via active learning**

1107 Another approach for assembling large data sets for DL is to try to increase the efficiency of
1108 collecting hand-labeled data to minimize the annotation cost. Active learning is one group of
1109 methods for increasing number of annotated data points by including human annotators in the

1110 loop of incremental learning and performance improvement. Two key aspects are usually
1111 considered for selecting candidate data for the expensive annotation process, uncertainty and
1112 representativeness of the candidate data.

1113 Different types of information could be utilized to measure the uncertainty and
1114 representativeness in order to select samples. Top et al.³³⁵ computed the uncertainty values of
1115 radius bone regions in the image for segmentation by considering boundary, regional,
1116 smoothness and entropy energies of those image regions. Annotators were then required to label
1117 those regions in a CT plane with maximum uncertainty. Zhu et al.³³⁶ leveraged the structured
1118 information (e.g., data from individual patients) when selecting batch of candidate unlabeled
1119 samples. The proposed learning framework enforced a set of specifically designed diversity
1120 constraints for the histopathological image annotation task. The visual saliency of objects³³⁷
1121 inside an image were considered as a measure for selecting samples. The similarities between
1122 labeled and unlabeled data were computed and encoded in a graph. Then, random walks were
1123 adopted for searching the most informative node (with largest classification uncertainty and
1124 minimum overlap with labeled data). Lee et al.³³⁸ believe the most informative instances (hard
1125 examples) are those closest to the SVM hyperplane. Together with balanced sampling, their
1126 proposed learning framework was able to achieve a more than 40% classification performance
1127 increase on the testing set.

1128 A batch mode based active learning³³⁹ method was proposed and applied to medical image
1129 classification applications. The Fisher information matrix was adopted to select informative
1130 unlabeled samples in a group-wise manner. The framework developed an efficient greedy
1131 searching algorithm to find a subset of the unlabeled data that can minimize the Fisher
1132 information of remaining unlabeled set. The experiments demonstrated the effectiveness of this

1133 batch-mode based active learning approach. Konyushkova et al.³⁴⁰ trained a segmentation
1134 classifier to decide if a set of supervoxels were most in need to be annotated in 3D image
1135 volumes. Geometric priors were utilized in this process to compute geometric uncertainty for
1136 each voxel, indicating whether a clear boundary was present. For segmenting electron
1137 microscopy images, the model trained using 100 selected pixels with annotations (less than
1138 0.03% of the total training set) achieved even higher classification performance than the one
1139 trained with all available labeled training pixels.

1140 Recent approaches further utilized DCNN features to compute and representativeness criteria.
1141 Yang et al.³⁴¹ presented a deep fully convolutional network based active learning framework to
1142 reduce annotation effort in image that contain multiple instances, e.g., pathological images. The
1143 uncertainty and similarity information computed from network activations is utilized to select the
1144 most cost-effective annotation areas. Zhou et al.³⁴² measured the uncertainty and diversity of
1145 candidate image samples using the CNN classification prediction values computed for all the
1146 image patches extracted from the candidate image. In comparison to previous methods, this
1147 method has the advantage that no seed labeled sample is required. A newly-annotated sample
1148 will further improve the candidate selection process after CNN mode is fine-tuned again based
1149 on the new training set. They demonstrated that the CNN's classification performance could be
1150 incrementally enhanced by continuously fine-tuning the CNN in an iterative manner.

1151 There are other methods that do not require even a small number of initial hand-labeled data.
1152 Gaur et al.³⁴³ started the selection process with a deep model trained on a similar domain. Then,
1153 they interpreted the active learning problem of increasing the size of limited labeled data set as
1154 an optimization problem by maximizing both the uncertainty and abundance. Only a minimum
1155 number of data fulfilling both criteria were selected and annotated by a human expert.

1156 Mosinska et al.³⁴⁴ tailored the uncertainty sampling based active learning approach for the
1157 delineation of complex linear structures problem, which significantly reduced the size (up to
1158 80%) of training data set while achieving equivalent performance. Multiple samples inside the
1159 same image were simultaneously presented to the annotator while the interactive annotation
1160 framework kept the selected samples informative, representative and diverse.

1161 **4.D. Expanding the training data set via domain adaptation**

1162 Instead of manually annotating selective number of data, another strategy for training data-
1163 hungry DL paradigms is to leverage labeled data from a different domain, e.g., ImageNet
1164 database of natural images, and then fine-tune based on the pre-trained CNN parameters in the
1165 target domain via transfer learning, as discussed in Sec. 3B. The assumption is that the essential
1166 pattern learned and recorded in CNN weights, especially in the earlier layers, to some extent are
1167 shared by different kinds of images from different domains. Under this assumption, transfer
1168 learning using a pre-trained model is rather straightforward, but the underlying differences of
1169 structures and features in data cross domains are overlooked. In contrast to this straightforward
1170 application of pre-training, domain adaptation attempts to alter a source domain to bring the
1171 distribution of the source closer to that of the target. In-depth analyses have been conducted to
1172 measure the distribution difference or nonlinear mapping of features between source and target
1173 domains for domain adaptation.

1174 Heimann et al.³⁴⁵ employed a discriminative learning based approach to localize the
1175 transesophageal echocardiography transducer in X-ray images. Instance weighting was applied
1176 on unlabeled fluoroscopy image samples to estimate the differences in feature space density and
1177 correct covariate shift to align the data distribution cross domains. Wachinger et al.³⁴⁶ employed
1178 a similar instance weighting strategy in a supervised domain adaptation problem with a small

1179 training set as supervision from the target domain. Conjeti et al.³⁴⁷ computed tissue-specific
1180 back-scattering signal statistics for calcified, lipidic and fibrotic arterial plaques and used
1181 decision forest based method to align the distribution shift of signal statistics between in-vitro
1182 and in-vivo image domains.

1183 Schlegl et al.²⁰⁵ trained a CNN in an unsupervised manner for learning more general low-level
1184 image features for images from multiple sites (as domains). Then, another CNN model was fine-
1185 tuned based on the previous CNN model (with domain information injected) to classify lung
1186 tissue in high-resolution CT data using a small set of annotated data from on site. Improved
1187 classification performance was demonstrated by adopting unsupervised pre-training with data
1188 cross domains.

1189 Different acquisition and staining processes can cause large variability of microscopic brain
1190 images even on the same part of brain.³⁴⁸ Normalized Cross Correlation was introduced to locate
1191 image patches in the images from target domain, which shared the similar selected features with
1192 an image patch from the source domain. Those located image patches will also share the same
1193 label as their counterpart from the annotated source domain. Then, a multiple instance learning
1194 based classification framework was used to utilize those newly labeled (and also possibly noisy)
1195 patches for the image classification task. For the same problem, Becker et al.³⁴⁹ proposed to learn
1196 a nonlinear mapping of the data features between two domains (acquisitions in this case),
1197 together with decision boundary for the regression based classification.

1198 Azizi et al.¹⁶ applied an unsupervised domain adaptation method based on DL for the prostate
1199 cancer detection problem. A deep belief network was trained using both B-mode (target domain)
1200 and radiofrequency (source domain) ultrasound images to effectively align features from two

1201 domains in a common latent feature space. The alignment was achieved by minimizing the
1202 divergence between the source and target distributions through the training. Similar ideas were
1203 presented for multiple sclerosis lesion segmentation in MR images using fully convolutional
1204 networks.³⁵⁰ A modified U-Net architecture was designed to take both labeled (source domain)
1205 and unlabeled (target domain) data and simultaneously minimize both the segmentation loss and
1206 the discrepancy between embedded features from two domains.

1207 **4.E. Data synthesis via generative adversarial networks**

1208 Generative adversarial networks have attracted tremendous attentions and have grown into a big
1209 family of methods in the past two years, from the original GAN framework³⁸ to recent
1210 CycleGAN.³⁷ The quality of synthesized images also evolved rapidly from 32*32 snapshots to
1211 high-resolution CT/MR images. There have been quite a few successful applications of GANs in
1212 the medical imaging domain. Compared to the conventional generative models based method,
1213 e.g., characteristic modeling,³⁵¹ random walk sampling,³⁵² and image decomposition,³⁵³ GANs
1214 intend to produce better images from an image appearance perspective. However, these images
1215 are often less meaningful from a clinical point of view since the image intensity on each pixel in
1216 a real clinical image has semantic meanings, e.g., high values in PET image usually represent
1217 high take-up tumor regions. To overcome such limitations, a variety of constraints and additional
1218 information need to be included to help produce more clinically meaningful medical images.

1219 Calimeri et al.³⁵⁴ cascaded the GAN models as a multi-scale pyramid based refinement
1220 framework with different size image inputs at each level so that a high-resolution MR image
1221 could be synthesized and then improved from coarse to fine. Frid-Adar et al.²¹⁵ started with
1222 standard data augmentation methods to create a larger data set that could be used to train a deep
1223 convolutional GAN. The synthetic data samples created for each lesion class, i.e. cysts,

1224 metastases and hemangiomas, by the GAN were then inputted to the training process of the final
1225 lesion classifier together with the enlarged training set from previous data augmentation. Lahiri
1226 et al.³⁵⁵ extended the discriminator for classifying patches from multiple categories in addition to
1227 answering the fake or real binary question. This design has proven to be more data efficient for
1228 adversarial training. Zhang et al.³⁵⁶ applied the same strategy on the semantic segmentation task,
1229 where the discriminator not only evaluated the segmentation results itself but also tried to
1230 differentiate the labeled and unlabeled data. The segmentation results from unlabeled data was
1231 weighted less (compared to the counterpart from labeled data) in the adversarial training
1232 procedure to produce more accurate results for the next iteration.

1233 Generating realistic images from scratch (initialized with noise vectors from the latent space) is
1234 extremely challenging, especially for medical images. However, more meaningful images could
1235 be synthesized if some prior knowledge was provided, e.g. an image similar to the target one but
1236 in different modality.³⁵⁷ Costa et al.³⁵⁸ proposed to generate retinal images by using
1237 corresponding vessel tree images. Different from the standard pair-wise GAN generative
1238 framework, an auto-encoder was first trained to learn the distribution of realistic retinal vessel
1239 trees and the retinal images were generated from the representations learned via the auto-
1240 encoder.

1241 Instead of using paired images for training, Chartsias et al.³⁵⁹ adopted the CycleGAN framework
1242 in synthesizing cardiac MR images and masks from view-aligned CT ones in a loosely
1243 supervised manner. The pair-wise constraints (e.g. paired images with similar anatomical
1244 structure) were eliminated in this case. A 15% increase in segmentation accuracy was
1245 demonstrated by using both real and synthetic data compared to using real data alone. The
1246 application of CycleGAN in the unpaired MRI to CT image synthesis was also demonstrated.³⁶⁰

1247 Although it is still in its early stage, GAN based medical image generation has provided a
1248 promising alternative to other data augmentation approaches. Chuquicusma et al.³⁶¹ reported a
1249 visual Turing test that involved two radiologists (with different years of experience) to evaluate
1250 the quality of the synthesized nodules. A mixed set of (benign or malignant) nodule patches was
1251 shown to the radiologists individually for determining whether they were real or generated. The
1252 results showed that the majority (67% and 100%, respectively) of the generated nodules were
1253 recognized as real by the two radiologists.

1254

1255 **5. CHALLENGES, LESSONS LEARNED, AND THE FUTURE**

1256 As discussed in previous sections, recent advances in DL show that computers can extract more
1257 information from images, more reliably, and more accurately than ever before. However, further
1258 developing and optimizing DL techniques for the characteristics of medical images and medical
1259 data remains an important and relevant research challenge.

1260 **5.A. Evaluation and robustness**

1261 As discussed previously, data augmentation is often used to alleviate the problem of limited data
1262 set sizes. Data augmentation is powerful, but must be used correctly. One cannot train a network
1263 on a set of images pertaining to a given case and then test this trained network on a different set
1264 of images pertaining to that same case. Similarly, when dealing with 3D images, it might be
1265 tempting to treat every image slice as an independent entity. This would be incorrect, however,
1266 since slices of the same case are correlated and slices of a given case either need to be all in the
1267 training/validation set or all in the test set. If not done correctly, the performance will be
1268 substantially overestimated and not be generalizable. It is also important to keep in mind that

1269 performance needs to be evaluated ‘by case’, whether a ‘case’ is a lesion, patient, or whatever is
1270 relevant to the clinical task at hand. No matter how one slices and dices the data, if there are 100
1271 patients, there really are only 100 patients, and evaluation needs to be done accordingly.

1272

1273 When DL is used as a feature extractor, even in transfer learning when a completely trained deep
1274 net is applied to new images, the sheer number of extracted features poses a challenge. With the
1275 use of data augmentation, one would hope that the number of features will not exceed the
1276 number of data points so that dimension reduction or feature selection is possible in a meaningful
1277 way before further classification with a different classifier such as a shallow neural net or
1278 support vector machine. Feature selection, however, is likely to be a rather unstable undertaking
1279 with different features being selected depending on how the data set is partitioned. Additionally,
1280 it is common practice to use p-values to choose which of numerous features should be used, but
1281 p-values themselves are highly variable.^{362, 363} P-values are data dependent statistics that vary
1282 from sample to sample even when underlying effects, population, and sampling are the same.³⁶⁴
1283 Hence, utmost care needs to be taken when using DL methods as feature extractors.

1284 Robustness and repeatability are concerns with any machine learning approach,³⁶⁵ and even more
1285 so with DL. Since medical image data sets are so difficult to come by compared to those of
1286 natural images and generally are of limited size, researchers like to re-use the same data for
1287 different tasks. Hence, correction for multiple comparisons^{366, 367} is crucial in the statistical
1288 evaluation of performance. The requirement that data sets need to be of sufficient size and
1289 quality is not unique to DL or medical imaging. It is, for example, reminiscent of issues observed
1290 in genomics where lack of reproducibility was observed when looking for predictive gene lists in

1291 small data sets (~100s of cases).^{368, 369} There, thousands of samples are needed to generate a
1292 robust gene list to predict the outcome in cancer.³⁶⁹ A 2012 study of 53 landmark papers in basic
1293 cancer research was able to replicate the original results of just 6 of these studies.³⁷⁰ Moreover, a
1294 study reviewing radiomics using texture features, i.e., ‘conventional’ radiomics, for the
1295 prediction of survival, found that all of the results of 9 published studies failed to reach statistical
1296 significance after properly correcting p-values for multiple comparisons and the use of an
1297 optimal cut-off (if applicable) in Kaplan-Meier analysis.³⁷¹ Results of DL-based methods, if
1298 analysis is not performed correctly, may be even less likely to hold up to scrutiny.

1299 **5.B. Data sets and curation**

1300 Perhaps the most important challenge when it comes to medical imaging data sets is to obtain
1301 data of a sufficiently large number of properly annotated cases. The bottleneck is not necessarily
1302 obtaining the images, but obtaining annotations and reference standards. For segmentation tasks,
1303 for example, the reference standard or ‘truth’ would be the manual outline of one, or preferably
1304 more, expert radiologists. For cancer classification tasks, for example, the reference standard
1305 would be the pathological truth as determined by biopsy or surgery which needs to be extracted
1306 from pathology reports. The reference standard has to be of high quality, especially when used
1307 for training but also for performance evaluation. Obtaining high quality image data, annotations,
1308 and reference standards is expensive and time consuming. Patient privacy laws, while absolutely
1309 necessary, further complicate data collection because all protected health information needs to be
1310 removed from image data and corresponding radiology, pathology, and other reports. Moreover,
1311 relevant information needs to be extracted from the radiology, pathology, and other text reports
1312 which is time consuming and potentially error prone when done manually and not trivial when
1313 performed automatically (section 4.B). There is immense value in sharing annotated image data

1314 and anonymized publicly accessible databases such as provided by the Cancer Imaging Archive
1315 (www.cancerimagingarchive.net/).

1316 Another challenge for medical image data sets is that imaging devices are not measurement
1317 devices. Unlike a ruler or a Volt meter, which are calibrated and expected to give consistent and
1318 correct results within the calibration accuracy, imaging devices generate images through often
1319 proprietary image processing techniques. Images are usually not quantitative and primarily
1320 designed to be interpretable by humans, not by computers. Robustness of ‘conventional’ and DL-
1321 based methods with respect to image manufacturer or image pre-processing methods needs to be
1322 investigated. There has been effort investigating robustness of ‘conventional’ methods with
1323 respect to manufacturer for breast cancer diagnosis on ultrasound,^{372,373} the assessment of risk of
1324 future breast cancer on digital mammography,³⁷⁴ and lung nodule features.³⁷⁵ Work has also been
1325 done towards the harmonization of image data with respect to different CT scanners.³⁷⁶ One of
1326 the advantages of DL-based methods, however, is that they may be less sensitive than
1327 ‘conventional’ methods to differences in images due to the use of imaging equipment of different
1328 manufacturers. Having been designed for natural images in which, for example, a dog in the
1329 shade is still a dog, may make them better able to deal with differences in image appearance and
1330 quality.

1331 Class imbalance is another challenge related to many medical imaging data sets, not only to DL
1332 based methods but to ‘conventional’ methods as well. In screening mammography, for example,
1333 the cancer prevalence is so low that developing a method to detect cancer without causing undue
1334 false-positives is a formidable task. One approach to alleviate the problem of class imbalance in
1335 the training of DL methods is to use data augmentation of the under-represented class only in
1336 classifier training as explained in more detail in Section 4.

1337 **5.C. Interpretability**

1338 When a deep neural net is used as a feature extractor thousands of features are extracted. Unlike
1339 engineered hand-crafted features these features do not directly relate to something radiologists
1340 can easily interpret. Engineered features often describe something directly related to
1341 characteristics radiologists use in their clinical assessment, such as lesion size or shape. Such
1342 characteristics can be described by multiple mathematical descriptors, i.e., engineered features.
1343 For example, the ‘simplest’ feature of maximum linear dimension is both used by a radiologist
1344 and can be automatically calculated by a radiomics method. It is then easy for a radiologist to
1345 assess whether to trust the radiomics output. But even for ‘traditional’ approaches, this direct
1346 interpretability diminishes for more ‘complicated’ features such as for the many that describe
1347 texture. For features extracted from deep neural nets, this interpretability is almost completely
1348 lost. Radiologists may not care about all the DL parameters and how an application works,
1349 however, and it may be more a matter of human trust in the capabilities of the proverbial DL
1350 ‘black box’. The ‘believability’ of DL approaches – both as classifiers and as feature extractors –
1351 then, relies on past performance reported for large independent test sets. For example, in
1352 diagnosis of breast cancer, the believability of the probability of malignancy output by a DL
1353 method relies on knowledge of past performance on independent test data. Acceptance of DL in
1354 medical imaging may benefit from success of DL in other applications such as self-driving cars
1355 and robotics. On the other hand, there may be legal implications to using DL in medical imaging
1356 applications since it will be more difficult than for ‘conventional’ applications to pinpoint
1357 exactly what went wrong if the output is incorrect (potentially negatively impacting patient care).

1358 Recently, there has been increasing interest in making AI methods (including those involving
1359 DL) transparent, interpretable, and explainable.³⁷⁷ This, in part, has been driven by the European

1360 general data protection regulation that will go into effect in May 2018 and will make ‘black-box’
1361 approaches difficult to use in business. These new rules require it to be at least possible to trace
1362 results on demand.³⁷⁷ Whereas traditional approaches tend to be at least interpretable in the sense
1363 that users can understand the underlying math of an algorithm, until recently, DL systems tended
1364 to be more opaque offering little or no insight into their inner workings. However, there has been
1365 increasing effort in making DL methods more transparent and methods have been proposed to
1366 assess the sensitivity of the prediction with respect to changes in the input or to decompose the
1367 decision in terms of the input variables.³⁷⁸

1368 It is possible to provide visual ‘explanations’, for example, to show heat maps visualizing the
1369 importance of each pixel for the prediction. These visualization techniques could help to further
1370 optimize a CNN training approach and ensure that the CNN is ‘paying attention’ to the correct
1371 regions of an image in analysis. For example, if a CNN were to be trained to detect
1372 pneumothorax on chest X-rays it would be important to know whether the CNN correctly
1373 ‘looked at’ the pneumothorax region of images or instead focused on chest tubes that are often
1374 present in patients with pneumothorax. Most popular visualization techniques are either
1375 perturbation-based or backpropagation-based. Perturbation-based methods modify parts of the
1376 image and study the effect on the CNN output.^{379, 380} Backpropagation-based methods propagate
1377 either the output probability score, or the gradient of the output with respect to the input in order
1378 to construct heatmaps. Some of the most popular backpropagation-based methods include the
1379 saliency map,³⁸¹ the class-activation map,³⁸² and the gradient-weighted class activation map.³⁸³
1380 Backpropagation-based methods are computationally cheaper because they use the fundamental
1381 property of propagating signals through convolutions, instead of propagating each modification
1382 through the network as in done in perturbation-based methods.

1383 **5.D. Competitive challenges**

1384 There have been a number of competitive challenges in the field of medical image analysis
1385 (https://grand-challenge.org/all_challenges/). The prevalence of DL based methods has clearly
1386 increased over the last couple of years and DL methods have become top performers in medical
1387 image analysis competitions. They often, but not always, perform as well as or better than
1388 ‘conventional’ methods. In a literature review on DL, Litjens et al.³⁸⁴ noted that the exact DL
1389 architecture does not seem to be the most important determinant in getting a good solution. For
1390 example, in the Kaggle Diabetic Retinopathy Challenge ([https://www.kaggle.com/c/diabetic-](https://www.kaggle.com/c/diabetic-retinopathy-detection)
1391 [retinopathy-detection](https://www.kaggle.com/c/diabetic-retinopathy-detection)), many researchers used the exact same architectures, the same type of
1392 networks, but obtained widely varying results. Data augmentation methods and preprocessing
1393 techniques seem to contribute substantially to good performance and robustness. It remains an
1394 open question how results from these competitive challenges can be leveraged to benefit the
1395 medical image analysis research community at large.

1396 **5.E. Lessons learned**

1397 Looking back into the history of medical image analysis, it appears that popularity of certain
1398 methods fluctuated in time. For example, ANNs gathered a lot of attention in the early 90’s, were
1399 replaced by support vector machines in many applications in late 1990’s and early 2000’s, only
1400 to make a comeback in the form of DL in the 2010’s. Likewise, the popularity of wavelet
1401 methods and feature extraction techniques such as SIFT evolved in time. The successes already
1402 achieved by DL methods, many of them discussed above, are undeniable and well-established.
1403 We believe that the application areas of DL will evolve in time like other methods, and will
1404 likely be supplemented and complemented by newer methods. However, one important lesson
1405 learned that will likely be maintained into the future is one about data quality, or the ‘garbage-in

1406 garbage-out' principle. Quality of the image data and annotations is crucial and analysis needs to
1407 be carried out correctly. Another important lesson is the difference between statistical
1408 significance and clinical significance/relevance. Although establishing statistical significance is a
1409 very important step in research and publications, we should never lose sight of what the
1410 clinically relevant questions are, and just because there is a newer more complicated CNN, does
1411 not necessarily mean that it will better help (or replace) radiologists. Expert knowledge about the
1412 clinical task can provide advantages that go beyond adding more layers to a CNN, and
1413 incorporating expert medical knowledge to optimize methods, for example through novel data
1414 preprocessing or augmentation techniques, for a specific clinical task is often crucial in obtaining
1415 good performance.

1416 Plenty of challenges remain for 'conventional' medical image analysis and DL-based methods,
1417 including computational and statistical aspects. We need to investigate and improve image data
1418 harmonization, develop standards for reporting as well as experiments, and have better access to
1419 annotated image data such as publicly available data sets to serve as independent benchmarks.

1420 **5.F. Future of deep learning in imaging and therapy**

1421 Machine learning, including DL, is a fast-moving research field that has great promise for future
1422 applications in imaging and therapy. It is evident that DL has already pervaded almost every
1423 aspect of medical image analysis. 'Conventional' image analysis methods were never intended to
1424 replace radiologists but rather to serve as a second opinion. Likewise, DL-based methods are
1425 unlikely to replace human experts any time soon. The performance of DL has equaled or
1426 surpassed human performance for some non-medical tasks such as playing computer games³⁸⁵
1427 and, as illustrated by the many cited publications in this paper, DL has also been quite successful
1428 in a variety of medical imaging applications. However, most medical imaging tasks are far from

1429 solved³⁸⁶ and the optimal deep learning method and architecture for each individual task and
1430 application area have not yet been established. Moreover, the integration of medical image
1431 analysis methods and other patient data - such as patient history, age, and demographics - also
1432 remains an area of active research that could further improve performance of clinical decision
1433 making aids.

1434 Three aspects that will drive the DL revolution are availability of big data, advances in DL
1435 algorithms, and processing power. As discussed above, there is abundant new research aimed at
1436 alleviating the limited data set size problem in medical imaging, and some of the custom DL
1437 architectures and algorithms specifically designed for medical imaging have shown great
1438 promise. There has been an explosion of research papers published on DL in medical imaging,
1439 most within the past couple of years, and this trend is expected continue. The emergence of
1440 conferences solely dedicated to DL in medical imaging (such as the ‘Medical Imaging with Deep
1441 Learning Conference’ to be held in July 2018, <https://midl.amsterdam/>) is very telling. The
1442 potential of DL in medical imaging has also not gone unnoticed by the healthcare industry.
1443 Companies, both big and small, are taking big steps in developing and commercializing new
1444 applications that are based on DL, and large medical imaging vendors have already made
1445 significant investments. Deep learning is here to stay, and its future in medical imaging and
1446 radiation therapy seems bright.

1447 **ACKNOWLEDGMENTS**

1448 MLG and KD were supported in part by NIH grants CA 195564, CA 166945, and CA 189240;
1449 and The University of Chicago CTSA UL1 TR000430 pilot awards. KHC was supported in part
1450 through a Critical Path grant from the U.S. Food and Drug Administration, and by an

1451 appointment to the Research Participation Program at the Center for Devices and Radiological
 1452 Health administered by the Oak Ridge Institute for Science and Education through an
 1453 interagency agreement between the U.S. Department of Energy and the U.S. Food and Drug
 1454 Administration. XW and RMS were supported by the Intramural Research Programs of the NIH
 1455 Clinical Center. The mention of commercial products, their sources, or their use in connection
 1456 with material reported herein is not to be construed as either an actual or implied endorsement of
 1457 such products by the Department of Health and Human Services.

1458 **CONFLICTS OF INTEREST**

1459 MLG is a stockholder in R2/Hologic, scientific advisor, co-founder, and equity holder in
 1460 Quantitative Insights, makers of QuantX, shareholder in Qview, and receives royalties from
 1461 Hologic, GE Medical Systems, MEDIAN Technologies, Riverain Medical, Mitsubishi, and
 1462 Toshiba. KD receives royalties from Hologic. RMS receives royalties from iCAD, Inc.,
 1463 Koninklijke Philips NV, ScanMed, LLC, and receives research support from Ping An Insurance
 1464 Company of China, Ltd., Carestream Health, Inc. and NVIDIA Corporation.

1465 **REFERENCES**

- 1466 1. D. Amodei, S. Ananthanarayanan, R. Anubhai, J. Bai, E. Battenberg, C. Case, J. Casper,
 1467 B. Catanzaro, Q. Cheng and G. Chen, "Deep speech 2: End-to-end speech recognition in
 1468 english and mandarin," International Conference on Machine Learning, 173-182, 2016.
- 1469 2. M. E. Peters, M. Neumann, M. Iyyer, M. Gardner, C. Clark, K. Lee and L. Zettlemoyer,
 1470 "Deep contextualized word representations," arXiv preprint arXiv:1802.05365 (2018).
- 1471 3. B. Zoph, V. Vasudevan, J. Shlens and Q. V. Le, "Learning transferable architectures for
 1472 scalable image recognition," arXiv preprint arXiv:1707.07012 2 (2017).
- 1473 4. D. Silver, A. Huang, C. J. Maddison, A. Guez, L. Sifre, G. Van Den Driessche, J.
 1474 Schrittwieser, I. Antonoglou, V. Panneershelvam and M. Lanctot, "Mastering the game of
 1475 Go with deep neural networks and tree search," Nature **529**, 484-489 (2016).
- 1476 5. D. Gandhi, L. Pinto and A. Gupta, "Learning to fly by crashing," arXiv:1704.05588
 1477 (2017).
- 1478 6. "Worldwide Semiannual Cognitive and Artificial Intelligence Systems Spending Guide",
 1479 (2016). At <https://www.idc.com/getdoc.jsp?containerId=prUS41878616>.

- 1480 7. "The Fourth Industrial Revolution: what it means, how to respond", (2016). At
 1481 <https://www.weforum.org/agenda/2016/01/the-fourth-industrial-revolution-what-it->
 1482 [means-and-how-to-respond/](https://www.weforum.org/agenda/2016/01/the-fourth-industrial-revolution-what-it-).
- 1483 8. E. Brynjolfsson and A. McAfee, *The second machine age: Work, progress, and*
 1484 *prosperity in a time of brilliant technologies.* (WW Norton & Company, 2014).
- 1485 9. K. Schwab, *The fourth industrial revolution.* (Crown Business, 2017).
- 1486 10. "Harnessing automation for a future that works", (2017). At
 1487 <https://www.mckinsey.com/global-themes/digital-disruption/harnessing-automation-for->
 1488 [a-future-that-works.](https://www.mckinsey.com/global-themes/digital-disruption/harnessing-automation-for-)
- 1489 11. Y. LeCun, Y. Bengio and G. Hinton, "Deep learning," *Nature* **521**, 436-44 (2015).
- 1490 12. J. Schmidhuber, "Deep learning in neural networks: an overview," *Neural Networks* **61**,
 1491 85-117 (2015).
- 1492 13. R. Caruana and A. Niculescu-Mizil, "An empirical comparison of supervised learning
 1493 algorithms," in *Proceedings of the 23rd international conference on Machine learning*,
 1494 (ACM, Pittsburgh, Pennsylvania, USA, 2006), pp. 161-168.
- 1495 14. S. J. Pan and Q. Yang, "A Survey on Transfer Learning," *IEEE Transactions on*
 1496 *Knowledge and Data Engineering* **22**, 1345-1359 (2010).
- 1497 15. K. Weiss, T. M. Khoshgoftaar and D. Wang, "A survey of transfer learning," *Journal of*
 1498 *Big Data* **3**, 9 (2016).
- 1499 16. S. Azizi, P. Mousavi, P. Yan, A. Tahmasebi, J. T. Kwak, S. Xu, B. Turkbey, P. Choyke,
 1500 P. Pinto, B. Wood and P. Abolmaesumi, "Transfer learning from RF to B-mode temporal
 1501 enhanced ultrasound features for prostate cancer detection," *International Journal of*
 1502 *Computer Assisted Radiology and Surgery* **12**, 1111-1121 (2017).
- 1503 17. R. K. Samala, H. P. Chan, L. Hadjiiski, M. A. Helvie, J. Wei and K. Cha, "Mass
 1504 detection in digital breast tomosynthesis: Deep convolutional neural network with
 1505 transfer learning from mammography," *Med Phys* **43**, 6654 (2016).
- 1506 18. A. Kumar, J. Kim, D. Lyndon, M. Fulham and D. Feng, "An ensemble of fine-tuned
 1507 convolutional neural networks for medical image classification," *IEEE Journal of*
 1508 *Biomedical and Health Informatics* **21**, 31-40 (2017).
- 1509 19. Y. Bengio, "Learning Deep Architectures for AI," *Foundations and Trends in Machine*
 1510 *Learning* **2**, 1-127 (2009).
- 1511 20. D. J. Felleman and D. C. Van Essen, "Distributed hierarchical processing in the primate
 1512 cerebral cortex," *Cereb Cortex* **1**, 1-47 (1991).
- 1513 21. C. M. Wessinger, J. VanMeter, B. Tian, J. Van Lare, J. Pekar and J. P. Rauschecker,
 1514 "Hierarchical organization of the human auditory cortex revealed by functional magnetic
 1515 resonance imaging," *Journal of Cognitive Neuroscience* **13**, 1-7 (2001).
- 1516 22. R. Caruana, N. Karampatziakis and A. Yessenalina, "An empirical evaluation of
 1517 supervised learning in high dimensions," in *Proceedings of the 25th international*
 1518 *conference on Machine learning*, (ACM, Helsinki, Finland, 2008), pp. 96-103.
- 1519 23. G. E. Hinton, S. Osindero and Y. W. Teh, "A fast learning algorithm for deep belief
 1520 nets," *Neural Comput* **18**, 1527-54 (2006).
- 1521 24. I. Sutskever, J. Martens, G. Dahl and G. Hinton, "On the importance of initialization and
 1522 momentum in deep learning," in *Proceedings of the 30th International Conference on*
 1523 *Machine Learning*, Vol. 28, edited by D. Sanjoy and M. David (PMLR, Proceedings of
 1524 *Machine Learning Research*, 2013), pp. 1139--1147.

- 1525 25. X. Glorot, A. Bordes and Y. Bengio, "Deep Sparse Rectifier Neural Networks," in
 1526 Proceedings of the Fourteenth International Conference on Artificial Intelligence and
 1527 Statistics, Vol. 15, edited by G. Geoffrey, D. David and D. Miroslav (PMLR,
 1528 Proceedings of Machine Learning Research, 2011), pp. 315--323.
- 1529 26. N. Srivastava, G. Hinton, A. Krizhevsky, I. Sutskever and R. Salakhutdinov, "Dropout: a
 1530 simple way to prevent neural networks from overfitting," *J. Mach. Learn. Res.* **15**, 1929-
 1531 1958 (2014).
- 1532 27. L. Wan, M. Zeiler, S. Zhang, Y. L. Cun and R. Fergus, "Regularization of Neural
 1533 Networks using DropConnect," in Proceedings of the 30th International Conference on
 1534 Machine Learning, Vol. 28, edited by D. Sanjoy and M. David (PMLR, Proceedings of
 1535 Machine Learning Research, 2013), pp. 1058--1066.
- 1536 28. J. Deng, W. Dong, R. Socher, L.-J. Li, K. Li and L. Fei-Fei, "Imagenet: A large-scale
 1537 hierarchical image database," Proceedings of the IEEE conference on computer vision
 1538 and pattern recognition, 248-255, 2009.
- 1539 29. A. Krizhevsky, I. Sutskever and G. E. Hinton, "ImageNet Classification with Deep
 1540 Convolutional Neural Networks," in *Advances in Neural Information Processing
 1541 Systems*, Vol. 25, edited by F. Pereira, C. J. C. Burges, L. Bottou and K. Q. Weinberger
 1542 (Curran Associates, Inc., 2012), pp. 1097--1105.
- 1543 30. Y. LeCun, K. Kavukcuoglu and C. Farabet, "Convolutional networks and applications in
 1544 vision," *IEEE International Symposium on Circuits and Systems*, 253-256, 2010.
- 1545 31. S. Hochreiter, #252 and r. Schmidhuber, "Long Short-Term Memory," *Neural Comput.* **9**,
 1546 1735-1780 (1997).
- 1547 32. O. Vinyals, A. Toshev, S. Bengio and D. Erhan, "Show and tell: A neural image caption
 1548 generator," *Computer Vision and Pattern Recognition (CVPR), 2015 IEEE Conference
 1549 on*, 3156-3164, 2015.
- 1550 33. H.-C. Shin, L. Lu, L. Kim, A. Seff, J. Yao and R. Summers, "Interleaved text/image deep
 1551 mining on a large-scale radiology database for automated image interpretation," *Journal
 1552 of Machine Learning Research* **17**, 2 (2016).
- 1553 34. A. Graves, A.-r. Mohamed and G. Hinton, "Speech recognition with deep recurrent
 1554 neural networks," *Acoustics, speech and signal processing (icassp), 2013 ieee
 1555 international conference on*, 6645-6649, 2013.
- 1556 35. I. Sutskever, O. Vinyals and Q. V. Le, "Sequence to sequence learning with neural
 1557 networks," *Advances in neural information processing systems*, 3104-3112, 2014.
- 1558 36. M. Arjovsky, S. Chintala and L. Bottou, "Wasserstein gan," *arXiv preprint
 1559 arXiv:1701.07875* (2017).
- 1560 37. J.-Y. Zhu, T. Park, P. Isola and A. A. Efros, "Unpaired Image-to-Image Translation using
 1561 Cycle-Consistent Adversarial Networks," *IEEE International Conference on Computer
 1562 Vision*, 2017.
- 1563 38. I. Goodfellow, J. Pouget-Abadie, M. Mirza, B. Xu, D. Warde-Farley, S. Ozair, A.
 1564 Courville and Y. Bengio, "Generative adversarial nets," *Advances in neural information
 1565 processing systems*, 2672-2680, 2014.
- 1566 39. M. Mardani, E. Gong, J. Y. Cheng, S. Vasanawala, G. Zaharchuk, M. Alley, N. Thakur,
 1567 S. Han, W. Dally and J. M. Pauly, "Deep generative adversarial networks for compressed
 1568 sensing automates MRI," *arXiv:1706.00051* (2017).

- 1569 40. P. H. Meyers, C. M. Nice, H. C. Becker, W. J. Nettleton, J. W. Sweeney and G. R.
1570 Meckstroth, "Automated computer analysis of radiographic images," *Radiology* **83**,
1571 1029-1034 (1964).
- 1572 41. H. C. Becker, W. J. Nettleton, P. H. Meyers, J. W. Sweeney and C. M. Nice, "Digital
1573 Computer Determination of a Medical Diagnostic Index Directly from Chest X-Ray
1574 Images " *IEEE Trans Biomed Eng* **11**, 67-72 (1964).
- 1575 42. G. S. Lodwick, T. E. Keats and J. P. Dorst, "The coding of roentgen images for computer
1576 analysis as applied to lung cancer," *Radiology* **81**, 185-200 (1963).
- 1577 43. H.-P. Chan, K. Doi, S. Galhotra, C. J. Vyborny, H. MacMahon and P. M. Jokich, "Image
1578 feature analysis and computer-aided diagnosis in digital radiography. 1. Automated
1579 detection of microcalcifications in mammography," *Med Phys* **14**, 538-548 (1987).
- 1580 44. M. L. Giger, K. Doi and H. MacMahon, "Image feature analysis and computer aided
1581 diagnosis in digital radiography. 3. Automated detection of nodules in peripheral lung
1582 fields.," *Med Phys* **15**, 158-66 (1988).
- 1583 45. K. Kanazawa, Y. Kawata, N. Niki, H. Satoh, H. Ohmatsu, R. Kakinuma, M. Kaneko, N.
1584 Moriyama and K. Eguchi, "Computer-aided diagnosis for pulmonary nodules based on
1585 helical CT images," *Computerized Medical Imaging and Graphics* **22**, 157-167 (1998).
- 1586 46. C. Abe, C. E. Kahn, K. Doi and S. Katsuragawa, "Computer-Aided Detection Of Diffuse
1587 Liver-Disease In Ultrasound Images," *Investigative Radiology* **27**, 71-77 (1992).
- 1588 47. K. Fukushima, S. Miyake and T. Ito, "Neocognitron: A neural network model for a
1589 mechanism of visual pattern recognition," *IEEE Transactions on Systems, Man, and
1590 Cybernetics* **SMC-13**, 826-834 (1983).
- 1591 48. J. S. Lin, P. A. Ligomenides, M. T. Freedman and S. K. Mun, "Application of artificial
1592 neural networks for reduction of false-positive detections in digital chest radiographs,"
1593 *Proc Annu Symp Comput Appl Med Care*, 434-8 (1993).
- 1594 49. S. C. Lo, S. L. Lou, J. S. Lin, M. T. Freedman and S. K. Mun, "Artificial convolution
1595 neural network techniques and applications to lung nodule detection," *IEEE Transactions
1596 on Medical Imaging* **14**, 711-718 (1995).
- 1597 50. H.-P. Chan, S. C. B. Lo, B. Sahiner, K. L. Lam and M. A. Helvie, "Computer-aided
1598 detection of mammographic microcalcifications: Pattern recognition with an artificial
1599 neural network," *Med Phys* **22**, 1555-1567 (1995).
- 1600 51. B. Sahiner, C. Heang-Ping, N. Petrick, W. Datong, M. A. Helvie, D. D. Adler and M. M.
1601 Goodsitt, "Classification of mass and normal breast tissue: a convolution neural network
1602 classifier with spatial domain and texture images," *IEEE Transactions on Medical
1603 Imaging* **15**, 598-610 (1996).
- 1604 52. W. Zhang, K. Doi, M. L. Giger, Y. Wu, R. M. Nishikawa and R. A. Schmidt,
1605 "Computerized detection of clustered microcalcifications in digital mammograms using a
1606 shift-invariant artificial neural network," *Med Phys* **21**, 517-524 (1994).
- 1607 53. W. Zhang, K. Doi, M. L. Giger, R. M. Nishikawa and R. A. Schmidt, "An improved
1608 shift-invariant artificial neural network for computerized detection of clustered
1609 microcalcifications in digital mammograms," *Med Phys* **23**, 595-601 (1996).
- 1610 54. K. Suzuki, S. G. Armato, F. Li, S. Sone and K. Doi, "Massive training artificial neural
1611 network (MTANN) for reduction of false positives in computerized detection of lung
1612 nodules in low-dose computed tomography," *Med. Phys* **30**, 1602-1617 (2003).
- 1613 55. K. Suzuki, F. Li, S. Sone and K. Doi, "Computer-Aided Diagnostic Scheme for
1614 Distinction Between Benign and Malignant Nodules in Thoracic Low-Dose CT by Use of

- 1615 Massive Training Artificial Neural Network," *IEEE Transactions on Medical Imaging* **24**,
 1616 1138-1150 (2005).
- 1617 56. K. M. He, X. Y. Zhang, S. Q. Ren and J. Sun, "Deep Residual Learning for Image
 1618 Recognition," in 2016 IEEE Conference on Computer Vision and Pattern Recognition,
 1619 (2016), pp. 770-778.
- 1620 57. M. Drozdal, E. Vorontsov, G. Chartrand, S. Kadoury and C. Pal, "The Importance of
 1621 Skip Connections in Biomedical Image Segmentation," in *Deep Learning and Data
 1622 Labeling for Medical Applications*, Vol. 10008, edited by G. Carneiro, D. Mateus, L.
 1623 Peter, A. Bradley, J. Tavares, V. Belagiannis, J. P. Papa, J. C. Nascimento, M. Loog, Z.
 1624 Lu, J. S. Cardoso and J. Cornebise (2016), pp. 179-187.
- 1625 58. H. Greenspan, B. van Ginneken and R. M. Summers, "Guest editorial deep learning in
 1626 medical imaging: Overview and future promise of an exciting new technique," *IEEE
 1627 Transactions on Medical Imaging* **35**, 1153-1159 (2016).
- 1628 59. K. Simonyan and A. Zisserman, "Very deep convolutional networks for large-scale
 1629 image recognition," arXiv:1409.1556 (2014).
- 1630 60. G. Huang, Z. Liu, L. Van Der Maaten and K. Q. Weinberger, "Densely Connected
 1631 Convolutional Networks," *CVPR*, 3, 2017.
- 1632 61. F. Chollet, "Xception: Deep Learning with Depthwise Separable Convolutions," 2017
 1633 IEEE Conference on Computer Vision and Pattern Recognition (CVPR), 1800-1807,
 1634 2017.
- 1635 62. C. Szegedy, V. Vanhoucke, S. Ioffe, J. Shlens and Z. Wojna, "Rethinking the inception
 1636 architecture for computer vision," *Proceedings of the IEEE Conference on Computer
 1637 Vision and Pattern Recognition*, 2818-2826, 2016.
- 1638 63. V. Gulshan, L. Peng, M. Coram, M. C. Stumpe, D. Wu, A. Narayanaswamy, S.
 1639 Venugopalan, K. Widner, T. Madams, J. Cuadros, R. Kim, R. Raman, P. C. Nelson, J. L.
 1640 Mega and R. Webster, "Development and Validation of a Deep Learning Algorithm for
 1641 Detection of Diabetic Retinopathy in Retinal Fundus Photographs," *Jama-Journal of the
 1642 American Medical Association* **316**, 2402-2410 (2016).
- 1643 64. T. Kooi, G. Litjens, B. van Ginneken, A. Gubern-Merida, C. I. Sanchez, R. Mann, A.
 1644 den Heeten and N. Karssemeijer, "Large scale deep learning for computer aided detection
 1645 of mammographic lesions," *Medical Image Analysis* **35**, 303-312 (2017).
- 1646 65. Y. Liu, K. Gadepalli, M. Norouzi, G. E. Dahl, T. Kohlberger, A. Boyko, S. Venugopalan,
 1647 A. Timofeev, P. Q. Nelson and G. S. Corrado, "Detecting cancer metastases on gigapixel
 1648 pathology images," arXiv:1703.02442 (2017).
- 1649 66. D. Ribli, A. Horváth, Z. Unger, P. Pollner and I. Csabai, "Detecting and classifying
 1650 lesions in mammograms with Deep Learning," *Sci Rep* **8**, 4165 (2018).
- 1651 67. N. Tajbakhsh, J. Y. Shin, S. R. Gurudu, R. T. Hurst, C. B. Kendall, M. B. Gotway and J.
 1652 M. Liang, "Convolutional Neural Networks for Medical Image Analysis: Full Training or
 1653 Fine Tuning?," *IEEE Transactions on Medical Imaging* **35**, 1299-1312 (2016).
- 1654 68. A. Coates, B. Huval, T. Wang, D. Wu, B. Catanzaro and N. Andrew, "Deep learning with
 1655 COTS HPC systems," *International Conference on Machine Learning*, 1337-1345, 2013.
- 1656 69. "Amazon Web Services". At <https://aws.amazon.com/>.
- 1657 70. "Nvidia GPU Cloud". At <https://www.nvidia.com/en-us/gpu-cloud/>.
- 1658 71. "Google Cloud TPU". At <https://cloud.google.com/tpu/>.

- 1659 72. M. Abadi, P. Barham, J. Chen, Z. Chen, A. Davis, J. Dean, M. Devin, S. Ghemawat, G.
1660 Irving and M. Isard, "TensorFlow: A System for Large-Scale Machine Learning," OSDI,
1661 265-283, 2016.
- 1662 73. Y. Jia, E. Shelhamer, J. Donahue, S. Karayev, J. Long, R. Girshick, S. Guadarrama and
1663 T. Darrell, "Caffe: Convolutional architecture for fast feature embedding," Proceedings
1664 of the 22nd ACM international conference on Multimedia, 675-678, 2014.
- 1665 74. R. Collobert, K. Kavukcuoglu and C. Farabet, "Torch7: A matlab-like environment for
1666 machine learning," BigLearn, NIPS workshop, 2011.
- 1667 75. F. Bastien, P. Lamblin, R. Pascanu, J. Bergstra, I. Goodfellow, A. Bergeron, N.
1668 Bouchard, D. Warde-Farley and Y. Bengio, "Theano: new features and speed
1669 improvements," arXiv:1211.5590 (2012).
- 1670 76. K. H. Cha, L. Hadjiiski, R. K. Samala, H. P. Chan, E. M. Caoili and R. H. Cohan,
1671 "Urinary bladder segmentation in CT urography using deep-learning convolutional neural
1672 network and level sets," *Med Phys* **43**, 1882 (2016).
- 1673 77. K. H. Cha, L. M. Hadjiiski, R. K. Samala, H. P. Chan, R. H. Cohan, E. M. Caoili, C.
1674 Paramagul, A. Alva and A. Z. Weizer, "Bladder Cancer Segmentation in CT for
1675 Treatment Response Assessment: Application of Deep-Learning Convolution Neural
1676 Network-A Pilot Study," *Tomography* **2**, 421-429 (2016).
- 1677 78. M. R. Avendi, A. Kheradvar and H. Jafarkhani, "Automatic segmentation of the right
1678 ventricle from cardiac MRI using a learning-based approach," *Magn Reson Med* **78**,
1679 2439-2448 (2017).
- 1680 79. T. A. Ngo, Z. Lu and G. Carneiro, "Combining deep learning and level set for the
1681 automated segmentation of the left ventricle of the heart from cardiac cine magnetic
1682 resonance," *Med Image Anal* **35**, 159-171 (2017).
- 1683 80. F. Lu, F. Wu, P. Hu, Z. Peng and D. Kong, "Automatic 3D liver location and
1684 segmentation via convolutional neural network and graph cut," *International Journal of*
1685 *Computer Assisted Radiology and Surgery* **12**, 171-182 (2017).
- 1686 81. F. Liu, Z. Zhou, H. Jang, A. Samsonov, G. Zhao and R. Kijowski, "Deep convolutional
1687 neural network and 3D deformable approach for tissue segmentation in musculoskeletal
1688 magnetic resonance imaging," *Magn Reson Med* **79**, 2379-2391 (2018).
- 1689 82. M. R. Avendi, A. Kheradvar and H. Jafarkhani, "A combined deep-learning and
1690 deformable-model approach to fully automatic segmentation of the left ventricle in
1691 cardiac MRI," *Med Image Anal* **30**, 108-119 (2016).
- 1692 83. B. Ibragimov and L. Xing, "Segmentation of organs-at-risks in head and neck CT images
1693 using convolutional neural networks," *Med Phys* **44**, 547-557 (2017).
- 1694 84. O. Ronneberger, P. Fischer and T. Brox, "U-Net: Convolutional Networks for
1695 Biomedical Image Segmentation," *International Conference on Medical Image*
1696 *Computing and Computer-Assisted Intervention (MICCAI)*, 234-241, Cham, 2015.
- 1697 85. M. U. Dalmis, G. Litjens, K. Holland, A. Setio, R. Mann, N. Karssemeijer and A.
1698 Gubern-Merida, "Using deep learning to segment breast and fibroglandular tissue in MRI
1699 volumes," *Med Phys* **44**, 533-546 (2017).
- 1700 86. D. Nie, L. Wang, R. Trullo, J. Li, P. Yuan, J. Xia and D. Shen, "Segmentation of
1701 Craniomaxillofacial Bony Structures from MRI with a 3D Deep-Learning Based Cascade
1702 Framework," *Mach Learn Med Imaging* **10541**, 266-273 (2017).
- 1703 87. R. Cheng, H. R. Roth, N. Lay, L. Lu, B. Turkbey, W. Gandler, E. S. McCreedy, T.
1704 Pohida, P. A. Pinto, P. Choyke, M. J. McAuliffe and R. M. Summers, "Automatic

- 1705 magnetic resonance prostate segmentation by deep learning with holistically nested
 1706 networks," *J Med Imaging (Bellingham)* **4**, 041302 (2017).
- 1707 88. Y. Zhuge, A. V. Krauze, H. Ning, J. Y. Cheng, B. C. Arora, K. Camphausen and R. W.
 1708 Miller, "Brain tumor segmentation using holistically nested neural networks in MRI
 1709 images," *Med Phys* **44**, 5234-5243 (2017).
- 1710 89. H. Lee, F. M. Troschel, S. Tajmir, G. Fuchs, J. Mario, F. J. Fintelmann and S. Do, "Pixel-
 1711 Level Deep Segmentation: Artificial Intelligence Quantifies Muscle on Computed
 1712 Tomography for Body Morphometric Analysis," *J Digit Imaging* **30**, 487-498 (2017).
- 1713 90. Y. Wang, Y. Qiu, T. Thai, K. Moore, H. Liu and B. Zheng, "A two-step convolutional
 1714 neural network based computer-aided detection scheme for automatically segmenting
 1715 adipose tissue volume depicting on CT images," *Comput Methods Programs Biomed*
 1716 **144**, 97-104 (2017).
- 1717 91. P. Hu, F. Wu, J. Peng, Y. Bao, F. Chen and D. Kong, "Automatic abdominal multi-organ
 1718 segmentation using deep convolutional neural network and time-implicit level sets,"
 1719 *International Journal of Computer Assisted Radiology and Surgery* **12**, 399-411 (2017).
- 1720 92. A. Mansoor, J. J. Cerrolaza, R. Idrees, E. Biggs, M. A. Alsharid, R. A. Avery and M. G.
 1721 Linguraru, "Deep Learning Guided Partitioned Shape Model for Anterior Visual Pathway
 1722 Segmentation," *IEEE Transactions on Medical Imaging* **35**, 1856-65 (2016).
- 1723 93. H. Choi and K. H. Jin, "Fast and robust segmentation of the striatum using deep
 1724 convolutional neural networks," *J Neurosci Methods* **274**, 146-153 (2016).
- 1725 94. P. Moeskops, M. A. Viergever, A. M. Mendrik, L. S. de Vries, M. J. Benders and I.
 1726 Isgum, "Automatic Segmentation of MR Brain Images With a Convolutional Neural
 1727 Network," *IEEE Transactions on Medical Imaging* **35**, 1252-1261 (2016).
- 1728 95. C. Wachinger, M. Reuter and T. Klein, "DeepNAT: Deep convolutional neural network
 1729 for segmenting neuroanatomy," *Neuroimage* **170**, 434-445 (2018).
- 1730 96. H. Chen, Q. Dou, L. Yu, J. Qin and P. A. Heng, "VoxResNet: Deep voxelwise residual
 1731 networks for brain segmentation from 3D MR images," *Neuroimage* **170**, 446-455
 1732 (2018).
- 1733 97. J. Dolz, C. Desrosiers and I. Ben Ayed, "3D fully convolutional networks for subcortical
 1734 segmentation in MRI: A large-scale study," *Neuroimage* **170**, 456-470 (2018).
- 1735 98. M. Kallenberg, K. Petersen, M. Nielsen, A. Y. Ng, P. Diao, C. Igel, C. M. Vachon, K.
 1736 Holland, R. R. Winkel, N. Karssemeijer and M. Lillholm, "Unsupervised Deep Learning
 1737 Applied to Breast Density Segmentation and Mammographic Risk Scoring," *IEEE*
 1738 *Transactions on Medical Imaging* **35**, 1322-1331 (2016).
- 1739 99. L. K. Tan, R. A. McLaughlin, E. Lim, Y. F. Abdul Aziz and Y. M. Liew, "Fully
 1740 automated segmentation of the left ventricle in cine cardiac MRI using neural network
 1741 regression," *J Magn Reson Imaging* (2018).
- 1742 100. L. K. Tan, Y. M. Liew, E. Lim and R. A. McLaughlin, "Convolutional neural network
 1743 regression for short-axis left ventricle segmentation in cardiac cine MR sequences," *Med*
 1744 *Image Anal* **39**, 78-86 (2017).
- 1745 101. L. Yu, Y. Guo, Y. Wang, J. Yu and P. Chen, "Segmentation of Fetal Left Ventricle in
 1746 Echocardiographic Sequences Based on Dynamic Convolutional Neural Networks,"
 1747 *IEEE Trans Biomed Eng* **64**, 1886-1895 (2017).
- 1748 102. T. L. Kline, P. Korfiatis, M. E. Edwards, J. D. Blais, F. S. Czerwiec, P. C. Harris, B. F.
 1749 King, V. E. Torres and B. J. Erickson, "Performance of an Artificial Multi-observer Deep

- 1750 Neural Network for Fully Automated Segmentation of Polycystic Kidneys," *J Digit*
 1751 *Imaging* **30**, 442-448 (2017).
- 1752 103. K. Sharma, C. Rupprecht, A. Caroli, M. C. Aparicio, A. Remuzzi, M. Baust and N.
 1753 Navab, "Automatic Segmentation of Kidneys using Deep Learning for Total Kidney
 1754 Volume Quantification in Autosomal Dominant Polycystic Kidney Disease," *Sci Rep* **7**,
 1755 2049 (2017).
- 1756 104. P. Hu, F. Wu, J. Peng, P. Liang and D. Kong, "Automatic 3D liver segmentation based on
 1757 deep learning and globally optimized surface evolution," *Phys Med Biol* **61**, 8676-8698
 1758 (2016).
- 1759 105. W. Kovacs, N. Hsieh, H. Roth, C. Nnamdi-Emeratom, W. P. Bandettini, A. Arai, A.
 1760 Mankodi, R. M. Summers and J. Yao, "Holistic segmentation of the lung in cine MRI," *J*
 1761 *Med Imaging (Bellingham)* **4**, 041310 (2017).
- 1762 106. A. Farag, L. Lu, H. R. Roth, J. Liu, E. Turkbey and R. M. Summers, "A Bottom-up
 1763 Approach for Pancreas Segmentation using Cascaded Superpixels and (Deep) Image
 1764 Patch Labeling," *IEEE Transactions on Image Processing* (2016).
- 1765 107. H. R. Roth, L. Lu, A. Farag, H.-C. Shin, J. Liu, E. B. Turkbey and R. M. Summers,
 1766 "Deeporgan: Multi-level deep convolutional networks for automated pancreas
 1767 segmentation," *International Conference on Medical Image Computing and Computer-*
 1768 *Assisted Intervention (MICCAI)*, 556-564, 2015.
- 1769 108. Y. Guo, Y. Gao and D. Shen, "Deformable MR Prostate Segmentation via Deep Feature
 1770 Learning and Sparse Patch Matching," *IEEE Transactions on Medical Imaging* **35**, 1077-
 1771 89 (2016).
- 1772 109. S. Liao, Y. Gao, A. Oto and D. Shen, "Representation learning: a unified deep learning
 1773 framework for automatic prostate MR segmentation," *International Conference on*
 1774 *Medical Image Computing and Computer-Assisted Intervention (MICCAI)*, 254-61, 2013.
- 1775 110. Z. Tian, L. Liu, Z. Zhang and B. Fei, "PSNet: prostate segmentation on MRI based on a
 1776 convolutional neural network," *J Med Imaging (Bellingham)* **5**, 021208 (2018).
- 1777 111. K. Men, J. Dai and Y. Li, "Automatic segmentation of the clinical target volume and
 1778 organs at risk in the planning CT for rectal cancer using deep dilated convolutional neural
 1779 networks," *Med Phys* **44**, 6377 (2017).
- 1780 112. X. Li, Q. Dou, H. Chen, C. W. Fu, X. Qi, D. L. Belavy, G. Armbrecht, D. Felsenberg, G.
 1781 Zheng and P. A. Heng, "3D multi-scale FCN with random modality voxel dropout
 1782 learning for Intervertebral Disc Localization and Segmentation from Multi-modality MR
 1783 Images," *Med Image Anal* **45**, 41-54 (2018).
- 1784 113. X. Zhou, R. Takayama, S. Wang, T. Hara and H. Fujita, "Deep learning of the sectional
 1785 appearances of 3D CT images for anatomical structure segmentation based on an FCN
 1786 voting method," *Med Phys* **44**, 5221-5233 (2017).
- 1787 114. Q. Dou, L. Yu, H. Chen, Y. Jin, X. Yang, J. Qin and P. A. Heng, "3D deeply supervised
 1788 network for automated segmentation of volumetric medical images," *Med Image Anal*
 1789 **41**, 40-54 (2017).
- 1790 115. V. Alex, K. Vaidhya, S. Thirunavukkarasu, C. Kesavadas and G. Krishnamurthi,
 1791 "Semisupervised learning using denoising autoencoders for brain lesion detection and
 1792 segmentation," *J Med Imaging (Bellingham)* **4**, 041311 (2017).
- 1793 116. P. Korfiatis, T. L. Kline and B. J. Erickson, "Automated Segmentation of Hyperintense
 1794 Regions in FLAIR MRI Using Deep Learning," *Tomography* **2**, 334-340 (2016).

- 1795 117. S. Iqbal, M. U. Ghani, T. Saba and A. Rehman, "Brain tumor segmentation in multi-
1796 spectral MRI using convolutional neural networks (CNN)," *Microsc Res Tech* **81**, 419-
1797 427 (2018).
- 1798 118. M. A. Al-antari, M. A. Al-masni, M.-T. Choi, S.-M. Han and T.-S. Kim, "A fully
1799 integrated computer-aided diagnosis system for digital X-ray mammograms via deep
1800 learning detection, segmentation, and classification," *International Journal of Medical*
1801 *Informatics* **117**, 44-54 (2018).
- 1802 119. R. Zhang, L. Huang, W. Xia, B. Zhang, B. Qiu and X. Gao, "Multiple supervised residual
1803 network for osteosarcoma segmentation in CT images," *Comput Med Imaging Graph* **63**,
1804 1-8 (2018).
- 1805 120. L. Huang, W. Xia, B. Zhang, B. Qiu and X. Gao, "MSFCN-multiple supervised fully
1806 convolutional networks for the osteosarcoma segmentation of CT images," *Comput*
1807 *Methods Programs Biomed* **143**, 67-74 (2017).
- 1808 121. K. Kamnitsas, C. Ledig, V. F. J. Newcombe, J. P. Simpson, A. D. Kane, D. K. Menon, D.
1809 Rueckert and B. Glocker, "Efficient multi-scale 3D CNN with fully connected CRF for
1810 accurate brain lesion segmentation," *Med Image Anal* **36**, 61-78 (2017).
- 1811 122. Y. Liu, S. Stojadinovic, B. Hrycushko, Z. Wardak, S. Lau, W. G. Lu, Y. L. Yan, S. B.
1812 Jiang, X. Zhen, R. Timmerman, L. Nedzi and X. J. Gu, "A deep convolutional neural
1813 network-based automatic delineation strategy for multiple brain metastases stereotactic
1814 radiosurgery," *Plos One* **12** (2017).
- 1815 123. M. Havaei, A. Davy, D. Warde-Farley, A. Biard, A. Courville, Y. Bengio, C. Pal, P. M.
1816 Jodoin and H. Larochelle, "Brain tumor segmentation with Deep Neural Networks," *Med*
1817 *Image Anal* **35**, 18-31 (2017).
- 1818 124. X. Zhao, Y. Wu, G. Song, Z. Li, Y. Zhang and Y. Fan, "A deep learning model
1819 integrating FCNNs and CRFs for brain tumor segmentation," *Med Image Anal* **43**, 98-
1820 111 (2018).
- 1821 125. L. Chen, P. Bentley and D. Rueckert, "Fully automatic acute ischemic lesion
1822 segmentation in DWI using convolutional neural networks," *Neuroimage Clin* **15**, 633-
1823 643 (2017).
- 1824 126. T. Brosch, L. Y. Tang, Y. Youngjin, D. K. Li, A. Traboulsee and R. Tam, "Deep 3D
1825 Convolutional Encoder Networks With Shortcuts for Multiscale Feature Integration
1826 Applied to Multiple Sclerosis Lesion Segmentation," *IEEE Transactions on Medical*
1827 *Imaging* **35**, 1229-1239 (2016).
- 1828 127. M. Ghafoorian, N. Karssemeijer, T. Heskes, I. W. M. van Uden, C. I. Sanchez, G.
1829 Litjens, F. E. de Leeuw, B. van Ginneken, E. Marchiori and B. Platel, "Location Sensitive
1830 Deep Convolutional Neural Networks for Segmentation of White Matter
1831 Hyperintensities," *Sci Rep* **7**, 5110 (2017).
- 1832 128. K. Men, X. Chen, Y. Zhang, T. Zhang, J. Dai, J. Yi and Y. Li, "Deep Deconvolutional
1833 Neural Network for Target Segmentation of Nasopharyngeal Cancer in Planning
1834 Computed Tomography Images," *Front Oncol* **7**, 315 (2017).
- 1835 129. J. Ma, F. Wu, T. Jiang, Q. Zhao and D. Kong, "Ultrasound image-based thyroid nodule
1836 automatic segmentation using convolutional neural networks," *International Journal of*
1837 *Computer Assisted Radiology and Surgery* **12**, 1895-1910 (2017).
- 1838 130. W. Li, F. Jia and Q. Hu, "Automatic segmentation of liver tumor in CT images with deep
1839 convolutional neural networks," *Journal of Computer and Communications* **3**, 146
1840 (2015).

- 1841 131. S. Wang, M. Zhou, Z. Liu, Z. Liu, D. Gu, Y. Zang, D. Dong, O. Gevaert and J. Tian,
1842 "Central focused convolutional neural networks: Developing a data-driven model for
1843 lung nodule segmentation," *Med Image Anal* **40**, 172-183 (2017).
- 1844 132. I. Noguees, L. Lu, X. Wang, H. Roth, G. Bertasius, N. Lay, J. Shi, Y. Tsehay and R. M.
1845 Summers, "Automatic lymph node cluster segmentation using holistically-nested neural
1846 networks and structured optimization in CT images," *International Conference on*
1847 *Medical Image Computing and Computer-Assisted Intervention (MICCAI)*, 388-397,
1848 2016.
- 1849 133. S. Trebeschi, J. J. M. van Griethuysen, D. M. J. Lambregts, M. J. Lahaye, C. Parmer, F.
1850 C. H. Bakers, N. Peters, R. G. H. Beets-Tan and H. Aerts, "Deep Learning for Fully-
1851 Automated Localization and Segmentation of Rectal Cancer on Multiparametric MR,"
1852 *Sci Rep* **7**, 9 (2017).
- 1853 134. M. H. Jafari, E. Nasr-Esfahani, N. Karimi, S. M. R. Soroushmehr, S. Samavi and K.
1854 Najarian, "Extraction of skin lesions from non-dermoscopic images for surgical excision
1855 of melanoma," *International Journal of Computer Assisted Radiology and Surgery* **12**,
1856 1021-1030 (2017).
- 1857 135. D. Yang, S. Zhang, Z. Yan, C. Tan, K. Li and D. Metaxas, "Automated anatomical
1858 landmark detection on distal femur surface using convolutional neural network," 2015
1859 *IEEE 12th International Symposium on Biomedical Imaging*, 17-21, 2015.
- 1860 136. H. Chen, D. Ni, J. Qin, S. L. Li, X. Yang, T. F. Wang and P. A. Heng, "Standard Plane
1861 Localization in Fetal Ultrasound via Domain Transferred Deep Neural Networks," *IEEE*
1862 *Journal of Biomedical and Health Informatics* **19**, 1627-1636 (2015).
- 1863 137. C. F. Baumgartner, K. Kamnitsas, J. Matthew, S. Smith, B. Kainz and D. Rueckert,
1864 "Real-Time Standard Scan Plane Detection and Localisation in Fetal Ultrasound Using
1865 Fully Convolutional Neural Networks," *International Conference on Medical Image*
1866 *Computing and Computer-Assisted Intervention (MICCAI)*, 203-211, 2016.
- 1867 138. A. Kumar, P. Sridar, A. Quinton, R. K. Kumar, D. Feng, R. Nanan and J. Kim, "Plane
1868 identification in fetal ultrasound images using saliency maps and convolutional neural
1869 networks," 2016 *IEEE 13th International Symposium on Biomedical Imaging*, 791-794,
1870 2016.
- 1871 139. F. C. Ghesu, E. Krubasik, B. Georgescu, V. Singh, Z. Yefeng, J. Hornegger and D.
1872 Comaniciu, "Marginal Space Deep Learning: Efficient Architecture for Volumetric
1873 Image Parsing," *IEEE Transactions on Medical Imaging* **35**, 1217-1228 (2016).
- 1874 140. H. Wu, C. Bailey, P. Rasoulinejad and S. Li, "Automatic Landmark Estimation for
1875 Adolescent Idiopathic Scoliosis Assessment Using BoostNet," *International Conference*
1876 *on Medical Image Computing and Computer-Assisted Intervention (MICCAI)*, 127-135,
1877 2017.
- 1878 141. K. Yan, L. Lu and R. M. Summers, "Unsupervised body part regression using
1879 convolutional neural network with self-organization," arXiv:1707.03891 (2017).
- 1880 142. Z. Yan, Y. Zhan, Z. Peng, S. Liao, Y. Shinagawa, S. Zhang, D. N. Metaxas and X. S.
1881 Zhou, "Multi-Instance Deep Learning: Discover Discriminative Local Anatomies for
1882 Bodypart Recognition," *IEEE Transactions on Medical Imaging* **35**, 1332-1343 (2016).
- 1883 143. F. C. Ghesu, B. Georgescu, T. Mansi, D. Neumann, J. Hornegger and D. Comaniciu, "An
1884 Artificial Agent for Anatomical Landmark Detection in Medical Images," *International*
1885 *Conference on Medical Image Computing and Computer-Assisted Intervention*
1886 *(MICCAI)*, 229-237, 2016.

- 1887 144. F. C. Ghesu, B. Georgescu, Y. Zheng, S. Grbic, A. Maier, J. Hornegger and D.
 1888 Comaniciu, "Multi-Scale Deep Reinforcement Learning for Real-Time 3D-Landmark
 1889 Detection in CT Scans," *IEEE Transactions on Pattern Analysis and Machine Intelligence*
 1890 (in print) (2017).
- 1891 145. F. C. Ghesu, B. Georgescu, S. Grbic, A. K. Maier, J. Hornegger and D. Comaniciu,
 1892 "Robust Multi-scale Anatomical Landmark Detection in Incomplete 3D-CT Data,"
 1893 *International Conference on Medical Image Computing and Computer-Assisted*
 1894 *Intervention (MICCAI)*, 194-202, 2017.
- 1895 146. Z. Xu, Q. Huang, J. Park, M. Chen, D. Xu, D. Yang, D. Liu and S. K. Zhou, "Supervised
 1896 Action Classifier: Approaching Landmark Detection as Image Partitioning,"
 1897 *International Conference on Medical Image Computing and Computer-Assisted*
 1898 *Intervention (MICCAI)*, 338-346, 2017.
- 1899 147. C. Payer, D. Štern, H. Bischof and M. Urschler, "Regressing Heatmaps for Multiple
 1900 Landmark Localization Using CNNs," *International Conference on Medical Image*
 1901 *Computing and Computer-Assisted Intervention (MICCAI)*, 230-238, 2016.
- 1902 148. Y. Cai, M. Landis, D. T. Laidley, A. Kornecki, A. Lum and S. Li, "Multi-modal vertebrae
 1903 recognition using Transformed Deep Convolution Network," *Computerized Medical*
 1904 *Imaging and Graphics* **51**, 11-19 (2016).
- 1905 149. N. Baka, S. Leenstra and T. v. Walsum, "Ultrasound Aided Vertebral Level Localization
 1906 for Lumbar Surgery," *IEEE Transactions on Medical Imaging* **36**, 2138-2147 (2017).
- 1907 150. Y. Zheng, D. Liu, B. Georgescu, H. Nguyen and D. Comaniciu, "3D Deep Learning for
 1908 Efficient and Robust Landmark Detection in Volumetric Data," *International Conference*
 1909 *on Medical Image Computing and Computer-Assisted Intervention (MICCAI)*, 565-572,
 1910 2015.
- 1911 151. H. Chen, Q. Dou, D. Ni, J.-Z. Cheng, J. Qin, S. Li and P.-A. Heng, "Automatic Fetal
 1912 Ultrasound Standard Plane Detection Using Knowledge Transferred Recurrent Neural
 1913 Networks," *International Conference on Medical Image Computing and Computer-*
 1914 *Assisted Intervention (MICCAI)*, 507-514, 2015.
- 1915 152. X. Lu, D. Xu and D. Liu, "Robust 3D Organ Localization with Dual Learning
 1916 Architectures and Fusion," *Deep Learning and Data Labeling for Medical Applications*,
 1917 12-20, 2016.
- 1918 153. H. R. Roth, C. T. Lee, H.-C. Shin, A. Seff, L. Kim, J. Yao, L. Lu and R. M. Summers,
 1919 "Anatomy-specific classification of medical images using deep convolutional nets,"
 1920 *Biomedical Imaging (ISBI), 2015 IEEE 12th International Symposium on*, 101-104, 2015.
- 1921 154. B. D. de Vos, J. M. Wolterink, P. A. de Jong, T. Leiner, M. A. Viergever and I. Išgum,
 1922 "ConvNet-Based Localization of Anatomical Structures in 3-D Medical Images," *IEEE*
 1923 *transactions on medical imaging* **36**, 1470-1481 (2017).
- 1924 155. J. Zhang, M. Liu and D. Shen, "Detecting Anatomical Landmarks From Limited Medical
 1925 Imaging Data Using Two-Stage Task-Oriented Deep Neural Networks," *IEEE*
 1926 *Transactions on Image Processing* **26**, 4753-4764 (2017).
- 1927 156. A. P. Harrison, Z. Xu, K. George, L. Lu, R. M. Summers and D. J. Mollura, "Progressive
 1928 and multi-path holistically nested neural networks for pathological lung segmentation
 1929 from CT images," *International Conference on Medical Image Computing and*
 1930 *Computer-Assisted Intervention*, 621-629, 2017.

- 1931 157. J. Yao, W. Kovacs, N. Hsieh, C.-Y. Liu and R. M. Summers, "Holistic segmentation of
1932 intermuscular adipose tissues on thigh MRI," *International Conference on Medical Image*
1933 *Computing and Computer-Assisted Intervention*, 737-745, 2017.
- 1934 158. M. L. Giger, H. P. Chan and J. Boone, "Anniversary Paper: History and status of CAD
1935 and quantitative image analysis: The role of Medical Physics and AAPM," *Med Phys* **35**,
1936 5799-5820 (2008).
- 1937 159. M. L. Giger, N. Karssemeijer and J. A. Schnabel, "Breast Image Analysis for Risk
1938 Assessment, Detection, Diagnosis, and Treatment of Cancer," in *Annual Review of*
1939 *Biomedical Engineering*, Vol 15, Vol. 15, edited by M. L. Yarmush (2013), pp. 327-357.
- 1940 160. H.-C. Shin, H. R. Roth, M. Gao, L. Lu, Z. Xu, I. Nogues, J. Yao, D. Mollura and R. M.
1941 Summers, "Deep convolutional neural networks for computer-aided detection: CNN
1942 architectures, dataset characteristics and transfer learning," *IEEE transactions on medical*
1943 *imaging* **35**, 1285-1298 (2016).
- 1944 161. M. H. Yap, G. Pons, J. Martí, S. Ganau, M. Sentís, R. Zwiggelaar, A. K. Davison and R.
1945 Martí, "Automated breast ultrasound lesions detection using convolutional neural
1946 networks," *IEEE Journal of biomedical and health informatics* (2017).
- 1947 162. P. M. Cheng, T. K. Tejura, K. N. Tran and G. Whang, "Detection of high-grade small
1948 bowel obstruction on conventional radiography with convolutional neural networks,"
1949 *Abdominal Radiology*, 1-8 (2017).
- 1950 163. S. Belharbi, C. Chatelain, R. Héroult, S. Adam, S. Thureau, M. Chastan and R.
1951 Modzelewski, "Spotting L3 slice in CT scans using deep convolutional network and
1952 transfer learning," *Computers in biology and medicine* **87**, 95-103 (2017).
- 1953 164. S. Albarqouni, C. Baur, F. Achilles, V. Belagiannis, S. Demirci and N. Navab, "Aggnet:
1954 deep learning from crowds for mitosis detection in breast cancer histology images," *IEEE*
1955 *Transactions on Medical Imaging* **35**, 1313-1321 (2016).
- 1956 165. J. I. Orlando, E. Prokofyeva, M. del Fresno and M. B. Blaschko, "An ensemble deep
1957 learning based approach for red lesion detection in fundus images," *Computer methods*
1958 *and programs in biomedicine* **153**, 115-127 (2018).
- 1959 166. H. R. Roth, L. Lu, J. Liu, J. Yao, A. Seff, K. Cherry, L. Kim and R. M. Summers,
1960 "Improving computer-aided detection using convolutional neural networks and random
1961 view aggregation," *IEEE transactions on medical imaging* **35**, 1170-1181 (2016).
- 1962 167. X. Yang, C. Liu, Z. Wang, J. Yang, H. Le Min, L. Wang and K.-T. T. Cheng, "Co-trained
1963 convolutional neural networks for automated detection of prostate cancer in multi-
1964 parametric MRI," *Medical image analysis* **42**, 212-227 (2017).
- 1965 168. A. A. Setio, F. Ciompi, G. Litjens, P. Gerke, C. Jacobs, S. J. van Riel, M. M. Wille, M.
1966 Naqibullah, C. I. Sanchez and B. van Ginneken, "Pulmonary Nodule Detection in CT
1967 Images: False Positive Reduction Using Multi-View Convolutional Networks," *IEEE*
1968 *Transactions on Medical Imaging* **35**, 1160-1169 (2016).
- 1969 169. Q. Dou, H. Chen, L. Yu, J. Qin and P. A. Heng, "Multilevel Contextual 3-D CNNs for
1970 False Positive Reduction in Pulmonary Nodule Detection," *IEEE Trans Biomed Eng* **64**,
1971 1558-1567 (2017).
- 1972 170. M. Ghafoorian, N. Karssemeijer, T. Heskes, M. Bergkamp, J. Wissink, J. Obels, K.
1973 Keizer, F. E. de Leeuw, B. V. Ginneken, E. Marchiori and B. Platel, "Deep multi-scale
1974 location-aware 3D convolutional neural networks for automated detection of lacunes of
1975 presumed vascular origin," *Neuroimage Clin* **14**, 391-399 (2017).

- 1976 171. J. Long, E. Shelhamer and T. Darrell, "Fully convolutional networks for semantic
1977 segmentation," Proceedings of the IEEE Conference on Computer Vision and Pattern
1978 Recognition, 3431-3440, 2015.
- 1979 172. D. Qi, C. Hao, Y. Lequan, Z. Lei, Q. Jing, W. Defeng, V. C. Mok, S. Lin and H. Pheng-
1980 Ann, "Automatic Detection of Cerebral Microbleeds From MR Images via 3D
1981 Convolutional Neural Networks," IEEE Transactions on Medical Imaging **35**, 1182-1195
1982 (2016).
- 1983 173. F. Ciompi, B. de Hoop, S. J. van Riel, K. Chung, E. T. Scholten, M. Oudkerk, P. A. de
1984 Jong, M. Prokop and B. van Ginneken, "Automatic classification of pulmonary peri-
1985 fissural nodules in computed tomography using an ensemble of 2D views and a
1986 convolutional neural network out-of-the-box," Medical image analysis **26**, 195-202
1987 (2015).
- 1988 174. S. Chen, J. Qin, X. Ji, B. Lei, T. Wang, D. Ni and J.-Z. Cheng, "Automatic scoring of
1989 multiple semantic attributes with multi-task feature leverage: A study on pulmonary
1990 nodules in CT images," IEEE transactions on medical imaging **36**, 802-814 (2017).
- 1991 175. A. Teramoto, H. Fujita, O. Yamamuro and T. Tamaki, "Automated detection of
1992 pulmonary nodules in PET/CT images: Ensemble false - positive reduction using a
1993 convolutional neural network technique," Med Phys **43**, 2821-2827 (2016).
- 1994 176. H. Jiang, H. Ma, W. Qian, M. Gao and Y. Li, "An automatic detection system of lung
1995 nodule based on multi-group patch-based deep learning network," IEEE Journal of
1996 Biomedical and Health Informatics **In print** (2017).
- 1997 177. Y. Bar, I. Diamant, L. Wolf, S. Lieberman, E. Konen and H. Greenspan, "Chest
1998 pathology detection using deep learning with non-medical training," Biomedical Imaging
1999 (ISBI), 2015 IEEE 12th International Symposium on, 294-297, 2015.
- 2000 178. M. Cicero, A. Bilbily, E. Colak, T. Dowdell, B. Gray, K. Perampaladas and J. Barfett,
2001 "Training and validating a deep convolutional neural network for computer-aided
2002 detection and classification of abnormalities on frontal chest radiographs," Investigative
2003 radiology **52**, 281-287 (2017).
- 2004 179. P. Lakhani and B. Sundaram, "Deep Learning at Chest Radiography: Automated
2005 Classification of Pulmonary Tuberculosis by Using Convolutional Neural Networks,"
2006 Radiology **284**, 574-582 (2017).
- 2007 180. X. Wang, Y. Peng, L. Lu, Z. Lu, M. Bagheri and R. M. Summers, "Chestx-ray8:
2008 Hospital-scale chest x-ray database and benchmarks on weakly-supervised classification
2009 and localization of common thorax diseases," 2017 IEEE Conference on Computer
2010 Vision and Pattern Recognition (CVPR), 3462-3471, 2017.
- 2011 181. Y. Bar, I. Diamant, L. Wolf and H. Greenspan, "Deep learning with non-medical training
2012 used for chest pathology identification," in Proc. SPIE Medical Imaging, Vol. 9414,
2013 edited by L. M. Hadjiiski and G. D. Tourassi (2015), pp. 94140V.
- 2014 182. T. Nakao, S. Hanaoka, Y. Nomura, I. Sato, M. Nemoto, S. Miki, E. Maeda, T.
2015 Yoshikawa, N. Hayashi and O. Abe, "Deep neural network - based computer - assisted
2016 detection of cerebral aneurysms in MR angiography," Journal of Magnetic Resonance
2017 Imaging **47**, 948-953 (2018).
- 2018 183. M. U. Dalmiş, S. Vreemann, T. Kooi, R. M. Mann, N. Karssemeijer and A. Gubern-
2019 Mérida, "Fully automated detection of breast cancer in screening MRI using
2020 convolutional neural networks," Journal of Medical Imaging **5**, 014502 (2018).

- 2021 184. J. Liu, D. Wang, L. Lu, Z. Wei, L. Kim, E. B. Turkbey, B. Sahiner, N. Petrick and R. M.
 2022 Summers, "Detection and diagnosis of colitis on computed tomography using deep
 2023 convolutional neural networks," *Med Phys* **44**, 4630-4642 (2017).
- 2024 185. J. J. Nappi, P. Pickhardt, D. H. Kim, T. Hironaka and H. Yoshida, "Deep learning of
 2025 contrast-coated serrated polyps for computer-aided detection in CT colonography," in
 2026 *Medical Imaging 2017: Computer-Aided Diagnosis*, Vol. 10134, edited by S. G. Armato
 2027 and N. A. Petrick (2017).
- 2028 186. H. R. Roth, L. Lu, A. Seff, K. M. Cherry, J. Hoffman, S. J. Wang, J. M. Liu, E. Turkbey
 2029 and R. M. Summers, "A New 2.5D Representation for Lymph Node Detection Using
 2030 Random Sets of Deep Convolutional Neural Network Observations," *International
 2031 Conference on Medical Image Computing and Computer-Assisted Intervention
 2032 (MICCAI)*, 520-527, 2014.
- 2033 187. R. Vivanti, A. Szeskin, N. Lev-Cohain, J. Sosna and L. Joskowicz, "Automatic detection
 2034 of new tumors and tumor burden evaluation in longitudinal liver CT scan studies,"
 2035 *International journal of computer assisted radiology and surgery* **12**, 1945-1957 (2017).
- 2036 188. J. Ma, F. Wu, T. a. Jiang, J. Zhu and D. Kong, "Cascade convolutional neural networks
 2037 for automatic detection of thyroid nodules in ultrasound images," *Med Phys* **44**, 1678-
 2038 1691 (2017).
- 2039 189. Y. Tsehay, N. Lay, X. Wang, J. T. Kwak, B. Turkbey, P. Choyke, P. Pinto, B. Wood and
 2040 R. M. Summers, "Biopsy-guided learning with deep convolutional neural networks for
 2041 Prostate Cancer detection on multiparametric MRI," *Biomedical Imaging (ISBI 2017),
 2042 2017 IEEE 14th International Symposium on*, 642-645, 2017.
- 2043 190. J. Liu, K. Chellamuthu, L. Lu, M. Bagheri and R. M. Summers, "A coarse-to-fine
 2044 approach for pericardial effusion localization and segmentation in chest CT scans," in
 2045 *Proc. SPIE Medical Imaging*, Vol. 10575, edited by N. Petrick and K. Mori (2018), pp.
 2046 105753B.
- 2047 191. K. Chellamuthu, J. Liu, J. Yao, M. Bagheri, L. Lu, V. Sandfort and R. M. Summers,
 2048 "Atherosclerotic vascular calcification detection and segmentation on low dose computed
 2049 tomography scans using convolutional neural networks," *Biomedical Imaging (ISBI
 2050 2017), 2017 IEEE 14th International Symposium on*, 388-391, 2017.
- 2051 192. H. Li, M. L. Giger, B. Q. Huynh and N. O. Antropova, "Deep learning in breast cancer
 2052 risk assessment: evaluation of convolutional neural networks on a clinical dataset of full-
 2053 field digital mammograms," *J Med Imaging (Bellingham)* **4**, 041304 (2017).
- 2054 193. A. A. Mohamed, W. A. Berg, H. Peng, Y. Luo, R. C. Jankowitz and S. Wu, "A deep
 2055 learning method for classifying mammographic breast density categories," *Med Phys* **45**,
 2056 314-321 (2018).
- 2057 194. S. F. Li, J. Wei, H. P. Chan, M. A. Helvie, M. A. Roubidoux, Y. Lu, C. Zhou, L. M.
 2058 Hadjiiski and R. K. Samala, "Computer-aided assessment of breast density: comparison
 2059 of supervised deep learning and feature-based statistical learning," *Phys Med Biol* **63**
 2060 (2018).
- 2061 195. J. Lee and R. M. Nishikawa, "Automated mammographic breast density estimation using
 2062 a fully convolutional network," *Med Phys* **45**, 1178-1190 (2018).
- 2063 196. B. Q. Huynh, H. Li and M. L. Giger, "Digital mammographic tumor classification using
 2064 transfer learning from deep convolutional neural networks," *J Med Imaging (Bellingham)*
 2065 **3**, 034501 (2016).

- 2066 197. N. Antropova, B. Q. Huynh and M. L. Giger, "A deep feature fusion methodology for
2067 breast cancer diagnosis demonstrated on three imaging modality datasets," *Med Phys* **44**,
2068 5162-5171 (2017).
- 2069 198. R. K. Samala, H. P. Chan, L. M. Hadjiiski, M. A. Helvie, C. Richter and K. Cha,
2070 "Evolutionary pruning of transfer learned deep convolutional neural network for breast
2071 cancer diagnosis in digital breast tomosynthesis," *Phys Med Biol* (2018).
- 2072 199. R. K. Samala, H. P. Chan, L. M. Hadjiiski, M. A. Helvie, K. H. Cha and C. D. Richter,
2073 "Multi-task transfer learning deep convolutional neural network: application to computer-
2074 aided diagnosis of breast cancer on mammograms," *Phys Med Biol* **62**, 8894-8908
2075 (2017).
- 2076 200. N. Antropova, H. Abe and M. L. Giger, "Use of clinical MRI maximum intensity
2077 projections for improved breast lesion classification with deep convolutional neural
2078 networks," *J Med Imaging (Bellingham)* **5**, 014503 (2018).
- 2079 201. N. Antropova, B. Huynh and M. L. Giger, "Long short-term memory networks for
2080 efficient breast DCE-MRI classification," in *NIPS: Neural Information Processing
2081 Systems, Medical Imaging Meets NIPS*, (2017).
- 2082 202. T. Kooi, B. van Ginneken, N. Karssemeijer and A. den Heeten, "Discriminating solitary
2083 cysts from soft tissue lesions in mammography using a pretrained deep convolutional
2084 neural network," *Med Phys* **44**, 1017-1027 (2017).
- 2085 203. B. B. Shi, L. J. Grimm, M. A. Mazurowski, J. A. Baker, J. R. Marks, L. M. King, C. C.
2086 Maley, E. S. Hwang and J. Y. Lo, "Prediction of Occult Invasive Disease in Ductal
2087 Carcinoma in Situ Using Deep Learning Features," *Journal of the American College of
2088 Radiology* **15**, 527-534 (2018).
- 2089 204. A. Nibali, Z. He and D. Wollersheim, "Pulmonary nodule classification with deep
2090 residual networks," *International Journal of Computer Assisted Radiology and Surgery*
2091 **12**, 1799-1808 (2017).
- 2092 205. T. Schlegl, J. Ofner and G. Langs, "Unsupervised Pre-training Across Image Domains
2093 Improves Lung Tissue Classification," *Medical Computer Vision: Algorithms for Big
2094 Data*, 82-93, 2014.
- 2095 206. M. Gao, U. Bagci, L. Lu, A. Wu, M. Buty, H.-C. Shin, H. Roth, G. Z. Papadakis, A.
2096 Depeursinge and R. M. Summers, "Holistic classification of CT attenuation patterns for
2097 interstitial lung diseases via deep convolutional neural networks," *Computer Methods in
2098 Biomechanics and Biomedical Engineering: Imaging & Visualization* **6**, 1-6 (2018).
- 2099 207. M. Anthimopoulos, S. Christodoulidis, L. Ebner, A. Christe and S. Mougiakakou, "Lung
2100 Pattern Classification for Interstitial Lung Diseases Using a Deep Convolutional Neural
2101 Network," *IEEE Transactions on Medical Imaging* **35**, 1207-1216 (2016).
- 2102 208. G. B. Kim, K. H. Jung, Y. Lee, H. J. Kim, N. Kim, S. Jun, J. B. Seo and D. A. Lynch,
2103 "Comparison of Shallow and Deep Learning Methods on Classifying the Regional
2104 Pattern of Diffuse Lung Disease," *J Digit Imaging* (2017).
- 2105 209. S. Christodoulidis, M. Anthimopoulos, L. Ebner, A. Christe and S. Mougiakakou,
2106 "Multisource Transfer Learning With Convolutional Neural Networks for Lung Pattern
2107 Analysis," *IEEE J Biomed Health Inform* **21**, 76-84 (2017).
- 2108 210. A. Masood, B. Sheng, P. Li, X. H. Hou, X. E. Wei, J. Qin and D. G. Feng, "Computer-
2109 Assisted Decision Support System in Pulmonary Cancer detection and stage classification
2110 on CT images," *Journal of Biomedical Informatics* **79**, 117-128 (2018).

- 2111 211. G. Gonzalez, S. Y. Ash, G. Vegas-Sanchez-Ferrero, J. O. Onieva, F. N. Rahaghi, J. C.
 2112 Ross, A. Diaz, R. S. J. Estepar, G. R. Washko, Copdgene and E. Investigator, "Disease
 2113 Staging and Prognosis in Smokers Using Deep Learning in Chest Computed
 2114 Tomography," *American Journal of Respiratory and Critical Care Medicine* **197**, 193-203
 2115 (2018).
- 2116 212. N. Lessmann, B. van Ginneken, M. Zreik, P. A. de Jong, B. D. de Vos, M. A. Viergever
 2117 and I. Isgum, "Automatic Calcium Scoring in Low-Dose Chest CT Using Deep Neural
 2118 Networks With Dilated Convolutions," *IEEE Transactions on Medical Imaging* **37**, 615-
 2119 625 (2018).
- 2120 213. W. F. Xue, G. Brahm, S. Pandey, S. Leung and S. Li, "Full left ventricle quantification
 2121 via deep multitask relationships learning," *Medical Image Analysis* **43**, 54-65 (2018).
- 2122 214. P. M. Cheng and H. S. Malhi, "Transfer Learning with Convolutional Neural Networks
 2123 for Classification of Abdominal Ultrasound Images," *Journal of Digital Imaging* **30**, 234-
 2124 243 (2017).
- 2125 215. M. Frid-Adar, E. Klang, M. Amitai, J. Goldberger and H. Greenspan, "Synthetic Data
 2126 Augmentation using GAN for Improved Liver Lesion Classification," *IEEE International
 2127 Symposium on Biomedical Imaging*, 2018.
- 2128 216. K. Yasaka, H. Akai, O. Abe and S. Kiryu, "Deep Learning with Convolutional Neural
 2129 Network for Differentiation of Liver Masses at Dynamic Contrast-enhanced CT: A
 2130 Preliminary Study," *Radiology* **286**, 899-908 (2018).
- 2131 217. R. Bharath and P. Rajalakshmi, "Deep Scattering Convolution Network based Features
 2132 for Ultrasonic Fatty Liver Tissue Characterization," in *2017 39th Annual International
 2133 Conference of the IEEE Engineering in Medicine and Biology Society*, (2017), pp. 1982-
 2134 1985.
- 2135 218. J. Lao, Y. Chen, Z. C. Li, Q. Li, J. Zhang, J. Liu and G. Zhai, "A Deep Learning-Based
 2136 Radiomics Model for Prediction of Survival in Glioblastoma Multiforme," *Sci Rep* **7**,
 2137 10353 (2017).
- 2138 219. D. B. Larson, M. C. Chen, M. P. Lungren, S. S. Halabi, N. V. Stence and C. P. Langlotz,
 2139 "Performance of a Deep-Learning Neural Network Model in Assessing Skeletal Maturity
 2140 on Pediatric Hand Radiographs," *Radiology* **287**, 313-322 (2018).
- 2141 220. H. Li, Y. Zhu, E. S. Burnside, E. Huang, K. Drukker, K. A. Hoadley, C. Fan, S. D.
 2142 Conzen, M. Zuley, J. M. Net, E. Sutton, G. J. Whitman, E. Morris, C. M. Perou, Y. Ji and
 2143 M. L. Giger, "Quantitative MRI radiomics in the prediction of molecular classifications
 2144 of breast cancer subtypes in the TCGA/TCIA data set," *NPJ Breast Cancer* **2** (2016).
- 2145 221. E. S. Burnside, K. Drukker, H. Li, E. Bonaccio, M. Zuley, M. Ganott, J. M. Net, E. J.
 2146 Sutton, K. R. Brandt, G. J. Whitman, S. D. Conzen, L. Lan, Y. Ji, Y. T. Zhu, C. C. Jaffe,
 2147 E. P. Huang, J. B. Freymann, J. S. Kirby, E. A. Morris and M. L. Giger, "Using
 2148 computer-extracted image phenotypes from tumors on breast magnetic resonance
 2149 imaging to predict breast cancer pathologic stage," *Cancer* **122**, 748-757 (2016).
- 2150 222. Y. T. Zhu, H. Li, W. T. Guo, K. Drukker, L. Lan, M. L. Giger and Y. Ji, "Deciphering
 2151 Genomic Underpinnings of Quantitative MRI-based Radiomic Phenotypes of Invasive
 2152 Breast Carcinoma," *Sci Rep* **5** (2015).
- 2153 223. H. Li, Y. T. Zhu, E. S. Burnside, K. Drukker, K. A. Hoadley, C. Fan, S. D. Conzen, G. J.
 2154 Whitman, E. J. Sutton, J. M. Net, M. Ganott, E. Huang, E. A. Morris, C. M. Perou, Y. Ji
 2155 and M. L. Giger, "MR Imaging Radiomics Signatures for Predicting the Risk of Breast

- 2156 Cancer Recurrence as Given by Research Versions of MammaPrint, Oncotype DX, and
 2157 PAM50 Gene Assays," *Radiology* **281**, 382-391 (2016).
- 2158 224. W. Guo, H. Li, Y. Zhu, L. Lan, S. Yang, K. Drukker, E. Morris, E. Burnside, G.
 2159 Whitman, M. L. Giger and Y. Ji, "Prediction of clinical phenotypes in invasive breast
 2160 carcinomas from the integration of radiomics and genomics data," *J Med Imaging*
 2161 (Bellingham) **2**, 041007 (2015).
- 2162 225. W. Q. Sun, T. L. Tseng, J. Y. Zhang and W. Qian, "Enhancing deep convolutional neural
 2163 network scheme for breast cancer diagnosis with unlabeled data," *Computerized Medical*
 2164 *Imaging and Graphics* **57**, 4-9 (2017).
- 2165 226. A. R. Jamieson, M. L. Giger, K. Drukker and L. L. Pesce, "Enhancement of breast CADx
 2166 with unlabeled data," *Med Phys* **37**, 4155-4172 (2010).
- 2167 227. S. Katsuragawa, K. Doi, H. MacMahon, L. MonnierCholley, T. Ishida and T. Kobayashi,
 2168 "Classification of normal and abnormal lungs with interstitial diseases by rule-based
 2169 method and artificial neural networks," *Journal of Digital Imaging* **10**, 108-114 (1997).
- 2170 228. B. van Ginneken, S. Katsuragawa, B. M. T. Romeny, K. Doi and M. A. Viergever,
 2171 "Automatic detection of abnormalities in chest radiographs using local texture analysis,"
 2172 *IEEE Transactions on Medical Imaging* **21**, 139-149 (2002).
- 2173 229. H. Li, M. L. Giger, L. Lan, J. Bancroft Brown, A. MacMahon, M. Mussman, O. I.
 2174 Olopade and C. Sennett, "Computerized analysis of mammographic parenchymal patterns
 2175 on a large clinical dataset of full-field digital mammograms: robustness study with two
 2176 high-risk datasets," *J Digit Imaging* **25**, 591-8 (2012).
- 2177 230. H. He, X. Yang, L. Wu, H. Yan, Z. Gao, Y. Feng and G. Townsend, "Dual Long Short-
 2178 Term Memory Networks for Sub-Character Representation Learning," arXiv:1712.08841
 2179 (2018).
- 2180 231. S. S. Garapati, L. Hadjiiski, K. H. Cha, H. P. Chan, E. M. Caoili, R. H. Cohan, A.
 2181 Weizer, A. Alva, C. Paramagul, J. Wei and C. A. Zhou, "Urinary bladder cancer staging
 2182 in CT urography using machine learning," *Med Phys* **44**, 5814-5823 (2017).
- 2183 232. M. Henglin, G. Stein, P. V. Hushcha, J. Snoek, A. B. Wiltschko and S. Cheng, "Machine
 2184 Learning Approaches in Cardiovascular Imaging," *Circulation-Cardiovascular Imaging*
 2185 **10** (2017).
- 2186 233. L. Zhang, L. Lu, R. M. Summers, E. Kebebew and J. Yao, "Convolutional Invasion and
 2187 Expansion Networks for Tumor Growth Prediction," *IEEE transactions on medical*
 2188 *imaging* **37**, 638-648 (2018).
- 2189 234. K. Suzuki, "A supervised 'lesion-enhancement' filter by use of a massive-training
 2190 artificial neural network (MTANN) in computer-aided diagnosis (CAD)," *Phys Med Biol*
 2191 **54**, S31-45 (2009).
- 2192 235. W. Yang, Y. Y. Chen, Y. B. Liu, L. M. Zhong, G. G. Qin, Z. T. Lu, Q. J. Feng and W. F.
 2193 Chen, "Cascade of multi-scale convolutional neural networks for bone suppression of
 2194 chest radiographs in gradient domain," *Medical Image Analysis* **35**, 421-433 (2017).
- 2195 236. S. Mori, "Deep architecture neural network-based real-time image processing for image-
 2196 guided radiotherapy," *Physica Medica-European Journal of Medical Physics* **40**, 79-87
 2197 (2017).
- 2198 237. H. Chen, Y. Zhang, W. Zhang, P. Liao, K. Li, J. Zhou and G. Wang, "Low-dose CT via
 2199 convolutional neural network," *Biomed Opt Express* **8**, 679-694 (2017).

- 2200 238. H. Chen, Y. Zhang, M. K. Kalra, F. Lin, Y. Chen, P. Liao, J. Zhou and G. Wang, "Low-
2201 Dose CT With a Residual Encoder-Decoder Convolutional Neural Network," *IEEE*
2202 *Transactions on Medical Imaging* **36**, 2524-2535 (2017).
- 2203 239. E. Kang, J. Min and J. C. Ye, "A deep convolutional neural network using directional
2204 wavelets for low-dose X-ray CT reconstruction," *Med Phys* **44**, e360-e375 (2017).
- 2205 240. X. Yang, V. De Andrade, W. Scullin, E. L. Dyer, N. Kasthuri, F. De Carlo and D.
2206 Gursoy, "Low-dose x-ray tomography through a deep convolutional neural network," *Sci*
2207 *Rep* **8**, 2575 (2018).
- 2208 241. L. Xiang, Y. Qiao, D. Nie, L. An, Q. Wang and D. Shen, "Deep Auto-context
2209 Convolutional Neural Networks for Standard-Dose PET Image Estimation from Low-
2210 Dose PET/MRI," *Neurocomputing* **267**, 406-416 (2017).
- 2211 242. K. H. Jin, M. T. McCann, E. Froustey and M. Unser, "Deep Convolutional Neural
2212 Network for Inverse Problems in Imaging," *IEEE Transactions on Image Processing* **26**,
2213 4509-4522 (2017).
- 2214 243. Y. B. Zhang, Y. Chu and H. Y. Yu, "Reduction of metal artifacts in x-ray CT images
2215 using a convolutional neural network," in *Developments in X-Ray Tomography Xi*, Vol.
2216 10391, edited by B. Muller and G. Wang (2017).
- 2217 244. Y. Han, J. Yoo, H. H. Kim, H. J. Shin, K. Sung and J. C. Ye, "Deep learning with domain
2218 adaptation for accelerated projection-reconstruction MR," *Magn Reson Med* (2018).
- 2219 245. V. Golkov, A. Dosovitskiy, J. I. Sper, M. I. Menzel, M. Czisch, P. Samann, T. Brox and
2220 D. Cremers, "q-Space Deep Learning: Twelve-Fold Shorter and Model-Free Diffusion
2221 MRI Scans," *IEEE Transactions on Medical Imaging* **35**, 1344-1351 (2016).
- 2222 246. K. Hammernik, T. Klatzer, E. Kobler, M. P. Recht, D. K. Sodickson, T. Pock and F.
2223 Knoll, "Learning a variational network for reconstruction of accelerated MRI data,"
2224 *Magn Reson Med* **79**, 3055-3071 (2018).
- 2225 247. J. Schlemper, J. Caballero, J. V. Hajnal, A. N. Price and D. Rueckert, "A Deep Cascade
2226 of Convolutional Neural Networks for Dynamic MR Image Reconstruction," *IEEE*
2227 *Transactions on Medical Imaging* **37**, 491-503 (2018).
- 2228 248. B. Zhu, J. Z. Liu, S. F. Cauley, B. R. Rosen and M. S. Rosen, "Image reconstruction by
2229 domain-transform manifold learning," *Nature* **555**, 487-492 (2018).
- 2230 249. G. Wu, M. Kim, Q. Wang, Y. Gao, S. Liao and D. Shen, "Unsupervised deep feature
2231 learning for deformable registration of MR brain images," *International Conference on*
2232 *Medical Image Computing and Computer-Assisted Intervention (MICCAI)*, 649-56, 2013.
- 2233 250. G. Wu, M. Kim, Q. Wang, B. C. Munsell and D. Shen, "Scalable High-Performance
2234 Image Registration Framework by Unsupervised Deep Feature Representations
2235 Learning," *IEEE Trans Biomed Eng* **63**, 1505-16 (2016).
- 2236 251. X. Yang, R. Kwitt, M. Styner and M. Niethammer, "Quicksilver: Fast predictive image
2237 registration - A deep learning approach," *Neuroimage* **158**, 378-396 (2017).
- 2238 252. J. Lv, M. Yang, J. Zhang and X. Y. Wang, "Respiratory motion correction for free-
2239 breathing 3D abdominal MRI using CNN-based image registration: a feasibility study,"
2240 *British Journal of Radiology* **91**, 9 (2018).
- 2241 253. S. Miao, Z. J. Wang and R. Liao, "A CNN Regression Approach for Real-Time 2D/3D
2242 Registration," *IEEE Transactions on Medical Imaging* **35**, 1352-1363 (2016).
- 2243 254. J. Zheng, S. Miao, Z. Jane Wang and R. Liao, "Pairwise domain adaptation module for
2244 CNN-based 2-D/3-D registration," *J Med Imaging (Bellingham)* **5**, 021204 (2018).

- 2245 255. D. Nie, X. Cao, Y. Gao, L. Wang and D. Shen, "Estimating CT Image from MRI Data
2246 Using 3D Fully Convolutional Networks," *Deep Learn Data Label Med Appl* (2016)
2247 **2016**, 170-178 (2016).
- 2248 256. X. Han, "MR-based synthetic CT generation using a deep convolutional neural network
2249 method," *Med Phys* **44**, 1408-1419 (2017).
- 2250 257. A. P. Leynes, J. Yang, F. Wiesinger, S. S. Kaushik, D. D. Shanbhag, Y. Seo, T. A. Hope
2251 and P. E. Z. Larson, "Direct PseudoCT Generation for Pelvis PET/MRI Attenuation
2252 Correction using Deep Convolutional Neural Networks with Multi-parametric MRI: Zero
2253 Echo-time and Dixon Deep pseudoCT (ZeDD-CT)," *J Nucl Med* (2017).
- 2254 258. F. Liu, H. Jang, R. Kijowski, T. Bradshaw and A. B. McMillan, "Deep Learning MR
2255 Imaging-based Attenuation Correction for PET/MR Imaging," *Radiology* **286**, 676-684
2256 (2018).
- 2257 259. D. Nie, R. Trullo, J. Lian, C. Petitjean, S. Ruan, Q. Wang and D. Shen, "Medical image
2258 synthesis with context-aware generative adversarial networks," *International Conference
2259 on Medical Image Computing and Computer-Assisted Intervention (MICCAI)*, 417-425,
2260 2017.
- 2261 260. H. Choi and D. S. Lee, "Generation of structural MR images from amyloid PET:
2262 Application to MR-less quantification," *J Nucl Med* (2017).
- 2263 261. A. Ben-Cohen, E. Klang, S. P. Raskin, M. M. Amitai and H. Greenspan, "Virtual PET
2264 Images from CT Data Using Deep Convolutional Networks: Initial Results,"
2265 *International Workshop on Simulation and Synthesis in Medical Imaging*, 49-57, 2017.
- 2266 262. L. Wu, J. Z. Cheng, S. Li, B. Lei, T. Wang and D. Ni, "FUIQA: Fetal Ultrasound Image
2267 Quality Assessment With Deep Convolutional Networks," *IEEE Transactions on
2268 Cybernetics* **47**, 1336-1349 (2017).
- 2269 263. J. Neylon, Y. G. Min, D. A. Low and A. Santhanam, "A neural network approach for
2270 fast, automated quantification of DIR performance," *Med Phys* **44**, 4126-4138 (2017).
- 2271 264. J. H. Lee, B. R. Grant, J. H. Chung, I. Reiser and M. L. Giger, "Assessment of diagnostic
2272 image quality of computed tomography (CT) images of the lung using deep learning," in
2273 *Proc. SPIE Medical Imaging*, Vol. 10573, (2018), pp. 105731M
- 2274 265. S. J. Esses, X. Lu, T. Zhao, K. Shanbhogue, B. Dane, M. Bruno and H. Chandarana,
2275 "Automated image quality evaluation of T2 -weighted liver MRI utilizing deep learning
2276 architecture," *J Magn Reson Imaging* **47**, 723-728 (2018).
- 2277 266. C. McCollough, "Low Dose CT Grand Challenge, the Mayo Clinic, the American
2278 Association of Physicists in Medicine, and grants EB017095 and grants EB017185 from
2279 the National Institute of Biomedical Imaging and Bioengineering," (2016).
- 2280 267. G. Delso, F. Wiesinger, L. I. Sacolick, S. S. Kaushik, D. D. Shanbhag, M. Hullner and P.
2281 Veit-Haibach, "Clinical Evaluation of Zero-Echo-Time MR Imaging for the
2282 Segmentation of the Skull," *Journal of Nuclear Medicine* **56**, 417-422 (2015).
- 2283 268. K. H. Cha, L. Hadjiiski, H. P. Chan, A. Z. Weizer, A. Alva, R. H. Cohan, E. M. Caoili, C.
2284 Paramagul and R. K. Samala, "Bladder Cancer Treatment Response Assessment in CT
2285 using Radiomics with Deep-Learning," *Sci Rep* **7** (2017).
- 2286 269. A. Nielsen, M. B. Hansen, A. Tietze and K. Mouridsen, "Prediction of Tissue Outcome
2287 and Assessment of Treatment Effect in Acute Ischemic Stroke Using Deep Learning,"
2288 *Stroke* **49**, 1394-1401 (2018).
- 2289 270. B. Q. Huynh, N. Antropova and M. L. Giger, "Comparison of Breast DCE-MRI Contrast
2290 Time Points for Predicting Response to Neoadjuvant Chemotherapy Using Deep

- 2291 Convolutional Neural Network Features with Transfer Learning," in Proc. SPIE Medical
 2292 Imaging, Vol. 10134, edited by S. G. Armato and N. A. Petrick (2017), pp. 101340U
 2293 271. K. Ravichandran, N. Braman, A. Janowczyk and A. Madabhushi, "A deep learning
 2294 classifier for prediction of pathological complete response to neoadjuvant chemotherapy
 2295 from baseline breast DCE-MRI," in Medical Imaging 2018: Computer-Aided Diagnosis,
 2296 Vol. 10575, edited by N. Petrick and K. Mori (2018).
 2297 272. K. Men, P. Boimel, J. Janopaul-Naylor, H. Zhong, M. Huang, H. Geng, C. Cheng, Y.
 2298 Fan, J. P. Plastaras, E. Ben-Josef and Y. Xiao, "Cascaded atrous convolution and spatial
 2299 pyramid pooling for more accurate tumor target segmentation for rectal cancer
 2300 radiotherapy," *Phys Med Biol* (2018).
 2301 273. M. Q. Ding, L. J. Chen, G. F. Cooper, J. D. Young and X. H. Lu, "Precision Oncology
 2302 beyond Targeted Therapy: Combining Omics Data with Machine Learning Matches the
 2303 Majority of Cancer Cells to Effective Therapeutics," *Molecular Cancer Research* **16**, 269-
 2304 278 (2018).
 2305 274. N. Tong, S. Gou, S. Yang, D. Ruan and K. Sheng, "Fully Automatic Multi-Organ
 2306 Segmentation for Head and Neck Cancer Radiotherapy Using Shape Representation
 2307 Model Constrained Fully Convolutional Neural Networks," *Med Phys* (2018).
 2308 275. P. Jackson, N. Hardcastle, N. Dawe, T. Kron, M. S. Hofman and R. J. Hicks, "Deep
 2309 Learning Renal Segmentation for Fully Automated Radiation Dose Estimation in
 2310 Unsealed Source Therapy," *Front Oncol* **8**, 215 (2018).
 2311 276. M. Shehata, F. Khalifa, A. Soliman, M. Ghazal, F. Taher, M. Abou El-Ghar, A. Dwyer,
 2312 G. Gimel'farb, R. Keynton and A. El-Baz, "Computer-Aided Diagnostic System for Early
 2313 Detection of Acute Renal Transplant Rejection Using Diffusion-Weighted MRI," *IEEE*
 2314 *Trans Biomed Eng* (2018).
 2315 277. B. Ibragimov, D. Toesca, D. Chang, Y. Yuan, A. Koong and L. Xing, "Development of
 2316 deep neural network for individualized hepatobiliary toxicity prediction after liver
 2317 SBRT," *Med Phys* (2018).
 2318 278. H. H. Tseng, Y. Luo, S. Cui, J. T. Chien, R. K. Ten Haken and I. El Naqa, "Deep
 2319 reinforcement learning for automated radiation adaptation in lung cancer," *Med Phys* **44**,
 2320 6690-6705 (2017).
 2321 279. M. D. Foote, B. Zimmerman, A. Sawant and S. Joshi, "Real-Time Patient-Specific Lung
 2322 Radiotherapy Targeting using Deep Learning," in International Conference on Medical
 2323 Imaging with Deep Learning (MIDL), (2018).
 2324 280. D. Nguyen, T. Long, X. Jia, W. Lu, X. Gu, Z. Iqbal and S. Jiang, "Dose prediction with
 2325 U-Net: a feasibility study for predicting dose distributions from contours using deep
 2326 learning on prostate IMRT patients," arXiv:1709.09233 (2017).
 2327 281. T. Kajikawa, N. Kadoya, K. Ito, Y. Takayama, T. Chiba, S. Tomori, K. Takeda and K.
 2328 Jingu, "Automated prediction of dosimetric eligibility of patients with prostate cancer
 2329 undergoing intensity-modulated radiation therapy using a convolutional neural network,"
 2330 *Radiol Phys Technol* **11**, 320-327 (2018).
 2331 282. M. Maspero, M. H. G. Savenije, A. M. Dinkla, P. R. Seevinck, M. P. W. Intven, I. M.
 2332 Jurgenliemk-Schulz, L. G. W. Kerkmeijer and C. A. T. van den Berg, "Fast synthetic CT
 2333 generation with deep learning for general pelvis MR-only Radiotherapy,"
 2334 arXiv:1802.06468 (2018).
 2335 283. X. Zhen, J. W. Chen, Z. C. Zhong, B. Hrycushko, L. H. Zhou, S. Jiang, K. Albuquerque
 2336 and X. J. Gu, "Deep convolutional neural network with transfer learning for rectum

- 2337 toxicity prediction in cervical cancer radiotherapy: a feasibility study," *Phys Med Biol*
 2338 **62**, 8246-8263 (2017).
- 2339 284. J. E. Bibault, P. Giraud, C. Durdux, J. Taieb, A. Berger, R. Coriat, S. Chaussade, B.
 2340 Dousset, B. Nordlinger and A. Burgun, "Deep Learning and Radiomics predict complete
 2341 response after neo-adjuvant chemoradiation for locally advanced rectal cancer," *Sci Rep*
 2342 **8**, 12611 (2018).
- 2343 285. M. L. Giger, "Machine Learning in Medical Imaging," *Journal of the American College*
 2344 *of Radiology* **15**, 512-520 (2018).
- 2345 286. K. Men, T. Zhang, X. Chen, B. Chen, Y. Tang, S. Wang, Y. Li and J. Dai, "Fully
 2346 automatic and robust segmentation of the clinical target volume for radiotherapy of breast
 2347 cancer using big data and deep learning," *Phys Med* **50**, 13-19 (2018).
- 2348 287. M. Everingham, S. M. A. Eslami, L. Van Gool, C. Williams, J. Winn and A. Zisserman,
 2349 "The Pascal Visual Object Classes Challenge: A Retrospective," *International journal of*
 2350 *computer vision* **111**, 98-136 (2015).
- 2351 288. T.-Y. Lin, M. Maire, S. Belongie, J. Hays, P. Perona, D. Ramanan, P. Dollár and C. L.
 2352 Zitnick, "Microsoft coco: Common objects in context," *European conference on*
 2353 *computer vision*, 740-755, 2014.
- 2354 289. A. Karpathy and L. Fei-Fei, "Deep Visual-Semantic Alignments for Generating Image
 2355 Descriptions," *IEEE transactions on pattern analysis and machine intelligence* **39**, 664-
 2356 676 (2017).
- 2357 290. H. Nam, J.-W. Ha and J. Kim, "Dual attention networks for multimodal reasoning and
 2358 matching," *The IEEE Conference on Computer Vision and Pattern Recognition (CVPR)*,
 2359 299-307, 2017.
- 2360 291. B. Dai, Y. Zhang and D. Lin, "Detecting Visual Relationships with Deep Relational
 2361 Networks," *The IEEE Conference on Computer Vision and Pattern Recognition (CVPR)*,
 2362 3076-3086, 2017.
- 2363 292. F. Dyson, "A meeting with Enrico Fermi," *Nature* **427**, 297 (2004).
- 2364 293. H. Mhaskar, Q. Liao and T. A. Poggio, "When and why are deep networks better than
 2365 shallow ones?," *Proceedings of the Thirty-First AAAI Conference on Artificial*
 2366 *Intelligence*, 2343--2349, San Francisco, CA, 2017.
- 2367 294. R. Schwartz-Ziv and N. Tishby, "Opening the black box of deep neural networks via
 2368 information," *arXiv:1703.00810* (2017).
- 2369 295. I. Goodfellow, Y. Bengio, A. Courville, G. I, I. Goodfellow, Y. Bengio and A. Courville,
 2370 "Regularization for Deep Learning," *Deep Learning*, 221-265 (2016).
- 2371 296. J. Prechelt, *Early stopping - But when?* (Springer Berlin Heidelberg, Berlin, Heidelberg,
 2372 2012).
- 2373 297. K. Fukunaga and R. R. Hayes, "Effects of sample size in classifier design," *IEEE*
 2374 *Transactions on Pattern Analysis and Machine Intelligence* **11**, 873-885 (1989).
- 2375 298. R. F. Wagner, H.-P. Chan, B. Sahiner, N. Petrick and J. T. Mossoba, "Finite-sample
 2376 effects and resampling plans: applications to linear classifiers in computer-aided
 2377 diagnosis," *Medical Imaging 1997: Image Processing*, 467-478, 1997.
- 2378 299. H. P. Chan, B. Sahiner, R. F. Wagner and N. Petrick, "Classifier design for computer -
 2379 aided diagnosis: Effects of finite sample size on the mean performance of classical and
 2380 neural network classifiers," *Med Phys* **26**, 2654-2668 (1999).

- 2381 300. B. Sahiner, H. P. Chan, N. Petrick, R. F. Wagner and L. Hadjiiski, "Feature selection and
2382 classifier performance in computer - aided diagnosis: The effect of finite sample size,"
2383 *Med Phys* **27**, 1509-1522 (2000).
- 2384 301. M. A. Kupinski, D. C. Edwards, M. L. Giger and C. E. Metz, "Ideal observer
2385 approximation using Bayesian classification neural networks," *IEEE transactions on*
2386 *medical imaging* **20**, 886-899 (2001).
- 2387 302. J. Cho, K. Lee, E. Shin, G. Choy and S. Do, "How much data is needed to train a medical
2388 image deep learning system to achieve necessary high accuracy?," arXiv:1511.06348
2389 (2015).
- 2390 303. C. Sun, A. Shrivastava, S. Singh and A. Gupta, "Revisiting unreasonable effectiveness of
2391 data in deep learning era," 2017 IEEE International Conference on Computer Vision
2392 (ICCV), 843-852, 2017.
- 2393 304. R. Zhang, Y. Zheng, T. W. C. Mak, R. Yu, S. H. Wong, J. Y. Lau and C. C. Poon,
2394 "Automatic detection and classification of colorectal polyps by transferring low-level
2395 CNN features from nonmedical domain," *IEEE Journal of Biomedical and Health*
2396 *Informatics* **21**, 41-47 (2017).
- 2397 305. B. van Ginneken, A. A. A. Setio, C. Jacobs and F. Ciompi, "Off-the-shelf convolutional
2398 neural network features for pulmonary nodule detection in computed tomography scans,"
2399 in 2015 IEEE 12th International Symposium on Biomedical Imaging, (2015), pp. 286-
2400 289.
- 2401 306. U. K. Lopes and J. F. Valiati, "Pre-trained convolutional neural networks as feature
2402 extractors for tuberculosis detection," *Computers in Biology and Medicine* **89**, 135-143
2403 (2017).
- 2404 307. A. Ben-Cohen, E. Klang, I. Diamant, N. Rozendorn, S. P. Raskin, E. Konen, M. M.
2405 Amitai and H. Greenspan, "CT Image-based Decision Support System for Categorization
2406 of Liver Metastases Into Primary Cancer Sites: Initial Results," *Academic Radiology* **24**,
2407 1501-1509 (2017).
- 2408 308. A. Z. Abidin, B. T. Deng, A. M. Dsouza, M. B. Nagarajan, P. Coan and A. Wismuller,
2409 "Deep transfer learning for characterizing chondrocyte patterns in phase contrast X-Ray
2410 computed tomography images of the human patellar cartilage," *Computers in Biology*
2411 *and Medicine* **95**, 24-33 (2018).
- 2412 309. H. Lee, S. Tajmir, J. Lee, M. Zissen, B. A. Yeshiwas, T. K. Alkasab, G. Choy and S. Do,
2413 "Fully Automated Deep Learning System for Bone Age Assessment," *J Digit Imaging* **30**,
2414 427-441 (2017).
- 2415 310. R. K. Samala, H.-P. Chan, L. Hadjiiski, M. A. Helvie, C. Richter and K. Cha, "Cross-
2416 domain and multi-task transfer learning of deep convolutional neural network for breast
2417 cancer diagnosis in digital breast tomosynthesis," *Medical Imaging 2018: Computer-*
2418 *Aided Diagnosis*, 105750Q, 2018.
- 2419 311. H. C. Shin, M. R. Orton, D. J. Collins, S. J. Doran and M. O. Leach, "Stacked
2420 autoencoders for unsupervised feature learning and multiple organ detection in a pilot
2421 study using 4D patient data," *IEEE Trans Pattern Anal Mach Intell* **35**, 1930-43 (2013).
- 2422 312. S. Wang, Y. Cong, H. Fan, L. Liu, X. Li, Y. Yang, Y. Tang, H. Zhao and H. Yu,
2423 "Computer-Aided Endoscopic Diagnosis Without Human-Specific Labeling," *IEEE*
2424 *Trans Biomed Eng* **63**, 2347-2358 (2016).
- 2425 313. X. Feng, J. Yang, A. F. Laine and E. D. Angelini, "Discriminative Localization in CNNs
2426 for Weakly-Supervised Segmentation of Pulmonary Nodules," *International Conference*

- 2427 on Medical Image Computing and Computer-Assisted Intervention (MICCAI) **10435**,
 2428 568-576 (2017).
- 2429 314. P. Rajpurkar, J. Irvin, K. Zhu, B. Yang, H. Mehta, T. Duan, D. Ding, A. Bagul, C.
 2430 Langlotz and K. Shpanskaya, "CheXNet: Radiologist-Level Pneumonia Detection on
 2431 Chest X-Rays with Deep Learning," arXiv:1711.05225 (2017).
- 2432 315. X. Chen, A. Shrivastava and A. Gupta, "NEIL: Extracting Visual Knowledge from Web
 2433 Data," Proc. of ICCV, 2013.
- 2434 316. J. Zech, M. Pain, J. Titano, M. Badgeley, J. Schefflein, A. Su, A. Costa, J. Bederson, J.
 2435 Lehar and E. K. Oermann, "Natural Language-based Machine Learning Models for the
 2436 Annotation of Clinical Radiology Reports," Radiology **287**, 570-580 (2018).
- 2437 317. M. Ghafoorian, J. Teuwen, R. Manniesing, F.-E. de Leeuw, B. van Ginneken, N.
 2438 Karssemeijer and B. Platel, "Student beats the teacher: deep neural networks for lateral
 2439 ventricles segmentation in brain MR," in Proc. SPIE Medical Imaging, Vol. 10574,
 2440 edited by E. D. Angelini and B. A. Landman (2018), pp. 105742U.
- 2441 318. L. Zhang, V. Gopalakrishnan, L. Lu, R. M. Summers, J. Moss and J. Yao, "Self-learning
 2442 to detect and segment cysts in lung CT images without manual annotation," Biomedical
 2443 Imaging (ISBI 2018), 2018 IEEE 15th International Symposium on, 1100-1103, 2018.
- 2444 319. A. Asperti and C. Mastronardo, "The Effectiveness of Data Augmentation for Detection
 2445 of Gastrointestinal Diseases from Endoscopic Images," the 5th International
 2446 Conference on Bioimaging, 2017.
- 2447 320. A. Pezeshk, N. Petrick, W. Chen and B. Sahiner, "Seamless Lesion Insertion for Data
 2448 Augmentation in CAD Training," IEEE Transactions on Medical Imaging **36**, 1005-1015
 2449 (2017).
- 2450 321. C. Zhang, W. Tavanapong, J. Wong, P. C. de Groen and J. Oh, "Real Data Augmentation
 2451 for Medical Image Classification," 67-76, 2017.
- 2452 322. A. Badano, A. Badal, S. Glick, C. G. Graff, F. Samuelson, D. Sharma and R. P. Zeng, "In
 2453 silico imaging clinical trials for regulatory evaluation: initial considerations for VICTRE,
 2454 a demonstration study," in Proc. SPIE Medical Imaging, Vol. 10132, edited by T. G.
 2455 Flohr, J. Y. Lo and T. G. Schmidt (2017), pp. 1013220.
- 2456 323. J. Cui, X. Liu, Y. Wang and H. Liu, "Deep reconstruction model for dynamic PET
 2457 images," PloS one **12**, e0184667 (2017).
- 2458 324. H.-C. Shin, L. Lu and R. M. Summers, "Natural Language Processing for Large-Scale
 2459 Medical Image Analysis Using Deep Learning," in Deep Learning for Medical Image
 2460 Analysis, (Elsevier, 2017), pp. 405-421.
- 2461 325. T. Schlegl, S. M. Waldstein, W.-D. Vogl, U. Schmidt-Erfurth and G. Langs, "Predicting
 2462 Semantic Descriptions from Medical Images with Convolutional Neural Networks,"
 2463 Information Processing in Medical Imaging, 437-448, 2015.
- 2464 326. H.-C. Shin, K. Roberts, L. Lu, D. Demner-Fushman, J. Yao and R. M. Summers,
 2465 "Learning to read chest x-rays: Recurrent neural cascade model for automated image
 2466 annotation," Proceedings of the IEEE Conference on Computer Vision and Pattern
 2467 Recognition, 2497-2506, 2016.
- 2468 327. X. Wang, L. Lu, H.-C. Shin, L. Kim, M. Bagheri, I. Noguees, J. Yao and R. M. Summers,
 2469 "Unsupervised joint mining of deep features and image labels for large-scale radiology
 2470 image categorization and scene recognition," 2017 IEEE Winter Conference on
 2471 Applications of Computer Vision (WACV), 998-1007, 2017.

- 2472 328. X. Wang, Y. Peng, L. Lu, Z. Lu and R. M. Summers, "TieNet: Text-Image Embedding
2473 Network for Common Thorax Disease Classification and Reporting in Chest X-rays,"
2474 International Conference of Computer Vision and Pattern Recognition, 2018.
- 2475 329. M. C. Chen, R. L. Ball, L. Yang, N. Moradzadeh, B. E. Chapman, D. B. Larson, C. P.
2476 Langlotz, T. J. Amrhein and M. P. Lungren, "Deep Learning to Classify Radiology Free-
2477 Text Reports," *Radiology* **286**, 845-852 (2018).
- 2478 330. K. Yan, X. Wang, L. Lu and R. M. Summers, "DeepLesion: Automated Deep Mining,
2479 Categorization and Detection of Significant Radiology Image Findings using Large-Scale
2480 Clinical Lesion Annotations," arXiv preprint arXiv:1710.01766 (2017).
- 2481 331. K. Yan, X. Wang, L. Lu, L. Zhang, A. Harrison, M. Bagheri and R. Summers, "Deep
2482 Lesion Graphs in the Wild: Relationship Learning and Organization of Significant
2483 Radiology Image Findings in a Diverse Large-scale Lesion Database," International
2484 Conference of Computer Vision and Pattern Recognition, 2018.
- 2485 332. J. E. Bibault, P. Giraud and A. Burgun, "Big Data and machine learning in radiation
2486 oncology: State of the art and future prospects," *Cancer Letters* **382**, 110-117 (2016).
- 2487 333. L. Dai, R. Fang, H. Li, X. Hou, B. Sheng, Q. Wu and W. Jia, "Clinical report guided
2488 retinal microaneurysm detection with multi-sieving deep learning," *IEEE Transactions on*
2489 *Medical Imaging* **37**, 1149-1161 (2018).
- 2490 334. Z. Zhang, P. Chen, M. Sapkota and L. Yang, "TandemNet: Distilling Knowledge from
2491 Medical Images Using Diagnostic Reports as Optional Semantic References,"
2492 International Conference on Medical Image Computing and Computer-Assisted
2493 Intervention (MICCAI), 320-328, 2017.
- 2494 335. A. Top, G. Hamarneh and R. Abugharbieh, "Active Learning for Interactive 3D Image
2495 Segmentation," International Conference on Medical Image Computing and Computer-
2496 Assisted Intervention (MICCAI), 603-610, Berlin, Heidelberg, 2011.
- 2497 336. Y. Zhu, S. Zhang, W. Liu and D. N. Metaxas, "Scalable histopathological image analysis
2498 via active learning," International Conference on Medical Image Computing and
2499 Computer-Assisted Intervention (MICCAI), 369-376, 2014.
- 2500 337. J. M. B. Dwarikanath Mahapatra, "Visual saliency-based active learning for prostate
2501 magnetic resonance imaging segmentation," *Journal of Medical Imaging* **3**, 3-3 (2016).
- 2502 338. J. Lee, Y. Wu and H. Kim, "Unbalanced data classification using support vector
2503 machines with active learning on scleroderma lung disease patterns," *Journal of Applied*
2504 *Statistics* **42**, 676-689 (2015).
- 2505 339. S. C. Hoi, R. Jin, J. Zhu and M. R. Lyu, "Batch mode active learning and its application
2506 to medical image classification," Proceedings of the 23rd international conference on
2507 Machine learning, 417-424, 2006.
- 2508 340. K. Konyushkova, R. Sznitman and P. Fua, "Introducing geometry in active learning for
2509 image segmentation," Proceedings of the IEEE International Conference on Computer
2510 Vision, 2974-2982, 2015.
- 2511 341. L. Yang, Y. Zhang, J. Chen, S. Zhang and D. Z. Chen, "Suggestive annotation: A deep
2512 active learning framework for biomedical image segmentation," International Conference
2513 on Medical Image Computing and Computer-Assisted Intervention (MICCAI), 399-407,
2514 2017.
- 2515 342. Z. Zhou, J. Shin, L. Zhang, S. Gurudu, M. Gotway and J. Liang, "Fine-Tuning
2516 Convolutional Neural Networks for Biomedical Image Analysis: Actively and

- 2517 Incrementally," *Computer Vision and Pattern Recognition (CVPR)*, 2017 IEEE
 2518 Conference on, 4761-4772, 2017.
- 2519 343. U. Gaur, M. Kourakis, E. Newman-Smith, W. Smith and B. S. Manjunath, "Membrane
 2520 segmentation via active learning with deep networks," 2016 IEEE International
 2521 Conference on Image Processing (ICIP), 1943-1947, 2016.
- 2522 344. A. Mosinska-Domanska, R. Sznitman, P. Glowacki and P. Fua, "Active learning for
 2523 delineation of curvilinear structures," *Computer Vision and Pattern Recognition (CVPR)*,
 2524 2016 IEEE Conference on, 5231-5239, 2016.
- 2525 345. T. Heimann, P. Mountney, M. John and R. Ionasec, "Learning without labeling: Domain
 2526 adaptation for ultrasound transducer localization," *International Conference on Medical
 2527 Image Computing and Computer-Assisted Intervention (MICCAI)*, 49-56, 2013.
- 2528 346. C. Wachinger and M. Reuter, "Domain adaptation for Alzheimer's disease diagnostics,"
 2529 *NeuroImage* **139**, 470-479 (2016).
- 2530 347. S. Conjeti, A. Katouzian, A. G. Roy, L. Peter, D. Sheet, S. Carlier, A. Laine and N.
 2531 Navab, "Supervised domain adaptation of decision forests: Transfer of models trained in
 2532 vitro for in vivo intravascular ultrasound tissue characterization," *Medical Image
 2533 Analysis* **32**, 1-17 (2016).
- 2534 348. R. Bermúdez-Chacón, C. Becker, M. Salzmann and P. Fua, "Scalable unsupervised
 2535 domain adaptation for electron microscopy," *International Conference on Medical Image
 2536 Computing and Computer-Assisted Intervention (MICCAI)*, 326-334, 2016.
- 2537 349. C. Becker, C. M. Christoudias and P. Fua, "Domain adaptation for microscopy imaging,"
 2538 *IEEE transactions on medical imaging* **34**, 1125-1139 (2015).
- 2539 350. C. Baur, S. Albarqouni and N. Navab, "Semi-supervised Deep Learning for Fully
 2540 Convolutional Networks," *International Conference on Medical Image Computing and
 2541 Computer-Assisted Intervention (MICCAI)*, 311-319, 2017.
- 2542 351. R. Saunders, E. Samei, J. Baker and D. DeLong, "Simulation of mammographic lesions,"
 2543 *Academic Radiology* **13**, 860-870 (2006).
- 2544 352. A. Rashidnasab, P. Elangovan, M. Yip, O. Diaz, D. R. Dance, K. C. Young and K. Wells,
 2545 "Simulation and assessment of realistic breast lesions using fractal growth model," *Phys
 2546 Med Biol* **58**, 5613-5627 (2013).
- 2547 353. F. J. Martinez-Murcia, J. M. Górriz, J. Ramírez, I. A. Illán, F. Segovia, D. Castillo-
 2548 Barnes and D. Salas-Gonzalez, "Functional Brain Imaging Synthesis Based on Image
 2549 Decomposition and Kernel Modeling: Application to Neurodegenerative Diseases,"
 2550 *Frontiers in neuroinformatics* **11**, 65 (2017).
- 2551 354. F. Calimeri, A. Marzullo, C. Stamile and G. Terracina, "Biomedical Data Augmentation
 2552 Using Generative Adversarial Neural Networks," *Artificial Neural Networks and
 2553 Machine Learning (ICANN)* 626-634, 2017.
- 2554 355. A. Lahiri, K. Ayush, P. K. Biswas and P. Mitra, "Generative adversarial learning for
 2555 reducing manual annotation in semantic segmentation on large scale microscopy images:
 2556 Automated vessel segmentation in retinal fundus image as test case," *Proceedings of the
 2557 IEEE Conference on Computer Vision and Pattern Recognition Workshops*, 42-48, 2017.
- 2558 356. L. Zhang, A. Gooya and A. F. Frangi, "Semi-supervised assessment of incomplete lv
 2559 coverage in cardiac mri using generative adversarial nets," *International Workshop on
 2560 Simulation and Synthesis in Medical Imaging*, 61-68, 2017.
- 2561 357. N. Bayramoglu, M. Kaakinen, L. Eklund and J. Heikkila, "Towards virtual h&e staining
 2562 of hyperspectral lung histology images using conditional generative adversarial

- 2563 networks," Proceedings of the IEEE Conference on Computer Vision and Pattern
 2564 Recognition, 64-71, 2017.
- 2565 358. P. Costa, A. Galdran, M. I. Meyer, M. Niemeijer, M. Abramoff, A. M. Mendonça and A.
 2566 Campilho, "End-to-end adversarial retinal image synthesis," IEEE transactions on
 2567 medical imaging (2017).
- 2568 359. A. Chartsias, T. Joyce, R. Dharmakumar and S. A. Tsaftaris, "Adversarial Image
 2569 Synthesis for Unpaired Multi-modal Cardiac Data," International Workshop on
 2570 Simulation and Synthesis in Medical Imaging, 3-13, 2017.
- 2571 360. J. M. Wolterink, A. M. Dinkla, M. H. Savenije, P. R. Seevinck, C. A. van den Berg and I.
 2572 Išgum, "Deep MR to CT synthesis using unpaired data," International Workshop on
 2573 Simulation and Synthesis in Medical Imaging, 14-23, 2017.
- 2574 361. M. J. Chuquicusma, S. Hussein, J. Burt and U. Bagci, "How to Fool Radiologists with
 2575 Generative Adversarial Networks?: A Visual Turing Test for Lung Cancer Diagnosis,"
 2576 IEEE International Symposium on Biomedical Imaging 2018.
- 2577 362. N. A. Obuchowski, H. X. Barnhart, A. J. Buckler, G. Pennello, X. F. Wang, J. Kalpathy-
 2578 Cramer, H. J. Kim, A. P. Reeves and C. E. W. Grp, "Statistical issues in the comparison
 2579 of quantitative imaging biomarker algorithms using pulmonary nodule volume as an
 2580 example," *Statistical Methods in Medical Research* **24**, 107-140 (2015).
- 2581 363. N. A. Obuchowski, A. P. Reeves, E. P. Huang, X. F. Wang, A. J. Buckler, H. J. Kim, H.
 2582 X. Barnhart, E. F. Jackson, M. L. Giger, G. Pennello, A. Y. Toledano, J. Kalpathy-
 2583 Cramer, T. V. Apanasovich, P. E. Kinahan, K. J. Myers, D. B. Goldgof, D. P. Barboriak,
 2584 R. J. Gillies, L. H. Schwartz, D. C. Sullivan and A. C. W. Grp, "Quantitative imaging
 2585 biomarkers: A review of statistical methods for computer algorithm comparisons,"
 2586 *Statistical Methods in Medical Research* **24**, 68-106 (2015).
- 2587 364. L. C. Lazzeroni, Y. Lu and I. Belitskaya-Levy, "P-values in genomics: Apparent
 2588 precision masks high uncertainty," *Molecular Psychiatry* **19**, 1336-1340 (2014).
- 2589 365. K. Drukker, L. Pesce and M. Giger, "Repeatability in computer-aided diagnosis:
 2590 Application to breast cancer diagnosis on sonography," *Med Phys* **37**, 2659-2669 (2010).
- 2591 366. S. Holm, "A Simple Sequentially Rejective Multiple Test Procedure," *Scandinavian
 2592 Journal of Statistics* **6**, 65-70 (1979).
- 2593 367. D. Curran-Everett, "Multiple comparisons: philosophies and illustrations," *American
 2594 Journal of Physiology-Regulatory Integrative and Comparative Physiology* **279**, R1-R8
 2595 (2000).
- 2596 368. L. Ein-Dor, I. Kela, G. Getz, D. Givol and E. Domany, "Outcome signature genes in
 2597 breast cancer: is there a unique set?," *Bioinformatics* **21**, 171-178 (2005).
- 2598 369. L. Ein-Dor, O. Zuk and E. Domany, "Thousands of samples are needed to generate a
 2599 robust gene list for predicting outcome in cancer," *Proceedings of the National Academy
 2600 of Sciences of the United States of America* **103**, 5923-5928 (2006).
- 2601 370. C. G. Begley and L. M. Ellis, "Raise standards for preclinical cancer research," *Nature*
 2602 **483**, 531-533 (2012).
- 2603 371. A. Chalkidou, M. J. O'Doherty and P. K. Marsden, "False Discovery Rates in PET and
 2604 CT Studies with Texture Features: A Systematic Review," *Plos One* **10** (2015).
- 2605 372. N. P. Grusauskas, K. Drukker, M. L. Giger, C. A. Sennett and L. L. Pesce,
 2606 "Performance of breast ultrasound computer-aided diagnosis: Dependence on image
 2607 selection," *Academic Radiology* **15**, 1234-1245 (2008).

- 2608 373. N. P. Gruszauskas, K. Drukker, M. L. Giger, R. F. Chang, C. A. Sennett, W. K. Moon
 2609 and L. L. Pesce, "Breast US Computer-aided Diagnosis System: Robustness across Urban
 2610 Populations in South Korea and the United States," *Radiology* **253**, 661-671 (2009).
- 2611 374. K. R. Mendel, H. Li, L. Lan, C. M. Cahill, V. Rael, H. Abe and M. L. Giger,
 2612 "Quantitative texture analysis: robustness of radiomics across two digital mammography
 2613 manufacturers' systems," *Journal of Medical Imaging* **5** (2018).
- 2614 375. J. Kalpathy-Cramer, A. Mamomov, B. S. Zhao, L. Lu, D. Cherezov, S. Napel, S.
 2615 Echegaray, D. Rubin, M. McNitt-Gray, P. Lo, J. C. Sieren, J. Uthoff, S. K. N. Dilger, B.
 2616 Driscoll, I. Yeung, L. Hadjiiski, K. Cha, Y. Balagurunathan, R. Gillies and D. Goldgof,
 2617 "Radiomics of Lung Nodules: A Multi-Institutional Study of Robustness and Agreement
 2618 of Quantitative Imaging Features," *Tomography* **2**, 430-437 (2016).
- 2619 376. L. E. Court, "Harmonization & Robustness in Radiomics," *Med Phys* **43**, 3695-3696
 2620 (2016).
- 2621 377. A. Holzinger, C. Biemann, C. S. Pattichis and D. B. Kell, "What do we need to build
 2622 explainable AI systems for the medical domain?," arXiv:1712.09923 (2017).
- 2623 378. W. Samek, T. Wiegand and K.-R. Müller, "Explainable Artificial Intelligence:
 2624 Understanding, Visualizing and Interpreting Deep Learning Models," arXiv:1708.08296
 2625 (2017).
- 2626 379. M. D. Zeiler and R. Fergus, "Visualizing and Understanding Convolutional Networks,"
 2627 arXiv:1311.2901 (2014).
- 2628 380. M. T. Ribeiro, S. Singh and C. Guestrin, "'Why Should I Trust You?': Explaining the
 2629 Predictions of Any Classifier," arXiv:1602.04938 (2016).
- 2630 381. K. Simonyan, A. Vedaldi and A. Zisserman, "Deep inside convolutional networks:
 2631 Visualising image classification models and saliency maps," arXiv:1312.6034 (2014).
- 2632 382. B. Zhou, A. Khosla, A. Lapedriza, A. Oliva and A. Torralba, "Learning Deep Features
 2633 for Discriminative Localization," arXiv:1512.04150 (2015).
- 2634 383. R. R. Selvaraju, M. Cogswell, A. Das, R. Vedantam, D. Parikh and D. Batra, "Grad-
 2635 CAM: Visual Explanations from Deep Networks via Gradient-based Localization,"
 2636 arXiv:1610.02391 (2017).
- 2637 384. G. Litjens, T. Kooi, B. E. Bejnordi, A. A. A. Setio, F. Ciompi, M. Ghafoorian, J. van der
 2638 Laak, B. van Ginneken and C. I. Sanchez, "A survey on deep learning in medical image
 2639 analysis," *Medical Image Analysis* **42**, 60-88 (2017).
- 2640 385. K. Adil, F. Jiang, S. H. Liu, A. Grigorev, B. B. Gupta and S. Rho, "Training an Agent for
 2641 FPS Doom Game using Visual Reinforcement Learning and VizDoom," *International*
 2642 *Journal of Advanced Computer Science and Applications* **8**, 32-41 (2017).
- 2643 386. R. M. Summers, "Are we at a crossroads or a plateau? Radiomics and machine learning
 2644 in abdominal oncology imaging," *Abdominal Radiology*, 1-5 (2018).

2645

2646

2647 **Figure Legends**

2648 Fig. 1: CNN with two convolution layers each followed by a pooling layer, and one fully connected layer.

2649 Fig. 2: Number of peer-reviewed publications in radiologic medical imaging that involved DL. Peer-
2650 reviewed publications were searched on PubMed using the criteria ("deep learning" OR "deep neural
2651 network" OR deep convolution OR deep convolutional OR convolution neural network OR "shift-
2652 invariant artificial neural network" OR MTANN) AND (radiography OR x-ray OR mammography OR
2653 CT OR MRI OR PET OR ultrasound OR therapy OR radiology OR MR OR mammogram OR SPECT).
2654 The search only covered the first three months of 2018 and the result was linearly extended to the rest of
2655 2018.

2656 Fig 3: Use of CNN as a feature extractor.¹⁹⁶ (a) Each ROI is sent through AlexNet and the outputs from
2657 each layer are preprocessed to be used as sets of features for an SVM. The filtered image outputs from
2658 some of the layers can be seen in the left column. The numbers in parentheses for the center column
2659 denote the dimensionality of the outputs from each layer. The numbers in parentheses for the right
2660 column denote the length of the feature vector per ROI used as an input for the SVM after zero-variance
2661 removal. (b) Performance in terms of area under the receiver operating characteristic curve for classifiers
2662 based on features from each layer of AlexNet in the task of distinguishing between malignant and benign
2663 breast tumors.

2664 Fig. 4: CNN-extracted and conventional features can be combined in a number of ways,
2665 including a traditional classifier such as an SVM.¹⁹⁶

2666 Fig. 5: The use of training, validation, and test sets for the design and performance evaluation of a
2667 supervised machine learning algorithm.

2668 Fig. 6: A disease image categorization framework using both images and texts.³²⁷

2669 Fig. 7: Eight sample disease keywords and images mined from PACS.¹⁸⁰

2670

2671 **Table Headings**

Author Manuscript

Table I: Organ and substructure segmentation summary and performance using DL.

Region	Segmentation Object	Network Input	Network Architecture Basis	Data Set (train/test)	Dice Coefficient on Test Set
Abdomen	Skeletal muscle ⁸⁹	Whole Image	FCN	250/150 patients	0.93
	Subcutaneous and visceral fat areas ⁹⁰	Image Patch	Custom	20/20 patients	0.92 - 0.98
	Liver, spleen, kidneys ⁹¹	Whole Image	Custom	140 scans 5-fold CV	0.94 – 0.96
Bladder	Bladder ⁷⁶	Image Patch	CifarNet	81/93 patients	0.86
Brain	Anterior visual pathway ⁹²	Whole Image	AE	165 patients LOO CV	0.78
	Bones ⁸⁶	Whole image	U-net	16 patients LOO CV	0.94
	Striatum ⁹³	Whole Image	Custom	15/18 patients	0.83
	Substructures ⁹⁴	Image Patch	Custom	15/20 patients	0.86 – 0.95
	Substructures ⁹⁵	Image Patch	Custom	20/10 patients	0.92
	Substructures ⁹⁶	Image Patch	Deep Residual Network ⁹²	18 patients 6-fold CV	0.69 – 0.83
	Substructures ⁹⁷	Whole Image	FCN	150/947 patients	0.86 – 0.92
Breast	Dense tissue and fat ⁹⁸	Image Patch	Custom	493 images 5-fold CV	0.63 – 0.95

	Breast and fibroglandular tissue ⁸⁵	Whole Image	U-net	66 patients 3-fold CV	0.85 – 0.94
Head and Neck	Organs-at-risk ⁸³	Image Patch	Custom	50 patients 5-fold CV	0.37 – 0.90
Heart	Left ventricle ⁷⁹	Whole Image	AE	15/15 patients	0.93
	Left ventricle ⁸²	Whole Image	AE	15/15 patients	0.94
	Left ventricle ⁹⁹	Image Patch	Custom	100/100 patients	0.86
	Left ventricle ¹⁰⁰	Image Patch	Custom	100/100 patients	0.88
	Fetal left ventricle ¹⁰¹	Image Patch	Custom	10/41 patients	0.95
	Right ventricle ⁷⁸	Whole Image	AE	16/16 patients	0.82
Kidney	Kidney ¹⁰²	Whole Image	Custom	2000/400 patients	0.97
	Kidney ¹⁰³	Whole Image	FCN	165/79 patients	0.86
Knee	Femur, femoral cartilage, tibia, tibial cartilage ⁸¹	Whole Image	Custom	60/40 images	-
Liver	Liver ⁸⁰	Image Patch	Custom	78/40 patients	-
	Liver ¹⁰⁴	Image Patch	Custom	109/32 patients	0.97
	Portal vein ⁸³	Image Patch	Custom	72 scans 8-fold CV	0.70

Lung	Lung ¹⁰⁵	Whole Image	HNN	62 slices/31 patients	0.96 – 0.97
Pancreas	Pancreas ¹⁰⁶	Image Patch	Custom	80 patients 6-fold CV	0.71
	Pancreas ¹⁰⁷	Image Patch	Custom	82 patients 4-fold CV	0.72
Prostate	Prostate ¹⁰⁸	Image Patch	AE	66 patients 2-fold CV	0.87
	Prostate ¹⁰⁹	Image Patch	Custom	30 patients LOO CV	0.87
	Prostate ¹¹⁰	Whole Image	FCN	41/99 patients	0.85
	Prostate ⁸⁷	Whole Image	HNN	250 patients 5-fold CV	0.90
Rectum	Organs-at-risk ¹¹¹	Whole Image	VGG-16	218/60 patients	0.88 – 0.93
Spine	Intervertebral disk ¹¹²	Image Patch	Custom	18/6 scans	0.91
Whole body	Multiple organs ¹¹³	Whole Image	FCN	228/12 scans	-
Multiple organs	Liver and heart (blood pool, myocardium) ¹¹⁴	Whole Image	Custom	Liver: 20/10 patients Heart: 10/10 patients	0.74 – 0.93

Note: A “-” on the performance metrics means that the authors report different segmentation accuracy metrics. Abbreviations: AE: Auto-encoder. FCN: Fully Convolutional Network. HNN: Holistically-Nested Network. LOO: Leave-one-out. CV: Cross-validation.

Table II: Lesion segmentation summary and performance using DL.

Region	Segmentation Object	Network Input	Network Architecture Basis	Data Set (train/test)	Dice Coefficient on Test Set
Bladder	Bladder lesion ⁷⁷	Image Patch	CifarNet	62 patients LOO CV	0.51
Breast	Breast lesion ¹¹⁸	Image Patch	Custom	107 patients 4-fold CV	0.93
Bone	Osteosarcoma ¹¹⁹	Whole Image	ResNet-50	15/8 patients	0.89
	Osteosarcoma ¹²⁰	Whole Image	FCN	1900/405 images from 23 patients	0.90
Brain	Brain lesion ¹²¹	Image Patch	Custom	61 patients 5-fold CV	0.65
	Brain metastases ¹²²	Image Patch	Custom	225 patients 5-fold CV	0.67
	Brain tumor ¹¹⁵	Image Patch	AE	HGG: 150/69 patients, LGG: 20/23 patients	HGG: 0.86 LGG: 0.82
	Brain tumor ¹¹⁷	Image Patch	Custom	HGG: 220, LGG: 54, 5-fold CV	HGG: 0.85 – 0.91 LGG: 0.83 – 0.86
	Brain tumor ¹²³	Whole Image	Custom	30/25 patients	0.88
	Brain tumor ¹²⁴	Whole Image	FCN	274/110 patients	0.82
	Brain tumor ⁸⁸	Whole Image	HNN	20/10 patients	0.83

	Ischemic lesions ¹²⁵	Whole Image	DeConvNet	380/381 patients	0.88
	Multiple sclerosis lesion ¹²⁶	Whole Image	Custom	250/77 patients	0.64
	White matter hyper-intensities ¹¹⁶	Image Patch	AE	100/135 patients	0.88
	White matter hyper-intensities ¹²⁷	Image Patch	Custom	378/50 patients	0.79
Head and neck	Nasopharyngeal cancer ¹²⁸	Whole Image	VGG-16	184/46 patients	0.81 – 0.83
	Thyroid nodule ¹²⁹	Image Patch	HNN	250 patients 5-fold CV	0.92
Liver	Liver lesion ¹³⁰	Image Patch	Custom	26 patients LOO CV	0.80
Lung	Lung nodule ¹³¹	Image Patch	Custom	350/493 nodules	0.82
Lymph nodes	Lymph nodes ¹³²	Whole Image	HNN	171 patients 4-fold CV	0.82
Rectum	Rectal cancer ¹³³	Image Patch	Custom	70/70 patients	0.68
Skin	Melanoma ¹³⁴	Image Patch	Custom	126 images 4-fold CV	-

Note: A “-” on the performance metrics means that the authors report different segmentation accuracy metrics. Abbreviations: AE: Auto-encoder. FCN: Fully Convolutional Network. HNN: Holistically-Nested Network. LOO: Leave-one-out. CV: Cross-validation. HGG: High Grade Glioma. LGG: Low Grade Glioma.

Table III: Organ and Anatomical structure detection summary and performance.

Organ	Detection Object	Network Input	Network Architecture Basis	Data Set (train/test)	Error (Mean±STD)
Bone	37 hand landmarks ¹⁴⁷	X-ray images	Custom CNN	895 images 3-fold CV	1.19±1.14 mm
	Femur bone ¹³⁵	MR 2.5D image patches	Custom 3D CNN	40/10 volumes	4.53±2.31 mm
	vertebrae ¹⁴⁸	MR/CT image patches	Custom CNN	1150 patches/ 110 images	3.81±2.98 mm
	vertebrae ¹⁴⁹	US/X-ray images	U-Net	22/19 patients	F1:0.90
Vessel	carotid artery ¹⁵⁰	CT 3D image patches	Custom 3D CNN	455 patient four-fold CV	2.64±4.98 mm
	ascending aorta ¹³⁹	3D US	Custom CNN	719/150 patients	1.04±0.50 mm
Fetal anatomy	Abdominal standard scan plane ^{136, 151}	US image patches	Custom CNN	11942/871 8 images	F1:0.71 ¹³⁶ , 0.75 ¹⁵¹
	12 standard scan planes ¹³⁷	US images	Custom CNN	800/200 images	F1:0.42- 0.93
	13 standard scan planes ¹³⁸	US images	AlexNet	5229/2339 images	Acc: 0.10- 0.94
Body	Body parts ¹⁵²	CT images	AlexNet + FCN	450/49 patients	3.9±4.7 voxels
	Body parts ¹⁵³	CT images	AlexNet	3438/860 images	AUC: 0.998
	Multiple	3D CT images	Custom CNN	200/200	F1:0.97

	Organ ¹⁵⁴			scans	
	Body parts ^{141,} 142	CT images	LeNet	2413/4043 images	F1:0.92
Brain	Brain landmarks ¹⁵⁵	MR images	FCN	350/350 images	2.94±1.58 mm
Lung	Pathologic Lung ¹⁵⁶	CT images	FCN	929 scans 5-fold CV	0.76±0.53 mm
Extremities	Thigh muscle ¹⁵⁷	MR images	FCN	15/10 patients	1.4±0.8 mm
Heart	Ventricle landmarks ¹⁴³⁻¹⁴⁵	MRI images	Custom CNN + RL	801/90 images	2.9±2.4 mm

Abbreviations: FCN: Fully Convolutional Network. RL: Reinforcement learning. F1: harmonic average of the precision (positive predictive value) and recall (sensitivity). AUC: Area under the receiver operating characteristic curve. CV: Cross-validation.

Table IV: Lesion detection using DL.

Detection Organ	Lesion Type	Data set (train/test)	Network Input	Network Architecture Basis
Lung and Thorax	Pulmonary Nodule	888 patients 5-fold CV ¹⁶⁸	Image Patch ^{168,} 169, 173-177 Whole Image ¹⁷⁸⁻¹⁸⁰	CNN ^{168, 169, 173,} 175-180 SDAE/CNN ¹⁷⁴
		888 patients 10-fold CV ¹⁶⁹		
		303 patients 10-fold CV ¹⁷³		
		2400 images 10-fold CV ¹⁷⁴		
		104 patients 5-fold CV ¹⁷⁵		
		1006 patients 10-fold CV ¹⁷⁶		
	Multiple	35,038/2,443		

	Pathologies	radiographs ¹⁷⁸		
		76,000/22,000 chest x-rays ¹⁸⁰		
		ImageNet Pre-training, 433 patients LOO CV ¹⁸¹		
	Tuberculosis	685/151 chest radiographs ¹⁷⁹		
Brain	Cerebral Aneurism	300/100 magnetic resonance angiography images ¹⁸²	Image Patch ¹⁸² Whole Image ^{170, 172}	CNN ¹⁸² FCN/CNN ^{170, 172}
	Cerebral microbleed	230/50 brain MR scans ¹⁷²		
	Lacune	868/111 brain MR scans ¹⁷⁰		
Breast	Solid Cancer	40,000/18,000 mammographic images ⁶⁴	Image Patch ^{17, 64, 183} Whole Image ^{66, 161}	CNN ^{17, 64, 66, 183} FCN/CNN ¹⁶¹
		161/160 Breast MR images ¹⁸³		
	Mass	Pre-training on ~2,300 mammography images, 277/47 DBT cases ¹⁷		
		ImageNet Pre-training, 306/163 breast ultrasounds images ¹⁶¹		
	Malignant mass & Mirco-calcification	ImageNet Pre-training, 3476/115 FFDM images ⁶⁶		
Colon	Polyp	394/792 CT colonography cases ¹⁶⁶	Whole Image ¹⁸⁴	CNN ^{166, 184, 185}

		101 CT colonography cases; 10-fold CV ¹⁸⁵	Image Patch ^{166, 185}	
	Colitis	ImageNet Pre-training, 160 abdominal CT cases; 4-fold CV ¹⁸⁴		
Multiple	Lymph Node	ImageNet Pre-training, 176 CT cases; 3-fold CV ¹⁶⁰	Image Patch ^{160, 166, 186}	CNN ^{160, 166, 186}
		69/17 abdominal CT cases ¹⁶⁶		
		176 abdominal CT cases; 3-fold CV ¹⁸⁶		
Liver	Tumor	NA/37 ¹⁸⁷	Image Patch ¹⁸⁷	CNN ¹⁸⁷
Thyroid	Nodule	21,523 Ultrasound images; 10-fold CV ¹⁸⁸	Image Patch ¹⁸⁸	CNN ¹⁸⁸
Prostate	Cancer	196 MR cases; 10-fold CV ¹⁸⁹	Whole Image ¹⁸⁹	FCN ¹⁸⁹
Pericardium	Effusion	20/5 CT cases ¹⁹⁰	Whole Image ¹⁹⁰	FCN ¹⁹⁰
Vascular	Calcification	ImageNet Pre-training; 84/28 ¹⁹¹	Image Patch ¹⁹¹	FCN ¹⁹¹

Abbreviations: SDAE: Stacked Denoising Auto-encoder. FCN: Fully Convolutional Network. LOO: Leave-one-out. CV: Cross-validation.

Table V: Characterization using DL.

Anatomic Site	Object or Task	Network Input	Network Architecture	Data Set (train/test)
Breast	Cancer risk	Mammograms	Pre-trained Alexnet	456 patients LOO

	assessment ¹⁹²		followed by SVM	CV
	Cancer risk assessment ¹⁹³	Mammograms	Modified AlexNet	14,000/1850 images randomly selected 20 times
	Cancer risk assessment ¹⁹⁴	Mammograms	Custom DCNN	478/183 mammograms
	Cancer risk assessment ¹⁹⁵	Mammograms	Fine-tuned a pre-trained VGG16Net	513/91 women
	Diagnosis ¹⁹⁶	Mammograms	Pre-trained AlexNet followed by SVM	607 cases 5-fold CV
	Diagnosis ¹⁹⁷	Mammograms, MRI, US	Pre-trained VGG19Net followed by SVM	690 MRI, 245 FFDM 1125 US, LOO CV
	Diagnosis ¹⁹⁸	Breast Tomosynthesis	Pre-trained Alexnet followed by evolutionary pruning	2682/89 masses
	Diagnosis ¹⁹⁹	Mammograms	Pre-trained AlexNet	1545/909 masses
	Diagnosis ²⁰⁰	MRI MIP	Pre-trained VGG19Net followed by SVM	690 cases with 5-fold CV
	Diagnosis ²⁰¹	DCE-MRI	LSTM	562/141 cases
	Solitary cyst diagnosis ²⁰²	Mammograms	Modified VGG Net	1,600 lesions 8-fold CV
	Prognosis ²⁰³	Mammograms	VGG16Net followed by logistic regression classifier	79/20 cases randomly selected 100 times
Chest - Lung	Pulmonary Nodule Classification ²⁰⁴	CT patches	ResNet	665/166 nodules

	Tissue Classification ²⁰⁵	CT patches	Restricted Boltzmann Machines	training 50/100/150/200; testing 20,000/1,000/20,000/20,000 image patches
	Interstitial Disease ²⁰⁶	CT patches	Modified AlexNet	100/20 patients
	Interstitial Disease ²⁰⁷	CT patches	Modified VGG	public: 71/23 scans local: 20/6 scans
	Interstitial Disease ²⁰⁸	CT patches	Custom	480/(120 and 240)
	Interstitial Disease ²⁰⁹	CT patches	Custom	36,106/1,050 patches
	Pulmonary Nodule Staging ²¹⁰	CT	DFCNet	11/7 patients
	Prognosis ²¹¹	CT	Custom	7,983/ (1000 and 2164) subjects
Chest - cardiac	Calcium Scoring ²¹²	CT	Custom	1181/506 scans
	Ventricle Quantification ²¹³	MR	Custom (CNN + RNN +Bayesian multitask)	145 cases, 5-fold CV
Abdomen	Tissue Classification ²¹⁴	Ultrasound	CaffeNet and VGGNet	136/49 Studies
	Liver Tumor Classification ²¹⁵	Portal Phase 2D CT	GAN	182 cases, 3-fold CV
	Liver Fibrosis ²¹⁶	DCE-CT	Custom CNN	460/100 scans

	Fatty Liver Disease ²¹⁷	US	Invariant Scattering Convolution Network	650 patients, 5- and 10-fold CV
Brain	Survival ²¹⁸	Multiparametric MR	Transfer learning as feature extractor, CNN-S	75/37 patients
Skeletal	Maturity ²¹⁹	Hand Radiographs	Deep Residual Network	14036/ (200 and 913) exams

Abbreviations: FCN: Fully Convolutional Network. LOO: Leave-one-out. CV: Cross-validation.

Table VI: Image processing and reconstruction with DL.

Task	Imaging Modality	Performance Measure	Network Output	Network Architecture Basis
Filtering	CT ²³⁴ Chest X-Ray ²³⁵ X-ray fluoro ²³⁶	MSE ²³⁴ , CAD Performance ²³⁴ PSNR ^{235, 236} SSIM ^{235, 236} Runtime ²³⁶	Likelihood of Nodule ²³⁴ Bone Image ²³⁵ CLAHE filtering ²³⁶	Custom CNN ^{234, 235} Residual CNN ²³⁶ Residual AE ²³⁶
Noise reduction	CT ²³⁷⁻²⁴⁰ PET ²⁴¹	PSNR ²³⁷⁻²⁴¹ RMSE ^{237, 238} SSIM ^{237, 238, 240} NRMSE ²³⁹ NMSE ²⁴¹	Noise-reduced image ²³⁷⁻²⁴¹	Custom CNN ²³⁷⁻²³⁹ Residual AE ^{237, 238} Concatenated CNNs ²⁴¹ U-net ²⁴⁰
Artifact reduction	CT ^{242, 243} MRI ²⁴⁴	SNR ^{242, 243} NMSE ²⁴⁴ Qualitative ²⁴³ Runtime ²⁴⁴	Sparse-view recon ^{242, 244} Metal artifact reduced image ²⁴³	U-net ^{242, 244} Custom CNN ²⁴³
Recons	MRI ²⁴⁵⁻²⁴⁸	RMSE ^{245, 248} Runtime ²⁴⁵ MSE ^{246, 247} NRMSE ²⁴⁶ SSIM ²⁴⁶ SNR ²⁴⁸	Image of scalar measures ²⁴⁵ MR reconstruction ²⁴⁶⁻²⁴⁸	Custom CNN ^{245, 248} Custom NN ²⁴⁶ Cascade of CNNs ²⁴⁷
Registration	MRI ²⁴⁹⁻²⁵² X-ray to	DICE ^{249, 250} Runtime ²⁵⁰ Target overlap ²⁵¹ SNR ²⁵²	Deformable registration ²⁴⁹⁻²⁵²	Custom CNN ^{249, 251-254} SAE ²⁵⁰

	3D ^{253, 254}	TRE ²⁵⁴ Image & vessel sharpness ²⁵² mTREproj ²⁵³	Rigid body 3D transformation ^{253, 254}	
Synthesis of one modality from another	CT from MRI ²⁵⁵⁻²⁵⁹ MRI from PET ²⁶⁰ PET from CT ²⁶¹	MAE ^{255, 256} PSNR ^{255, 259} ME ²⁵⁶ MSE ²⁵⁶ Pearson Correl ²⁵⁶ PET Image Quality ^{257, 258} SSIM ²⁶⁰ SUVR of MR-less methods ²⁶⁰ Tumor detection by radiologist ²⁶¹	Synthetic CT ²⁵⁵⁻²⁵⁸ Synthetic MRI ²⁶⁰ Synthetic PET ²⁶¹	Custom 3D FCN ²⁵⁵ GAN ²⁵⁹⁻²⁶¹ U-net ^{256, 257} AE ²⁵⁸
Image quality assessment	US ²⁶² CT ^{263, 264} MRI ²⁶⁵	AUC ^{262, 264} IOU ²⁶² Correlation between TRE estimation and ground truth ²⁶³ Concordance with readers ²⁶⁵	ROI localization & classification ²⁶² TRE estimation ²⁶³ estimate of image diagnostic value ^{264, 265}	Custom CNN ^{262, 265} Custom NN ²⁶³ VGG19 ²⁶⁴

Abbreviations: MSE: Mean-squared error, RMSE: Root MSE, NSME: Normalized MSE, NRMSE: Normalized RMSE, SNR: signal-to-noise ratio, PSNR: Peak SNR, SSIM: Structural similarity, DICE: Segmentation overlap index, TRE: Target registration error, mTREproj: mean TRE in projection direction, MAE: Mean absolute error, ME: Mean error, SUVr: Standardized uptake value ratio, AUC: Area under the receiver operating characteristic curve, IOU: Intersection over union, CLAHE: Contrast-limited adaptive histogram equalization.

Table VII: Radiotherapy and assessment of response to treatment with DL.

Anatomic Site	Object or Task	Network Input	Network Architecture	Dataset (train/test)
Bladder	Treatment response assessment ²⁶⁸	CT	CifarNet	82/41 patients
Brain	Glioblastoma multiforme treatment options and survival prediction ²¹⁸	MRI	Custom	75/37 patients
	Assessment of treatment effect in acute ischemic	MRI	CNN based on	158/29 patients

	stroke ²⁶⁹		SegNet	
Breast	Response to neoadjuvant chemotherapy ²⁷⁰	MRI	Pre-trained VGGNet followed by LDA	561 exams from 64 subjects LOO CV
	Response to neoadjuvant chemotherapy ²⁷¹	MRI	Custom	133/33 patients
	Segmentation of clinical target volume ²⁷²	CT	Deep Dilated Residual Network	800 patients 5-fold CV
Cancer cell lines	Prediction of drug effectiveness in cancer cell lines ²⁷³	Multiple omics data from cancer cells (gene expression data, copy number variation data, mutation data, and cell line annotations)	Deep autoencoder	520/104 cell lines
Head and Neck	Organ segmentation ²⁷⁴	CT	U-Net based with shape retention model	22/10 scans
Kidney	Renal segmentation ²⁷⁵	CT	Custom	89/24 patients
	Early detection of acute renal transplant rejection ²⁷⁶	DWI-MRI	Stacked autoencoders	100 patients 4-fold, 10-fold and LOO CV
Liver	Hepatobiliary toxicity prediction after liver SBRT ²⁷⁷	CT and patient demographics, clinical information	Custom CNN trained on other organs, fine-tuned on liver	125 patients 20-fold CV

			SBRT	
Lung	Estimation of dose protocols in Radiotherapy ²⁷⁸	FDG-PET/CT, clinical, genetic, imaging radiomics features, tumor and lung dosimetric variables, treatment plans	Deep Q-Network	114 real train / 4000 synthesized test cases
	Dynamic tracking during therapy ²⁷⁹	DRRs from 4D CT	DenseNet	1/9 volumes
Prostate	Prediction of dose from patient image contours ²⁸⁰	IMRT	U-Net	80/8 patients
	Prediction of dosimetric eligibility of prostate cancer patients undergoing IMRT ²⁸¹	CT	Fine-tuned AlexNet	60 patients 5-fold CV
Pelvis	Generating synthetic CTs from MR-only radiotherapy ²⁸²	MRI	cGAN	123/59 patients
	Assessment of toxicity to normal organs and tissue ²⁸³	Rectum surface dose maps	Fine-tuned VGG-16	42 patients 10-fold and LOO CV
Rectum	Segmentation of rectal tumors on T2-MRI and clinical target volume segmentation on CT ²⁷²	T2-MRI or CT	Novel CNN involving cascaded atrous convolution and spatial pyramid pooling	70 T2-MR and 100 CT 5-fold CV
	Prediction of pathologic	CT	DNN Classifier	95 patients 5-

	complete response after chemoradiation ²⁸⁴		Custom Estimator	fold CV
--	--	--	---------------------	---------

Abbreviations: IMRT: Intensity-modulated radiation therapy. SBRT: Stereotactic body radiotherapy. DWI: Diffusion-weighted MRI. DRR: Digitally reconstructed radiographs. LDA: Linear discriminant analysis. LOO: Leave-one-out. CV: Cross-validation.

Author Manuscript

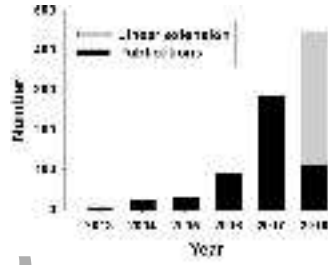
Author Manuscript



Created by Universal Document Converter

mp_13264_f1.tif


Author Manuscript



Created by Universal Document Converter

mp_13264_f2.tif

Author Manuscript

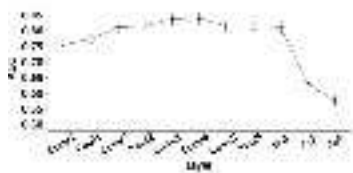


1	1	1
2	2	2
3	3	3
4	4	4
5	5	5
6	6	6
7	7	7
8	8	8
9	9	9
10	10	10
11	11	11
12	12	12
13	13	13
14	14	14
15	15	15
16	16	16
17	17	17
18	18	18
19	19	19
20	20	20
21	21	21
22	22	22
23	23	23
24	24	24
25	25	25
26	26	26
27	27	27
28	28	28
29	29	29
30	30	30
31	31	31
32	32	32
33	33	33
34	34	34
35	35	35
36	36	36
37	37	37
38	38	38
39	39	39
40	40	40
41	41	41
42	42	42
43	43	43
44	44	44
45	45	45
46	46	46
47	47	47
48	48	48
49	49	49
50	50	50
51	51	51
52	52	52
53	53	53
54	54	54
55	55	55
56	56	56
57	57	57
58	58	58
59	59	59
60	60	60
61	61	61
62	62	62
63	63	63
64	64	64
65	65	65
66	66	66
67	67	67
68	68	68
69	69	69
70	70	70
71	71	71
72	72	72
73	73	73
74	74	74
75	75	75
76	76	76
77	77	77
78	78	78
79	79	79
80	80	80
81	81	81
82	82	82
83	83	83
84	84	84
85	85	85
86	86	86
87	87	87
88	88	88
89	89	89
90	90	90
91	91	91
92	92	92
93	93	93
94	94	94
95	95	95
96	96	96
97	97	97
98	98	98
99	99	99
100	100	100

Created by Universal Document Converter

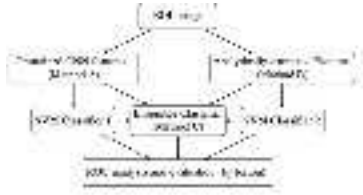
mp_13264_f3a.tif

Author Manuscript



Created by Universal Document Converter

mp_13264_f3b.tif

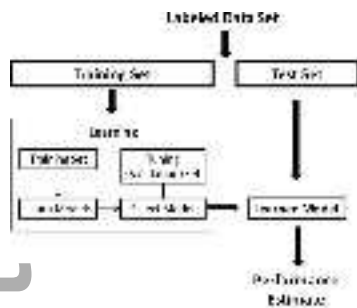


Author Manuscript

Created by Universal Document Converter

mp_13264_f4.tif

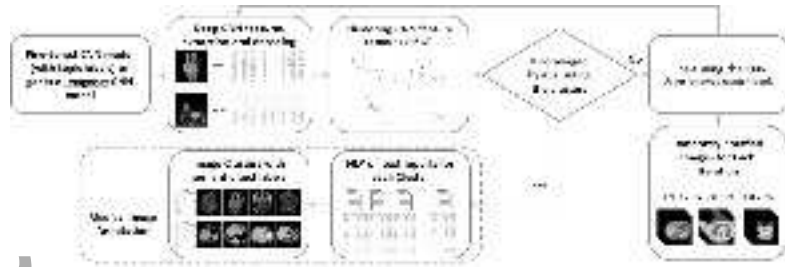
Author Manuscript



Created by Universal Document Converter

mp_13264_f5.tif

Author Manuscript



Created by Universal Document Converter

mp_13264_f6.tif



Author Manuscript

Created by Universal Document Converter

mp_13264_f7.tif